FREQUENCY-DOMAIN EQUALIZATION FOR MULTI-H CONTINUOUS PHASE MODULATION

A Thesis
Presented to
The Academic Faculty

by

Sajid Saleem

In Partial Fulfillment
of the Requirements for the Degree
Doctor of Philosophy in the
School of Electrical and Computer Engineering

Georgia Institute of Technology
December 2013

FREQUENCY-DOMAIN EQUALIZATION FOR MULTI-H CONTINUOUS PHASE MODULATION

Approved by:

Professor Gordon L. Stüber, Advisor
School of Electrical and Computer Engineering
Georgia Institute of Technology

Professor Faramarz Fekri
School of Electrical and Computer Engineering
Georgia Institute of Technology

Professor Geoffrey Ye Li
School of Electrical and Computer Engineering
Georgia Institute of Technology

Professor John McCuan
School of Mathematics
Georgia Institute of Technology

Professor John R. Barry
School of Electrical and Computer Engineering
Georgia Institute of Technology

Date Approved: November 12th, 2013

To my parents.

ACKNOWLEDGEMENTS

My life at Georgia Tech, as a graduate student, has been very exciting and enriching. Many individuals and institutions colored these very special years of my life. The great sense of accomplishment on completing my doctoral degree, at such a distinguished school, is coupled with a strong realization of the importance of the support and contribution of others. This journey has been truly enlightening for me, and the one which instilled immense humility. I take this as an opportunity to thank everyone who supported me by investing their technical, emotional and/or financial resources in my graduate education and research. To all these people, I owe my deepest gratitude and earnest appreciation for believing in my abilities.

First and foremost, I am very grateful to my advisor, Prof. Gordon L. Stüber. It has been a great privilege to work under his supervision. I have no words that can express my gratitude. This dissertation was not possible, in its current form, without his unwavering support, patient mentoring, and invaluable advice. His mere presence, at times, was sufficient to inspire new ideas. He maintained his trust and faith in me despite my repeated mistakes and shortcomings.

I would like to thank Prof. John R. Barry and Prof. Geoffrey Ye Li for taking time out of their hectic schedules to serve on my reading committee. Without their feedback and suggestions, this work would not have been even half as good. I also want to thank Prof. Faramraz Fekri and Prof. John McCuan for serving on my committee and providing useful comments, which played a significant role in improving the dissertation. I did not know much about communications or analysis before I took their wonderfully taught graduate courses. Their teaching philosophy and pedagogical technique will inspire me perpetually for the rest of my career.

Most of my doctoral research was supported by grants from Institute of International Education (IIE), United States Educational Foundation in Pakistan (USEFP), and Georgia Tech. I am truly indebted to them for providing me this great opportunity.

My deepest appreciation for the great camaraderie I enjoyed at the Wireless Systems Lab with my fellow graduate students, and special thanks to Seok-Chul (Sean) Kwon, Hyungseok Yu, and Sami Almalfouh for providing a very productive environment in the lab. I treasure all the thoughts, ideas, and knowledge that I gained through long conversations and meetings with people on- and off-campus. I am also thankful to Syed Ali Hassan, Haejoon Jung, and Obaidullah Fayyaz for their fellowship during lunch and coffee breaks, for providing hope in times of despair, and for sharing joy on the eve of paper acceptance. Hussain, Minhaj, Hassan, Ahmad, Saad, Haider, Ali, and Bashir are among many friends who passed the test of time though I may have failed them at times. I accept unconditionally that it was impossible without their help.

Finally, I am grateful to the most important people in my life: my parents and my siblings. Without family, there is no meaning to life, and there are no achievements. There is no way to acknowledge or thank for their countless prayers and encouraging messages. Their sacrifice and patience is the greatest cost of my education at Tech.

TABLE OF CONTENTS

LIST OF TABLES

LIST OF FIGURES

ABBREVIATIONS

ZF	Zero-forcing
BER	Bit-error rate
FFT	Fast Fourier Transform
IFFT	Inverse Fast Fourier Transform
FSM	Finite-state Machine
PM	Phase Modulator
TS	Terminating Sequence
AWGN	Additive White Gaussian Noise
PCM/FM	Pulse-code Modulation/Frequency Modulation
OFDM	Orthogonal Frequency-division Multiplexing
GSM	Global System for Mobile Communications
MLSE	Maximum-likelihood Sequence Estimation
ISI	Intersymbol Interference
VA	Viterbi Algorithm
PAPR	Peak-to-average-power Ratio
RSSE	Reduced-state Sequence Estimation
CPE	Continuous Phase Encoder
LDE	Linear Diophantine Equation

TSS	Terminating Solution Set
FN	Frobenius Number
FDE	Frequency-domain Equalization
CPFSK	Continuous Phase Frequency Shift Keying
MSK	Minimum Shift Keying
PSD	Power Spectral Density
SCFDE	Single-carrier Frequency-domain Equalization
CPM	Continuous Phase Modulation
IRIG	Inter-Range Instrumentation Group
MIL-STD	Military Standard
ARTM	Advanced Range Telemetry
SO-QPSK	Shaped-offset Quadri-phase Shift Keying
MMSE	Minimum Mean Square Error

SUMMARY

Continuous phase modulation (CPM) is a non-linear constant-envelope modulation scheme with memory, known for its bandwidth and power efficiency. Multi-h CPM uses multiple modulation indices in successive symbol intervals to improve the error performance as compared to single-h CPM (basic CPM that utilizes only a single modulation index). One of the major applications of multi-h CPM is in aeronautical telemetry systems. Aeronautical telemetry is witnessing a data deluge similar to other applications of wireless communications. Modern aeronautical devices host an increasing number of sensors, which can transmit flight-test data to the ground station. However, this excess data transfer requires more bandwidth, making the behavior of the aeronautical channel increasingly selective in the frequency domain. To get acceptable performance, channel equalization is required. Frequency-domain equalization (FDE) offers low-complexity, as compared to both the optimal maximum-likelihood sequence detection (MLSD) and the time-domain equalizer, for a channel with large delay spread. The objective of our research is to develop FDE techniques for multi-h CPM waveforms.

FDE is a block-based approach, and it mandates the transmitter to compose symbol blocks resulting in a cyclic transmitted signal. For a modulation scheme with memory, such as CPM, the cyclic constraint on the block necessitates the use of an extra segment of symbols, called intrafix or tail segment, in each block. The computation of these intrafix symbols and their quantity is related to the memory of the modulator. To characterize the memory of the multi-h CPM modulator, we have shown that it can be decomposed into a finite-state machine (FSM) with periodic

transitions and a memoryless phase modulator (PM). First, we discuss the process of terminating the tilted-phase component of the multi-h CPM signal. We have used very simple geometric arguments to derive upper and lower bounds on the length of the intrafix in terms of the parameters of the modulation scheme and the Frobenius number. It is concluded that the length of the intrafix for multi-h CPM schemes is typically shorter than those required for single-h modulation schemes.

After composing a signal suitable for FDE at the receiver, the next step is to design the equalizer and demodulator for multi-h CPM. We propose two receiver architectures; one uses a matched-filter front end, while the other utilizes a fractional-sampling front end. We develop circulant matrix models for both receiver architectures, and use these models to develop equalizers. Various simplifications are proposed for each architecture, and the trade-off between receiver complexity and performance is analyzed and verified through detailed simulation studies. For performance evaluation, we consider a dual-h CPM waveform (used in the IRIG-106 telemetry standard) affected by a wideband aeronautical telemetry channel model.

Our theoretical results and proposed architectures for FDE of multi-h CPM will be an important contribution towards achieving fast and reliable aeronautical telemetry.

CHAPTER I

INTRODUCTION

1.1 Motivation

Continuous phase modulation (CPM) represents a family of non-linear coded modulation schemes characterized by a constant envelope and continuity of the phase [1]. The constant envelope permits the use of very efficient non-linear power amplifiers in the transmitter, while smooth phase variations result in a compact spectrum. Typical CPM schemes use a single modulation index that controls the sensitivity of phase with respect to the source symbols. These modulations are classified as single-h CPM schemes and have been used in various standards, such as GSM [2], Bluetooth [3], etc. A variant of CPM, called multi-h CPM, has a set of modulation indices, and the modulator selects one from the set, in a round-robin fashion, in successive symbol intervals [4]. The use of multiple modulation indices introduces asymmetries in the demodulating trellis of multi-h CPM signal, which delays the first merge, thereby increasing the coding gain relative to single-h CPM. Multi-h CPM has been used for voice-over-satellite communications (MIL-STD-188-181B) [5], and has been included as the most sophisticated modulation scheme in IRIG-106 aeronautical telemetry standard [6].

Aeronautical telemetry is witnessing a data deluge similar to other applications of wireless communications. Modern aeronautical devices host an increasing number of sensors, which can transmit flight testing data to the ground station. However, this excess data transfer requires more bandwidth making the behavior of the aeronautical channel increasingly selective in the frequency domain [7, 8]. The effect of the frequency-selective channel in the time domain is to introduce interference

among the neighboring symbols called intersymbol interference (ISI). To get acceptable performance, this effect has to be mitigated/equalized at the receiver, prior to demodulation, by using an equalizer. Frequency-domain equalization (FDE) is a single-carrier technique that has low-complexity, as compared to both the optimal maximum-likelihood sequence detection (MLSD) and the time-domain equalizer, for a channel with large delay spread [9]. Our objective is to develop a comprehensive framework to enable frequency-domain equalization (FDE) of multi-h continuous phase modulation (CPM). This involves design of a transmit block to generate a cyclic modulated signal, and to develop low-complexity receiver architectures that can equalize and demodulate multi-h CPM signal received from a frequency-selective channel.

FDE is a block-based approach, and it mandates the transmitter to compose symbol blocks such that the resulting transmitted signal is cyclic over the duration of the block [10]. For a modulation scheme with memory, such as CPM, cyclic constraint on the block necessitates the use of an extra segment of symbols in each block [11]. These extra symbols are collectively referred to as a tail segment [11] or an intrafix [12]. This intrafix is in addition to the regular cyclic prefix required for memoryless modulation schemes [13]. Computation of these intrafix symbols and their quantity is related to the memory of the modulator. To characterize the memory of multi-h CPM modulator, it is shown that the modulator can be decomposed into a finite-state machine (FSM) with periodic transitions and a memoryless phase modulator (PM). The periodic FSM generates a tilted-phase signal [14], which after tilt correction, results in excess phase. The excess phase is modulated by the PM. Cyclic constraint on the signal can thus be posed as a constraint on state of the FSM. First, the process of terminating the tilted-phase component of the multi-h CPM signal is discussed. It is shown that an arbitrary state can be reached by controlling the input symbols of the state machine. The process of minimizing the length of the terminating sequence

(TS) is posed as a discrete optimization problem, and it is observed that this problem is closely related to a celebrated problem in number theory called the Diophantine Frobenius problem [15]. Very simple geometric arguments are used to derive upper and lower bounds on the length of the TS in terms of parameters of the modulation scheme and the Diophantine Frobenius number. It is concluded that the length of intrafix for multi-h CPM schemes is typically shorter than that required for single-h modulation schemes. Later, it is shown that the problem of intrafix computation to form a cyclic multi-h CPM signal can be reduced to a search of the terminating sequence for the tilted-phase trellis; hence, the results on the length of the TS can be applied to the length of the intrafix.

CPM schemes use a power-efficient transmitter owing to its constant envelope, while its compact spectrum makes it desirable for bandwidth-constrained channels. This clemency on the transmitter and channel, however, complicates the receiver. After composing a signal suitable for FDE at the receiver, the next step is to design an equalizer and a demodulator for multi-h CPM. Owing to the memory inherent in CPM, optimal receivers become very complicated [1, 4]. Even for an additive white-Gaussian-noise (AWGN) channel, an optimal CPM receiver requires a trellis-based sequence detection because of CPM's inherent memory arising from the phase continuity property [1]. Both the size of the matched-filter (MF) bank and the number of states in the trellis contribute to the complexity of the receiver, which increases exponentially relative to the inherent memory. The reduction in complexity is typically achieved by a sub-optimal receiver that is based upon one or another decomposition of the CPM signal as a superposition of multiple amplitude modulated pulses (see [16], [17], and references therein). The most elegant and frequently used decomposition is Laurent decomposition. It was first discovered for binary single-h CPM schemes [18] and later developed for the M-ary single-h CPM waveforms [19]. A simplified AWGN receiver for single-h CPM, based upon the Laurent decomposition,

was proposed by Kaleh [20]. By ignoring the pulses with negligible energy, Laurent decomposition enables the reduction of both the number of MFs and the number of states in the demodulator.

Laurent decomposition has been recently extended to multi-h CPM schemes [21], and it is observed that the set of Laurent pulses vary from one symbol interval to the next, and the pulses have a periodic behavior similar to that of modulation indices. For example, for a modulation scheme with two distinct modulation indices, the Laurent pulses appear in two distinct sets (one set corresponding to even symbol intervals and the other to odd symbol intervals). A reduced complexity receiver design for AWGN channels has been proposed for multi-h CPM [22] using similar principles as Kaleh's receiver except that it uses a dynamic MF bank – the received signal is correlated with the current set of Laurent pulses.

As mentioned earlier, equalization is required at the receiver for signals transmitted over frequency-selective channels. There are two hurdles in designing a practical frequency-domain equalizer for multi-h CPM; the requirement of a cyclic transmitted signal for the scope of the block and the exorbitant complexity of the receiver. The problem of constructing a cyclic signal by using a cyclic prefix and an intrafix has been examined in detail in [23] and Chapter 4 for single-h and multi-h CPM, respectively. The use of FDE itself reduces the complexity of the receiver as compared to the optimal MLSD receiver, but it can still be too high for partial-response modulation schemes. There are two basic approaches to an FDE-based receiver design proposed previously for single-h CPM suffering from ISI; one that has a MF bank front end [11] and the other that utilizes a single low-pass filter followed by fractional sampling [24, 25]. Both these architectures utilize Laurent decomposition, and it has been reported that they have similar performance at comparable receiver complexities. We discuss both these architectures for multi-h CPM in Chapter 5.

Matched-filter (MF) Front end Receiver: Using Laurent decomposition for multi-h CPM signal, a matched-filter bank can be used to gather sufficient statistics for detection [1, 10, 26]. Non-orthogonality of Laurent's pulses and their periodicity, in case of multi-h CPM, causes the noise at output of the matched filters to be correlated and cyclo-stationary. Moreover, the pseudo symbols are also correlated. Thus, the equalizer design must also consider second order statistics of both signal and noise components of the sampled outputs of the matched filters. As discussed in Chapter 5, this design requires an equalizer for each branch of the matched-filter bank. Each equalizer is preceded by an FFT block, and followed by an IFFT block. Complexity reduction can be obtained by omitting matched filters corresponding to Laurent pulses with smaller amplitudes. Also, the demodulator can be simplified by state reduction techniques as discussed in [27]. It will be shown that the suboptimality caused by this complexity reduction impacts performance of the receiver.

Sampling-based Equalizer and Demodulator: Since the CPM spectrum is very compact, it is expected that sampling the signal at the rate of two samples per symbol interval may not cause much aliasing. Using this idea, the matched-filter bank could be replaced by a single anti-aliasing filter followed by sampling at twice the symbol rate. This approach has been used in equalizer design for single-h CPM in [24, 25]. However, the framework is not directly applicable to multi-h CPM because of the periodicity of its Laurent pulses. In the latter half of the Chapter 5, a polyphase decomposition model is developed for multi-h CPM that can isolate the effect of channel and the modulation memory. This will enable channel equalization in the frequency domain followed by detection in the time domain. It is expected that the complexity of the equalizer, in this approach, becomes independent of the number of Laurent pulses.

Performance and Complexity Comparison: Performance of the proposed FDE schemes is compared by performing simulations on the dual-h CPM adavnced range telemetry (ARTM) waveform. For this purpose, a wideband channel model for aeronautical telemetry is used [7]. A complexity and performance comparison in terms of the number of operations required per block and the achieved bit error rate (BER), respectively, will help in determining the trade-offs involved in the choice of one of these different approaches.

Previous Related Work: To the best of our knowledge, equalization for multi-h CPM has only been considered in [28] and [29]. In [28], equalization is performed for a specific full-response dual-h CPM waveform that is affected by the satellite-transponder filters. The proposed approach is that of decision-feedback sequence estimation (DFSE), which is performed on a super-trellis representing both ISI and the memory of the modulation scheme. However, this approach becomes infeasible or ineffective for partial-response waveforms and longer/non-minimum phase channels. The authors in [29] proposed an FDE approach for general multi-h schemes based upon the MF-bank and a differential-phase demodulator. Unfortunately, the circulant discrete model derived for the output of the MFs omits the cross-correlation between different Laurent pulses, which makes the results reported in [29] optimistic and unrealistic.

1.2 Thesis Contributions

Important contributions of this thesis are summarized as follows:

- A decomposition for mult-h CPM modualtor has been developed as the cascade of a periodic recursive continuous phase encoder (CPE) and memoryless phase modualtor (PM).

- Trellis termination of multi-h CPM has been considered in detail. It has been shown that the constraints assume the form of a set of linear Diophantine equations (LDEs). A method has been proposed to minimize the length of the terminating sequence (TS).

- Bounds are derived on the length of the TS in terms of the parameters of multi-h CPM modulation. The length of the TS has also been found to be related to the Frobenius Number.

- A detailed procedure has been proposed for the construction of a block that generates a cyclic multi-h CPM signal. Theoretical justifications are provided to establish the correspondence between the problem of minimizing the length of the intrafix and the tilted-phase trellis termination.

- Two different receiver techniques are proposed for frequency-domain equalization of multi-h CPM. One of them utilizes a matched-filter bank and the other utilizes a simple fractional sampler. Matrix models with a circulant substructure are developed for both types of receivers, and using these models, we have proposed the design of equalizers and demodulators.

1.3 Thesis Outline

The remainder of this dissertation is organized as follows. In Chapter 2, we provide background information about continuous phase modulation, single-carrier frequency-domain equalization, and Laurent decomposition of CPM signals. Moreover, we also provide a brief literature review of the area. Chapter 3 explains the structure of multi-h CPM transmitter and its trellis termination. Bounds are computed for the length of terminating sequence, and a relationship of the length of terminating sequence is found with the Diophantine Frobenius problem. In Chapter 4, we build upon theoretical results of Chapter 3, and propose various methods to compute the intrafix

segment. A procedure is specified for the construction of a cyclic transmit block such that the length of the intrafix is minimized. Chapter 5 deals with the receiver design, i.e, the most challenging part of the problem. We propose two different receiver architectures for frequency-domain equalization of multi-h CPM; one of them based upon a matched-filter front end, and the other one based upon a fractional sampling front end. For each model, we provide the derivation of the circulant matrix models, analyze the computational requirements, and perform simulation-based studies. Finally, in Chapter 6, we conclude our thesis with a summary of important contributions and a list of future research directions.

CHAPTER II

BACKGROUND

As mentioned in the previous chapter, the objective of our research is the frequency-domain equalization (FDE) of multi-h continuous phase modulation (CPM). In this chapter, we introduce continuous phase modulation (CPM), motivate the need for equalization in a frequency-selective channel, identify the challenges involved and the advantages gained by performing equalization in the frequency domain, and provide a brief review of the existing transceiver techniques for single-h and multi-h CPM in frequency-selective channels.

2.1 Continous Phase Modulation

Continuous phase modulation (CPM) is a group name for a family of constant envelope and bandwidth efficient modulation schemes [1]. Over the years, specific forms of CPM have been adopted in various personal and mobile communication standards, such as GSM and Bluetooth. The standard single-h CPM transmitter uses a single modulation index for all the symbols. An important sub-group of CPM schemes is multi-h CPM, which acquires superior minimum distance properties as compared to single-h CPM schemes, through the use of a cyclic set of modulation indices [4]. A quaternary dual-h CPM scheme (with two modulation indices) is part of the IRIG-106 Aeronautical Telemetry standard [6].

2.2 Channel Equalization

The effect of multipath fading on the transmitted signal is to introduce interference among the neighbouring symbols. This effect is called intersymbol interference (ISI) [10, 26]. In the frequency domain, the multipath effect manifests itself as a

frequency-dependent gain of the channel, and a channel with such behaviour is said to be frequency selective. As the data rate increases, the effect of multipath becomes more and more dominant. Continuous phase modulation (CPM) schemes have an inherent memory owing to the partial-response character of the phase pulse and the continuity of the phase [4, 30, 31]. A frequency-selective channel induces memory in addition to this inherent memory [10, 26].

In case of a frequency-selective channel, a direct approach to the receiver design is to perform joint sequential detection using a trellis that incorporates both the inherent memory of CPM and the memory introduced by the channel [32]. The Viterbi algorithm (VA) is used to reduce the complexity of sequential detection [33]. However, the complexity still rises exponentially as a function of the partial-response length of CPM and the delay spread of the channel. Suboptimal approaches such as decision-feedback sequence estimation (DFSE) [34] and reduced-state sequence estimation (RSSE) [35] reduce the complexity of the receiver at the cost of performance. Another approach is to mitigate/equalize the effect of a frequency-selective channel prior to detection so that an acceptable performance can be obtained [10, 26]. This process of equalization can be performed in the time domain using a linear transversal equalizer. However, the complexity of a linear equalizer also rises at increased data rates. For linear modulation schemes, orthogonal frequency-division multiplexing (OFDM) is a very effective multi-carrier transmission technique. OFDM reduces the complexity of equalization by performing it in the frequency domain. Unfortunately, OFDM is not readily applicable to a non-linear modulation scheme, such as CPM. OFDM also suffers from large peak-to-average-power ratio (PAPR) and sensitivity to frequency synchronization [36]. Single-carrier frequency-domain equalization (SCFDE) is widely acknowledged as an alternative technique to OFDM for time-dispersive communication channels [9, 37, 38]. The advantage of FDE, over time-domain equalization, is its ability to equalize long channels at relatively low complexity.

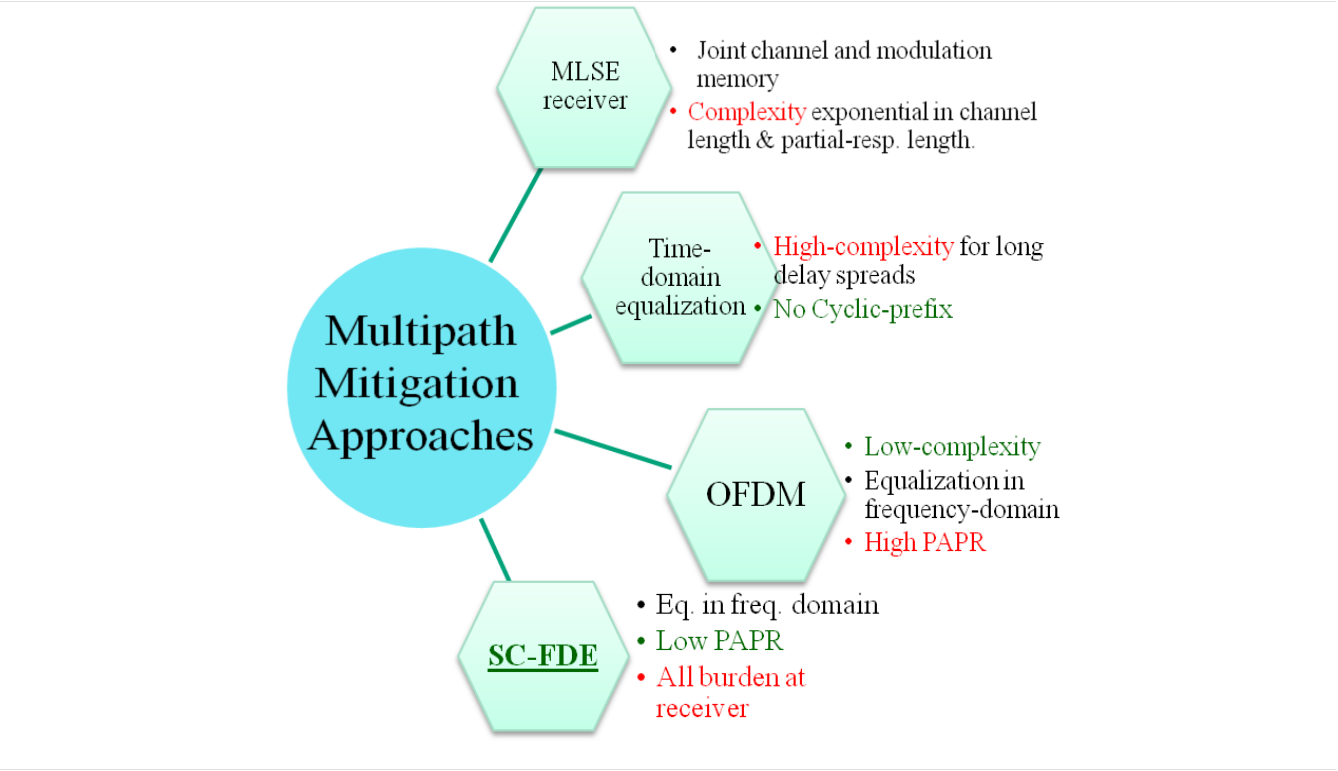

Figure 1: A chart of various techniques for multipath mitigation (channel equalization). Their merits and demerits are also listed.

2.3 Cyclic Signal Generation for Frequency-domain Equalization

As mentioned in the previous section, the major advantage of performing equalization in the frequency domain, rather than in the time domain, is to get a low-complexity receiver. The reduction in complexity is achieved by the use of very efficient fast Fourier transform (FFT) and inverse fast Fourier transform (IFFT) operations in the receiver. However, the use of FFT requires a circulant channel matrix, which imposes a cyclic constraint on the transmitted block. For linear modulation schemes, this constraint can be satisfied by simply appending a cyclic guard interval to each transmitted block. For non-linear modulation schemes, such as CPM, the insertion of a guard interval alone is insufficient owing to the continuous-phase requirement of CPM waveform [11, 12, 24, 39]. A segment consisting of a few symbols, sometimes called a tail sequence [11] or an intrafix [12], must be inserted in a block to force the

transmitter to reach the same state it had at the start of the block. This concept, first introduced in [11], specified the need for two such tail sequences. One of these sequences was shown to be redundant in [24]. Later, [12] introduced the term intrafix and devised an ingenious approach that eliminated the dependence of this segment on the symbols of previous blocks.

The tilted-phase decomposition for single-h CPM, proposed by Rimoldi in [14], represents a CPM transmitter as the cascade of a recursive continuous phase encoder (CPE) and a memoryless phase modulator (PM). The CPE has a shift-register structure, and the number of states are finite for a modulation scheme with a rational modulation index. This transformation of the excess phase to the tilted phase results in a time-invariant phase trellis [14]. Moreover, this transformation reduces the effective number of states by half for certain modulation schemes. These schemes are characterized by a modulation index with an odd positive numerator.

The excess-phase trellis of a multi-h CPM scheme is periodic with period $2H$, where H is the cardinality of the set of modulation indices [4]. A decomposition approach similar to Rimoldi's decomposition is outlined in [40] for multi-h CPM. Like Rimoldi's decomposition, this decomposition also uses the lowest phase trajectory to define the transformation between the excess- and the tilted-phase trellis. In Section 3, this tilted-phase transformation is further developed for multi-h CPM, and it is proved that the resulting trellis is periodic with period H. The number of states in the maximum-likelihood sequence detector (MLSD) is reduced to half [27] when at least one of the H modulation indices has a numerator that is an odd integer. This transformation also enables the representation of a multi-h CPM transmitter as the cascade of a periodic recursive CPE and a PM.

2.4 Trellis Termination

The memory inherent in the CPM scheme owing to phase continuity and partial response must be used in the receiver to get an adequate performance. For this purpose, trellis-based decoding techniques, such as the Viterbi Algorithm (VA), are used to implement the optimal MLSD receiver [33]. In a packetized-transmission mode, it is necessary to start and terminate the phase trellis in a known state to provide uniform protection to all the information bits [41]. This process referred to as trellis termination is important for satisfactory performance of trellis-based receivers [42, 43]. Trellis termination is also required for SCFDE of modulation schemes with memory, such as CPM. The continuity of CPM signal is ascertained by starting and terminating the cyclic prefix in a known state. This problem is discussed for single-h CPM in [11, 25, 44].

In Chapter 3, the problem of trellis termination is discussed for the tilted-phase multi-h CPM scheme. Trellis termination is achieved by appending a terminating-sequence (TS) to the block. It is observed that finding the TS for a given modulation scheme and an initial state of the CPE is equivalent to finding a non-negative solution to a linear Diophantine equation (LDE) with H integer variables [45]. An analytical proof of the existence of a finite-length TS is furnished. Since the TS is an overhead and results in a loss of bandwidth efficiency, it is interesting to find the worst-case length of the TS for different initial and terminating states. An equivalent mathematical criterion is found for the minimal-length TS, and bounds are derived on the length of the TS for arbitrary modulation parameters and initial conditions. A connection of this problem is established with the Diophantine Frobenius problem (FP) [15], and it is shown that the upper bound is closely related to the Frobenius Number (FN).

2.5 Laurent Decomposition of a CPM Signal

As discussed earlier, the complexity of the MLSD receiver increases exponentially with partial-response length of the phase function. This rise in complexity occurs because of the increase in the number of states in the decoder and the number of matched filters in the receiver front end. Several suboptimal approaches are proposed for the receiver in additive white-Gaussian-noise (AWGN) channel [20, 31, 46]. These techniques are invariably based upon a decomposition of the CPM signal, e.g., the Laurent decomposition [18], orthogonal decomposition [17], non-symmetric non-orthogonal exponential expansion (nSnOEE) [47], etc. The purpose of these decompositions is to write the CPM signal as a combination of pulses. The shape, duration, and number of these pulses depends upon the form of decomposition. The coefficients of these pulses, also called pseudo-symbols, have a non-linear dependence upon the source symbols. The Laurent decomposition is the most popular decomposition because it results in a reduction in both the number of states and the number of matched filters. The Laurent decomposition was originally available only for binary single-h CPM and was first used by Kaleh [20] to introduce reduced-complexity receiver design. This decomposition was later extended to the case of non-binary single-h CPM [19] and multi-h CPM [21]. Based upon this decomposition, Perrins and Rice [27] proposed suboptimal low-complexity receivers for multi-h CPM.

The decompositions of CPM have also been employed in the low-complexity design of equalizers. Tan and Stüber [11] proposed frequency-domain equalizers for single-h CPM based upon both the Laurent and orthogonal decomposition. The receiver has a matched-filter front end, a frequency-domain equalizer for each pulse, and a demodulator based upon the Viterbi Algorithm. The reduction in complexity of each component is obtained by leaving out the low-energy pulses. Later approaches [24, 25] used sampling-based receivers, in which the receiver front end consists of a single low-pass filter. Although these designs employ the Laurent decomposition, but the

complexity of the equalizer becomes independent of the number of Laurent pulses used. It was claimed in [24] that the performance for sampling-based approach is very close to that of [11] for a given receiver complexity. A polyphase decomposition was proposed for single-h CPM in [25]. This decomposition enables the receiver to isolate the effect of the channel and the memory of CPM. The equalizer works only upon the channel, while a CPM detector for AWGN is used afterwards. This technique improves performance considerably.

2.6 Notation

We utilize the following notation (some of which is borrowed from [25]). Time-domain vectors (matrices) are denoted by lower-case underlined (doubly underlined) letters, respectively. Frequency-domain vectors (matrices) are denoted by upper-case underlined (doubly underlined) letters, respectively. $(a)_b$ denotes the modulo-reduced value of a w.r.t b. The set of natural numbers $\{0, 1, 2, ...\}$, integers, and strictly positive integers are denoted by $\mathbb{N}$, $\mathbb{Z}$, and $\mathbb{Z}^+$, respectively. For integers a and b, $a|b$ is used to denote that b is divisible by a. The set $\{0, 1, ..., A-1\}$, for $A \in \mathbb{Z}^+$ is denoted by $\mathbb{N}_A$. An ordered n-tuple synthesized from consecutive terms of a sequence x_n, i.e., $(x_i, x_{i+1}, ..., x_j)$ is represented by $\mathbf{x}_i^j$. For a matrix $\underline{\underline{a}}$, the m, n-th element is represented by $[\underline{\underline{a}}]_{m,n}$. The Kronecker product between two matrices $\underline{\underline{A}}$ and $\underline{\underline{B}}$ is denoted by $\underline{\underline{A}} \otimes \underline{\underline{B}}$, while the Hermitian transpose of a matrix $\underline{\underline{A}}$ is written as $\underline{\underline{A}}^H$. The Hadamard product of two matrices of equal size is the entrywise product represented as $\underline{\underline{A}} \odot \underline{\underline{B}}$. A horizontal (vertical) concatenation of two matrices or vectors is denoted by $[\underline{\underline{A}}, \underline{\underline{B}}]$ ($[\underline{\underline{A}}; \underline{\underline{B}}]$). The identity matrix of size $N \times N$ is written as $\underline{\underline{I}}_N$, while an all-ones-matrix of size $N \times N$ is denoted by $\underline{\underline{J}}_N$. The cardinality of a set X is denoted by $|X|$. We use $\mathbf{1}_{(.)}$ to denote an all-ones-vector with dimension specified by the argument, and $||\ .\ ||_\infty$ represents the largest among the absolute values of the components of a vector.

2.7 Signal Description for Multi-h CPM

The complex envelope of a multi-h CPM waveform with H different modulation indices is given by

$$s(t, \mathbf{x}) = \sqrt{\frac{E}{T}} \exp j(\phi(t, \mathbf{x}) + \phi_o), \quad t \leq nT, \tag{1}$$

where E is the energy per symbol, T is the symbol interval, and ϕ_o is a constant phase term. ϕ_o can be ignored if phase synchronization is assumed. The time-varying phase $\phi(t, \mathbf{x})$, also called the excess phase, is defined as

$$\phi(t, \mathbf{x}) = 2\pi \sum_{i=-\infty}^{n} h_{(i)_H} x_i q(t - iT), \quad t \leq nT. \tag{2}$$

Here $(\cdot)_H$ denotes modulo-H and the modulation index for each symbol interval is chosen cyclically from the set $\{h_0, h_1, ..., h_{H-1}\}$. The symbols x_n are chosen from an M-ary alphabet, defined as $\mathbb{M} := \{\pm 1, \pm 3, \ldots, \pm(M-1)\}$ for even M and $\mathbb{M} := \{0, \pm 2, \ldots, \pm(M-1)\}$ for odd M. Together they constitute the sequence $\mathbf{x} = \{x_0, x_1, \ldots, x_n, \ldots\}$. The function $q(t)$ in (2) is called the phase shaping function, and its derivative is known as the frequency shaping function $f(t)$. The phase shaping function $q(t)$ satisfies the following constraints. It is non-zero only for positive time, increases to $\frac{1}{2}$ during the interval $[0, LT]$, and stays constant beyond $t = LT$, where L is a positive integer that determines the memory of the modulation scheme. Modulation schemes with $L = 1$ are called full response, whereas those with $L > 1$ are called partial-response schemes. To ensure a finite number of states in the decoding trellis, modulation indices are restricted to the set of rational numbers with a common denominator P, such that $h_i = K_i/P$ for $i \in \mathbb{N}_H$. The denominator P is always chosen such that $\gcd(K_0, K_1, ..., K_{H-1}, P) = 1$, where $\gcd(\cdot)$ denotes the greatest common divisor of the arguments. The notation $\mathbb{K}$ is used for the set of numerators $\{K_0, K_1, ..., K_{H-1}\}$. For spectrally efficient modulation schemes, $\sup(\mathbb{K}) < P$.

The state vector for the transmitter can be defined as

$$\chi_n(\mathbf{x}) := \left(\tau_{n-L}, \mathbf{x}_{n-L+1}^{n-1}, (n)_H\right), \tag{3}$$

Table 1: Parameters for Tier-2 IRIG-106 dual-h CPM waveform

Alphabet size	$M = 4$ (Quaternary)
Symbol set	$x_n \in \{\pm 1, \pm 3\}$
Partial-response length	$L = 3$
Modulation indices ($H = 2$)	$(h_0, h_1) = \left(\frac{4}{16}, \frac{5}{16}\right)$
Frequency shaping function	Raised-cosine pulse

where $\tau_n := \left(\sum_{i=-\infty}^{i=n} K_{(i)_H} x_i\right)_{2P}$. The Laurent decomposition for multi-h CPM was proposed by Perrins et al. [21],

$$s(t, \mathbf{x}) = \sum_{i=-\infty}^{n} \sum_{q=0}^{Q-1} a_{q,i} g_{q,(i)_H}(t - iT), t \leq nT, \tag{4}$$

where $g_{q,(i)_H}(t)$ are the Laurent pulses and $a_{q,i}$ are the corresponding pseudo-symbols. The number of pulses in one symbol interval are given by $Q = 2^{\zeta(L-1)}(2^{\zeta} - 1)$, where ζ satisfies $2^{\zeta} < M \leq 2^{\zeta}$. For a detailed account of multi-h CPM, see [4].

2.8 Aeronautical Telemetry Waveform

A dual-h ($H = 2$) CPM scheme has been included as the Tier-2 modulation scheme in the IRIG-106 standard. Similarly, a PCM/FM scheme is defined as Tier-0, while two modulation schemes, namely shaped-offset quadri-phase shift keying (SO-QPSK) and Feher-patented quadri-phase shift keying (F-QPSK), are defined as Tier-1 modulations in the IRIG-106 suite. We use this Tier-2 modulation scheme repeatedly to provide as an illustration for our theoretical and simulation results. For example, we use it in Chapter 3 to discuss the trellis termination problem, in Chapter 4 to explain the intrafix insertion, and in Chapter 5 to provide numerical simulation results for our proposed frequency-domain equalizers. The parameters of this modulation scheme are defined in Table 1.

From the table, it is clear that it is a quaternary ($M = 4$), partial response ($L = 3$) waveform with two modulation indices 4/16 and 5/16. The symbols are chosen from the alphabet $\mathbb{M} = \{\pm 1, \pm 3\}$. The frequency shaping function $f(t)$ is a

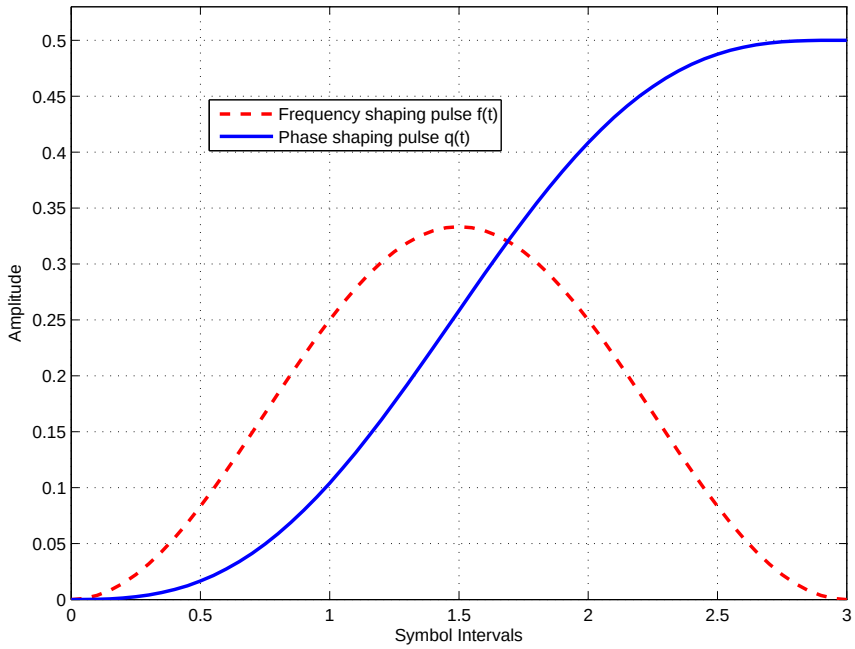

Figure 2: Frequency shaping function $f(t)$ and phase shaping function $q(t)$ for IRIG-106 dual-h CPM scheme.

raised-cosine pulse with support $3T$. Both the frequency shaping function $f(t)$ and the phase shaping function $q(t)$ for this modulation scheme are shown in Fig. 2. From the definitions in Section 2.7, it can be seen that $H = 2$, $P = 16$, $(K_0, K_1) = (4, 5)$. Number of Laurent pulses, per symbol interval, for this modulation scheme are given as $Q = 2^{2.2}(2^2 - 1) = 48$. The set of 48 Laurent pulses, for even symbol intervals, are shown in Fig. 3 and for odd symbol intervals are shown in Fig. 4. For further details about the Laurent decomposition of multi-h CPM signals, see [21].

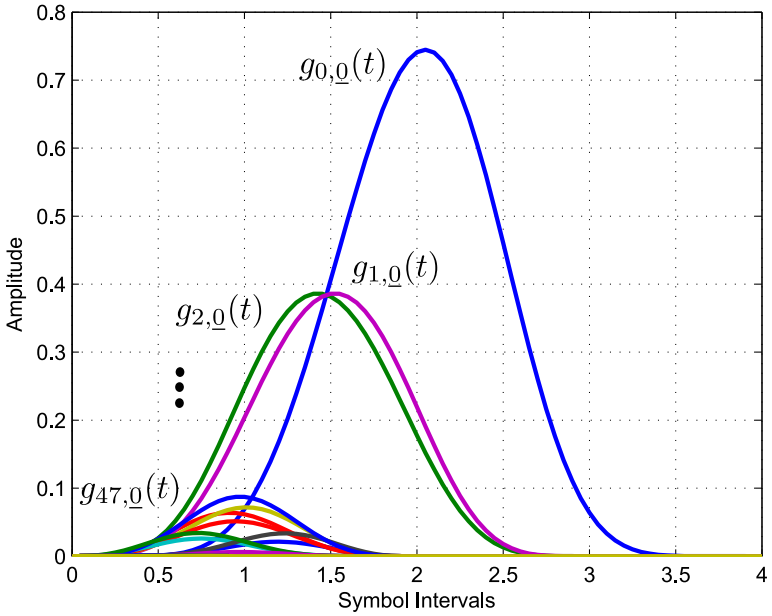

Figure 3: Laurent Pulses for Tier-2 IRIG-106 dual-h CPM waveform in even symbol intervals.

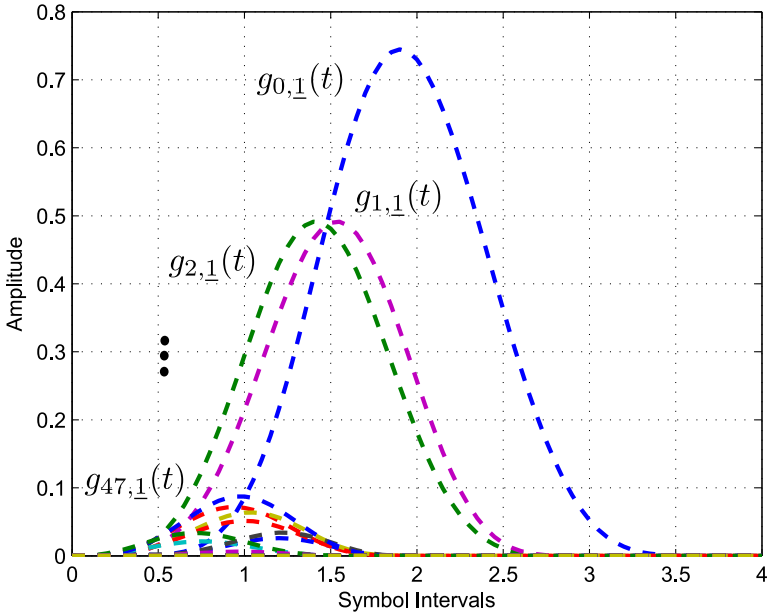

Figure 4: Laurent Pulses for Tier-2 IRIG-106 dual-h CPM waveform in odd symbol intervals.

CHAPTER III

TRELLIS TERMINATION OF MULTI-H CPM AND THE DIOPHANTINE FROBENIUS PROBLEM

This chapter presents a method for terminating the phase trellis of multi-h continuous phase modulation (CPM). It is shown that the tilted-phase trellis for multi-h CPM signals is periodic, and enables the representation of the multi-h CPM modulator as a cascade of a periodic recursive continuous-phase encoder (CPE) and a phase modulator (PM). The problem of finding the minimum number of symbols that will terminate the phase trellis in a known state of the modulator is posed, and a connection of its solution to the Diophantine Frobenius problem (FP) is established. Analytical results are obtained for the existence of a terminating sequence, and bounds are derived on its length for arbitrary modulation parameters. It is shown that the terminating symbols and their quantity depend upon the initial state of the encoder, the set of modulation indices, the CPE memory order, and the number of bits per modulated symbol. It is further shown that required overhead for trellis termination can be significant for schemes with integer modulation indices.

The rest of this chapter is organized as follows. Analytical results for the periodicity of the tilted-phase representation of multi-h CPM signals are presented in Section 3.1. A CPE representation for the modulator is also developed in Section 3.1. The problem of trellis termination for multi-h CPM is treated in Section 3.2, and bounds are proposed and derived for the length of the terminating sequence in Section 3.3. The Diophantine Frobenius problem (FP) is used to derive a bound in Section 3.3. In Section 3.4, various examples of single-h and multi-h CPM are discussed to illustrate the earlier developed theoretical results. Conclusions are drawn

in Section 3.5.

The multi-h CPM waveform and modulation parameters are described in Section 2.7, and the notation used in this chapter is defined in Section 2.6.

3.1 Tilted-phase Decomposition of Multi-h CPM Modulator

Rimoldi presented a tilted-phase description of the single-h CPM signals in [14] by shifting the carrier frequency from f_o to $f_o + \frac{\pi h(M-1)}{2T}$, where h is the modulation index. The resulting modified-phase (tilted-phase) trellis is time invariant, and the single-h CPM modulator can be interpreted as a cascade of a linear CPE and a memoryless PM. In this section, it is shown that the tilted-phase representation of multi-h CPM signals results in a periodic phase trellis, which enables the decomposition of multi-h CPM modulator as a cascade of a periodic recursive CPE and a memoryless PM. This section concludes with a finite-state machine (FSM) based representation of CPE and a description of its state vector.

3.1.1 Tilted-phase Trellis and its Periodicity

The excess phase in (2) can be written as

$$\phi(t, \mathbf{x}) = \pi \sum_{i=-\infty}^{n-L} h_{(i)_H} x_i + 2\pi \sum_{i=n-L+1}^{n} h_{(i)_H} x_i q(t - iT), \tag{5}$$

for the time interval $t \in [nT, (n+1)T]$. A change of variable in the second summation results in

$$\phi(t, \mathbf{x}) = \pi \sum_{i=-\infty}^{n-L} h_{(i)_H} x_i + 2\pi \sum_{i=0}^{L-1} h_{(n-i)_H} x_{n-i} q(t - (n-i)T). \tag{6}$$

Define $U_n := \frac{x_n+(M-1)}{2}$ as the non-negative symbols such that $U_n \in \mathbb{N}_M$. Using this transformation in (6),

$$\phi(t, \mathbf{U}) = \pi \sum_{i=-\infty}^{n-L} h_{(i)_H}(2U_i - (M-1)) + 2\pi \sum_{i=0}^{L-1} [h_{(n-i)_H}(2U_{n-i} - (M-1))q(t-(n-i)T)], \tag{7}$$

where $\mathbf{U} = \{U_n\}$ denotes the sequence of symbols. Note that unlike [27], U_n is substituted for x_n not only in the first term but also in the second term. This substitution will help develop the required structure for the multi-h CPM modulator, and establish the periodicity of the phase trellis. Substituting $\tau = t - nT$ such that the interval $t \in [nT, (n+1)T]$ is equivalent to $\tau \in [0, T]$, (7) becomes

$$\phi(\tau + nT, \mathbf{U}) = 2\pi \sum_{i=-\infty}^{n-L} h_{(i)_H} U_i + 4\pi \sum_{i=0}^{L-1} h_{(n-i)_H} U_{n-i} q(\tau + iT) - 2\pi(M-1) \sum_{i=0}^{L-1} h_{(n-i)_H} q(\tau + iT) - \pi(M-1) \sum_{i=-\infty}^{n-L} h_{(i)_H}, \tag{8}$$

where the first term in (8) is called the cumulative phase state, and is denoted by

$$\theta_{n-L} := \left[2\pi \sum_{i=-\infty}^{n-L} h_{(i)_H} U_i \right] \bmod 2\pi. \tag{9}$$

The second term contains the input term ($i = 0$) and the correlative state terms ($i \neq 0$). The input term depends upon the current symbol, while the correlative state term is determined by the $L-1$ most recent symbols.

The tilted phase $\psi(t, \mathbf{x})$ for $t \in [nT, (n+1)T]$ is defined as

$$\psi(t, \mathbf{x}) := \phi(t, \mathbf{x}) + \pi(M-1) \sum_{i=-\infty}^{n-1} h_{(i)_H} + \frac{\pi(M-1)h_{(n)_H}(t-nT)}{T}. \tag{10}$$

Note that the sum of second and third term is actually negative of the lowest trajectory of the excess-phase trellis. When written in terms of τ and $\mathbf{U}$, where $\tau \in [0, T]$, and substituting $\phi(\tau + nT, \mathbf{U})$ from (8), (10) becomes

$$\psi(\tau + nT, \mathbf{U}) = \phi(\tau + nT, \mathbf{U}) + \pi(M-1) \sum_{i=0}^{n-1} h_{(i)_H} + \frac{\pi(M-1)h_{(n)_H}\tau}{T}. \tag{11}$$

Substituting from (10), we get

$$\begin{aligned}\psi(\tau+nT,\mathbf{U}) &= 2\pi\sum_{i=0}^{n-L} h_{(i)_H}U_i + 4\pi\sum_{i=0}^{L-1} h_{(n-i)_H}U_{n-i}q(\tau+iT)\\ &\quad - 2\pi(M-1)\sum_{i=0}^{L-1} h_{(n-i)_H}q(\tau+iT) - \pi(M-1)\sum_{i=0}^{n-L} h_{(i)_H}\\ &\quad + \pi(M-1)\sum_{i=0}^{n-1} h_{(i)_H} + \frac{\pi(M-1)h_{(n)_H}\tau}{T}, \end{aligned} \tag{12}$$

and after combining the terms, we arrive at

$$\begin{aligned}\psi(\tau+nT,\mathbf{U}) &= 2\pi\sum_{i=-\infty}^{n-L} h_{(i)_H}U_i + 4\pi\sum_{i=0}^{L-1} h_{(n-i)_H}U_{n-i}q(\tau+iT)\\ &\quad - 2\pi(M-1)\sum_{i=0}^{L-1} h_{(n-i)_H}q(\tau+iT) + \pi(M-1)\sum_{i=1}^{L-1} h_{(n-i)_H}\\ &\quad + \frac{\pi(M-1)h_{(n)_H}\tau}{T}. \end{aligned} \tag{13}$$

All the terms in $\psi(\tau+nT,\mathbf{U})$ are periodic in n, and depend only on the time-translated variable τ. Thus we reach the conclusion that the tilted-phase transformation is a periodic function of time with period H.

3.1.2 FSM Representation of CPE

On the time interval, $t \in [nT,(n+1)T]$, (13) can be expressed as

$$\psi(t,\mathbf{U}) = 2\pi\sum_{i=-\infty}^{n-L} h_{(i)_H}U_i + R(t-nT) + 4\pi\sum_{i=0}^{L-1} h_{(n-i)_H}U_{n-i}q(t-(n-i)T), \tag{14}$$

where $R(t)$ is a data independent term, and is defined as

$$R(t) := \pi(M-1)\sum_{i=1}^{L-1} h_{(n-i)_H} + \frac{\pi(M-1)h_{(n)_H}t}{T} - 2\pi(M-1)\sum_{i=0}^{L-1} h_{(n-i)_H}q(t+iT). \tag{15}$$

The tilted phase is generated from the input symbols by the CPE of (14). The CPE is a finite-state machine (FSM) with a periodic coefficient $K_{(n)_H}$. Based on the relationship between excess and tilted phase (10), the CPE in (14), and the phase

modulator in (1), one can represent the multi-h CPM modulator as a periodic CPE followed by a PM, as shown in Fig. 5. Here

$$Q_i(n,t) := \frac{4\pi}{P} q(t-(n-i)T), \tag{16}$$

the block labelled "TT" is the transformation in (10), and the double circled symbol denotes a modulo-P adder.

3.1.3 State Vector for CPE

Unlike single-h CPM, where the state vector is defined as the cascade of the cumulative phase and the $L-1$ previous input symbols, for multi-h CPM, one must also take the periodicity of the state machine into account. The state vector is defined as

$$\chi_n^{(\theta)} := \left\{\theta_{n-L}, \mathbf{U}_{n-L+1}^{n-1}, (n)_H\right\}, \tag{17}$$

where $\mathbf{U}_{n-L+1}^{n-1} := \{U_{n-L+1}, U_{n-L+2}, ..., U_{n-1}\}$ is the set of past symbols determining the correlative terms in the tilted phase. If one defines $\gamma_n := \theta_n \frac{P}{2\pi}$, then $\gamma_n \in \mathbb{N}_P$, and an equivalent state vector for the system of Fig. 5 is

$$\chi_n^{(\gamma)} = \left\{\gamma_{n-L}, \mathbf{U}_{n-L+1}^{n-1}, (n)_H\right\}. \tag{18}$$

Note that $(n)_H$ is incorporated in the state vector to conform to the usual definition of a state machine, i.e., the next state and output of the CPE is determined solely by the knowledge of the previous state and current input symbol. A few more comments are made on this in the next section, where it is discussed how to reach a specified state in the phase trellis given an initial state vector.

3.2 Trellis Termination

In this section, the focus is on the problem of forcing the time-varying recursive CPE of Fig. 5 to any desired state from an arbitrary initial state. Trellis termination is achieved by appending a sequence (henceforth, called the terminating sequence (TS))

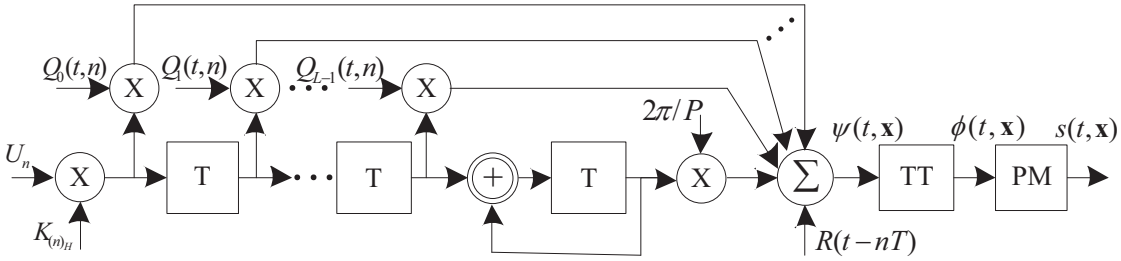

Figure 5: Finite-state machine representation of multi-h CPM modulator (The tilt transformation in (10) is denoted by TT).

to a block $\mathbf{U}_0^{N-1}$ of N data symbols. The symbols in the TS are chosen by imposing algebraic constraints on them for reaching the desired state in the tilted-phase trellis. As described earlier, owing to the trellis periodicity, the desired state vector will also put a constraint on the time index of the last symbol of the TS, and thus upon its length $T^{(H)}$. A simplifying assumption that can be made here is to allow only those desired states that have a time index equivalent modulo-H to the time index of the initial state. It is then possible to exclude $(n)_H$ from the state-vector definition, and assume that both the length N of the block to be terminated, and length $T^{(H)}$ of TS are a multiple of H. However, it is not difficult to avoid this assumption, as becomes clear from the process of trellis termination discussed in the sequel.

It is of interest to determine the length of the required terminating sequence, $T^{(H)}$, and the sequence $\mathbf{U}_N^{N+T^{(H)}-1}$ itself, where N is also the index of the first terminating symbol. It will be shown later that for $H > 1$, it is not possible to determine a closed-form expression for $T^{(H)}$ as a function of the modulation parameters. Thus, upper and lower bounds are derived on $T^{(H)}$ for arbitrary initial states and modulation scheme parameters. However, for a fixed modulation scheme (defined values of $P, \mathbb{K}, M$, and L), initial state $\chi_N^{(\gamma)}$ and desired state $\chi_{N+T^{(H)}}^{(\gamma)} : \left\{\gamma^{(D)}, \mathbf{U}^{(\mathbf{D})}{}_{N+T_H-L+1}^{N+T_H-1}, D\right\}$, one can compute the terminating sequence by following a three step procedure. Each step defines a segment of the TS that terminates exactly one component of the state vector.

Three Segments of TS:

1. First, the cumulative phase state is forced to reach its desired value, i.e., $\gamma^{(D)}$, by choosing the first segment of the TS. Let $T_\gamma^{(H)}$ be defined as the number of symbols in this segment. Selection of these symbols depends upon current state and the desired state, and can be translated into a set of algebraic constraints. This problem is discussed in detail later.

2. Second, an appropriate number of zero symbols, $T_Z^{(H)}$ are inserted. The number of zero symbols are chosen such that the desired time index D modulo-H is attained after the end of the TS, i.e., $(N + T^{(H)})_H = D$. Note that $T_Z^{(H)} \in \mathbb{N}_H$.

3. Third, a segment of length $T_L^{(H)} \in \mathbb{N}_L$ symbols is appended. For most of the states, $T_L^{(H)} = L - 1$, and each symbol in the segment is taken equal to the corresponding symbol in the desired correlative state vector. For some trivial pairs of initial and desired states, only a subset of the correlative state vector has to modified to reach the desired state. Such cases may result in $T_L^{(H)} < L - 1$.

The total length of the TS is the sum of the lengths of these three individual segments, i.e.,

$$T^{(H)} = T_\gamma^{(H)} + T_Z^{(H)} + T_L^{(H)}. \tag{19}$$

The overall data block created by appending the TS to the original block is shown in Fig. 6. Note that the sequence of these steps is important because it is undesirable to modify the components of the state vector that have already reached their required values. Followings observations can be made in support of the selection of the three step process described above:

1. The correlative state is determined only by the last $L - 1$ symbols that enter the CPE. This is a consequence of the structure of Fig. 1 and the fact that only the selection of the TS can be made. Hence, the segment terminating the correlative symbols must appear at the end of the TS.

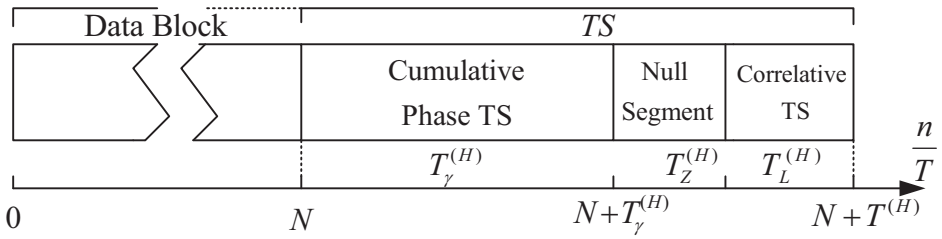

Figure 6: Structure of a terminated block with various segments of the terminating sequence (TS).

2. Even if a single symbol is required in the first segment to complete the termination of cumulative phase state, it must be followed by at least $L-1$ TS symbols to push all $T_\gamma^{(H)}$ symbols of this segment into the feedback section of CPE (see Fig. 5).

3. In the chosen scheme, segments 2 and 3 do not alter the cumulative phase state reached by segment 1.

4. Though the order of segments 1 and 2 can be interchanged, it will not change the overall length $T^{(H)}$ of the TS.

The choice of second and third segments is straightforward, and will not be discussed further. Next, the algebraic constraints on the symbols of the first segment of the TS that immediately follows the data block are evaluated. Just before the first symbol in the TS is incorporated in the feedback portion of the CPE, the state vector is as follows:

$$\chi_{N+L-1}^{(\gamma)} = \left\{\gamma_{N-1}, \mathbf{U}_N^{N+L-2}, (N+L-1)_H\right\}, \tag{20}$$

where

$$\gamma_{N-1} = \gamma_{N-L} + \sum_{i=1}^{L-1} U_{N-i} K_{(N-i)_H} \tag{21}$$

is the evolution of γ_{N-L} with the symbols already present in the shift register. When the symbol $U_{N+T_\gamma^{(H)}}$ is at the input, the state vector becomes

$$\chi_{N+T_\gamma^{(H)}}^{(\gamma)} = \left\{\gamma_{N-L+T_\gamma^{(H)}}, \mathbf{U}_{N+T_\gamma^{(H)}-L+1}^{N+T_\gamma^{(H)}-1}, (N+T_\gamma^{(H)})_H\right\}, \tag{22}$$

where

$$\gamma_{N-L+T_\gamma^{(H)}} = \gamma_{N-L} + \sum_{i=-T_\gamma^{(H)}+1}^{L-1} U_{N-i} K_{(N-i)_H}. \tag{23}$$

Separating the term with symbols from the TS, (23) can be rewritten as

$$\gamma_{N-L+T_\gamma^{(H)}} = \gamma_{N-1} + \sum_{i=0}^{T_\gamma^{(H)}-1} U_{N+i} K_{(N+i)_H}. \tag{24}$$

Making the cumulative phase state equal to $\gamma^{(D)}$ at the end of $T_\gamma^{(H)}$ TS symbols is equivalent to requiring that

$$\gamma_{N-1} + \sum_{i=0}^{T_\gamma^{(H)}-1} U_{N+i} K_{(N+i)_H} \equiv \gamma^{(D)} \bmod \mathrm{P}, \tag{25}$$

or

$$\sum_{i=0}^{T_\gamma^{(H)}-1} U_{N+i} K_{(N+i)_H} + \Gamma \equiv 0 \bmod \mathrm{P}, \tag{26}$$

where $\Gamma = (\gamma_{N-1} - \gamma^{(D)})_P$.

The remainder of this section deals with finding the solution to (26). Eq. (26) can be reformulated by combining the symbols corresponding to each element of $\mathbb{K}$. By defining the sum of symbols corresponding to $K_k, \forall k \in \mathbb{N}_H$ as $V_k^{(\Gamma)}$, (26) becomes

$$\sum_{k=0}^{H-1} K_k V_k^{(\Gamma)} = mP - \Gamma, \tag{27}$$

where $m \in \mathbb{N}$. Unlike the symbols U_n, which are constrained such that $0 \leq U_n \leq M-1$, the coefficients $V_k^{(\Gamma)}$ are only required to be non-negative integers. It is easy to see that a solution to (26) can be found once (27) is solved for $\mathbf{V^{(\Gamma)}} = [V_0^{(\Gamma)}, V_1^{(\Gamma)}, ..., V_{(H-1)}^{(\Gamma)}]$ for a given Γ (corresponding to a specified initial state), i.e., $\lceil \frac{V_k^{(\Gamma)}}{M-1} \rceil$ number of symbols are required corresponding to the modulation index numerator, K_k.

It can be observed that for a fixed m and Γ, (27) is a linear Diophantine equation (LDE) [45, 48] of H non-negative integer variables $V_k^{(\Gamma)}$ and positive coefficients $\{K_0, K_1, ..., K_{H-1}\}$. From the Bézout Identity [48] and Theorem 3.19 in [45], the following can be deduced about the solutions of this equation:

1. An integer solution to this LDE exists iff $d|(mP - \Gamma)$, where $d := \gcd(\mathrm{K}_0, \mathrm{K}_1, ..., K_{H-1})$.

2. If the above condition is satisfied for an LDE, and all its coefficients are positive integers, then it will have a non-negative solution when m is large enough.

Let $\mathbf{V} = \{\mathbf{V}^{(\mathbf{\Gamma})} | \Gamma \in \mathbb{N}_P\}$ be defined as the terminating solution set (TSS) for a given modulation scheme. A closed-form expression for the symbols in the TSS, or an expression for $T_\gamma^{(H)}$, in terms of modulation parameters in not possible by virtue of the fact that closed-form integer solutions for LDEs cannot be written in terms of their coefficients. In fact, the Euclidean Algorithm [45] is used to solve LDEs, which is an iterative procedure. However, it can shown that the TSS always exists.

Theorem 1 *Let* $\mathbb{K} = \{K_i\}_{i=0}^{H-1}$ *be non-negative integers such that*

$$d := \gcd(\mathbb{K}), \tag{28}$$

and

$$\gcd(\mathbb{K}, \mathrm{P}) = 1. \tag{29}$$

For each $\Gamma \in \{0, 1, ..., P-1\}$*, there exists an* $m \in \mathbb{N}$*, and hence a non-negative integer solution* $\mathbf{V}^{(\mathbf{\Gamma})} = [V_0^{(\Gamma)}, V_1^{(\Gamma)}, ..., V_{H-1}^{(\Gamma)}]$ *that satisfies the LDE in* (27)*.*

Proof: See Appendix A.

In this section, the process of trellis termination is discussed, and a set of constraints are derived for various segments of the TS. The TSS discussed in the proof of *Theorem 1* (see Appendix A) is sufficient for existence. However, it is not unique, and far from optimal. In fact, there can be multiple solutions even for a single value of m. In the next section, a procedure is proposed to choose a TSS in a way that minimizes the number of symbols required for trellis termination.

3.3 Minimal-length Criterion and Bounds on Number of Symbols

In a packetized-transmission mode, such as with single-carrier frequency domain equalization, length of the data block N and that of the terminating sequence $T^{(H)}$ is fixed. This will be done so as to allow trellis termination for all possible states of the system. Thus, it is of interest to minimize the worst case length of the TS. In this section, an optimization criterion is introduced for the choice of such a TS. Moreover, upper and lower bounds are derived on the required number of TS symbols in terms of modulation scheme parameters. To make the analysis less cumbersome, an additional constraint is introduced on the structure of the TS, i.e., $T_\gamma^{(H)}$ is taken to be a multiple of H. Under this assumption, the criterion of best solution (minimum number of symbols) is equivalent to the choice of $\mathbf{V}^{(\mathbf{\Gamma})}$ such that

$$\zeta = \max_{\Gamma \in \mathbf{N}_P} \{ \min_{m \geq 0} \| \mathbf{V}^{(\mathbf{\Gamma})} \|_\infty \}, \tag{30}$$

is minimized, where $\|.\|_\infty$ denotes the largest component of the vector argument. It is observed that a smaller value of m, for a given Γ, may not result in a minimal-length TS. Parameter ζ is an important quantity of interest since it not only defines the required optimization criterion, but is also related to the worst case number of termination symbols required for a multi-h CPM modulation scheme. The worst case length of the first segment of the TS is

$$T_\gamma^{(H)} = H \left\lceil \frac{\zeta}{M-1} \right\rceil, \tag{31}$$

and the total worst case length of TS is

$$T^{(H)} = H \left\lceil \frac{\zeta}{M-1} \right\rceil + L - 1 + H - 1. \tag{32}$$

From now on, $T_\gamma^{(H)}$ and $T^{(H)}$ will refer to their worst case values given in (31) and (32), respectively . Since ζ is a quantity based on the solutions $\mathbf{V}^{(\mathbf{\Gamma})}$ of LDEs, a closed-form expression for ζ, $T_\gamma^{(H)}$, and $T^{(H)}$ does not exist in general. To get an insight into the

dependence of these quantities upon the modulation parameters, various bounds on ζ are established in the next section.

3.3.1 Geometric Interpretation of TSS and Bounds on ζ

Define $C := mP - \Gamma$. Then for each value of C, (27) is actually an $(H-1)$-simplex in the H-dimensional Euclidean space $\mathbb{R}^H$, with vertices $\frac{C}{K_k}e_{k+1}$, $0 \leq k \leq (H-1)$, where e_k is the kth row of the $H \times H$ identity matrix. Each solution, $\mathbf{V}^{(\mathbf{\Gamma})}$, of (27) corresponds to a lattice point (a point with all integer coordinates) in the first orthant. A TSS is a collection of P such lattice points, each on a different simplex, corresponding to distinct values of Γ. By the criterion of minimum number of symbols, the best TSS is one for which all these lattice points are contained in a $\|.\|_\infty$-norm closed ball of smallest possible radius. These geometrical ideas are used in the proof of the following theorem, which proposes a lower and upper bound on ζ, and hence, on the length of the TS.

Theorem 2 *ζ, as defined in* (30)*, satisfies the following:*

$$\sqrt[H]{P} - 1 \leq \zeta \leq P - 1. \tag{33}$$

Proof: See Appendix B.

3.3.2 Diophantine Frobenius Problem and bounds on ζ

The bounds on ζ proposed above are independent of modulation indices, and are not always tight. In this section, a better upper bound on ζ, and hence on $T^{(H)}$, is computed for the special case when the elements of the set $\mathbb{K}$ are relatively prime. In this case, any P successive simplex curves, as explained above, correspond to P unique values of Γ. A classical problem in number theory, the Diophantine Frobenius Problem (FP)[15], is defined in the following. Consider an LDE

$$\sum_{k=0}^{H-1} K_k V_k^{(\Gamma)} = C, \tag{34}$$

where $K_k > 1, \forall k \in \mathbb{N}_H$, and $C \in \mathbb{N}$. There exists greatest positive number $g(K_0, K_1, ..., K_{H-1})$, henceforth, also referred to as $g(\mathbb{K})$, such that for $C > g(\mathbb{K})$, a non-negative solution $V_k^{(\Gamma)}$ to this equation can be found. This number $g(\mathbb{K})$ is called the Frobenius Number (FN) [15], and is the largest positive integer that cannot be represented as a non-negative linear integer combination of $K_k, k \in \mathbb{N}_H$. The FP is closely related to the money changing problem[49] and the Integer Knapsack problem[50], both of which are classical problems in combinatorial optimization.

With the definition of the FN in mind, *Theorem 3* is introduced, which specifies a lower and an upper bound on ζ. The upper bound is a function of the FN, which may not have a general closed-form expression for $H \geq 3$. When such an expression does not exist, $g(\mathbb{K})$ may be replaced by an upper bound $G(\mathbb{K})$. This issue is discussed further towards the end of the next section.

Theorem 3 *ζ, as defined in* (30)*, satisfies the following when* $\mathrm{gcd}(\{\mathrm{K_k}\}_{\mathrm{k=0}}^{\mathrm{H-1}}) = 1$ *and* $g(\mathbb{K})$ *exists:*

$$\frac{P-1}{\sum_{k=0}^{H-1} K_k} \leq \zeta \leq \frac{g(\mathbb{K})+P}{\min_k K_k} \leq \frac{G(\mathbb{K})+P}{\min_k K_k}, \tag{35}$$

where $G(\mathbb{K})$ is any upper bound of $g(\mathbb{K})$.

Note: Since $g(\mathbb{K})$ is not defined when $\min(\mathbb{K}) = 1$*, a convenient value in such a case may be taken as $g(\mathbb{K}) = -1$. The lower bound is effective even when the above conditions on the elements of $\mathbb{K}$ are not satisfied. However, as clarified by the proof, one can hope to achieve this lower bound only when the condition of relative primality on the elements of $\mathbb{K}$ holds.*

Proof: See Appendix C.

For convenience of reference in next section, the following notation is introduced for the bounds. The lower and upper bounds on ζ in (33) are denoted by ζ_{PL} and ζ_{PU}, respectively. Similarly, the lower and upper bounds in (35) will be referenced by ζ_{FL} and ζ_{FP}, respectively.

3.4 Examples

In this section, trellis termination is discussed for several modulation schemes to illustrate the proposed procedure, and the earlier derived results for the length of TS are applied.

3.4.1 Single-h CPM

Single-h CPM can be considered as a trivial case of multi-h CPM with $H = 1$, and is unique in the sense that one can obtain a closed-form expression for $T^{(1)}$. Both the upper and the lower bound on ζ in *Theorem 2* are equal for this case, i.e.,

$$\zeta_{PL} = \zeta_{PU} = P - 1. \tag{36}$$

This implies that $\zeta = P - 1$, and from (32), the length of the required TS is

$$T^{(1)} = T_{\gamma}^{(1)} + (L-1) = \left\lceil \frac{P-1}{M-1} \right\rceil + (L-1), \tag{37}$$

since $T_Z^{(1)} = 0$. Note that the FN does not exist for $H = 1$, since the set of non-negative numbers that cannot be expressed as a multiple of K_0 is not finite for $K_0 > 1$. Thus, the upper bound ζ_{FU} does not exist. The lower bound ζ_{FL} is applicable, though of little interest, since it is always smaller than ζ_{PL}. An expression for $T^{(1)}$ computed for single-h CPM in [44] is slightly different from (37), and is given as

$$T^{(1)} = \left\lfloor \frac{P-1}{M-1} \right\rfloor + L. \tag{38}$$

This expression is valid for partial-response single-h CPM schemes only. The two expressions agree for partial-response schemes unless $(M-1)|(P-1)$. Otherwise, (37) correctly computes the length of TS to be one symbol less than that predicted by (38).

Minimum-shift Keying (MSK) is perhaps the simplest, though, a significant example of full-response single-h CPM with a rectangular frequency shaping function. Its parameters are $K_0 = 1$, $P = 2$, $M = 2$ and $L = 1$, and only one symbol is required to

reach a desired state in the two-state tilted-phase trellis diagram. Quaternary 3-RC is a partial response single-h modulation scheme, which is spectrally very efficient due to its use of a raised cosine frequency shaping function. Its parameters are $K_0 = 1$, $P = 2$, $M = 4$, and $L = 3$, and the required number of symbols in the TS is $T^{(1)} = 3$.

Now, consider the relatively interesting case of another modulation scheme with parameters $K_0 = 5$, $P = 16$, $M = 4$, and $L = 3$. Equations (37) and (38) suggest that $T^{(1)} = 7$ and $T^{(1)} = 8$, respectively. However, it is clear that any desired state can be reached with 7 symbols, since at most 5 symbols are required for the desired cumulative phase, and 2 symbols are required to set the correlative state vector.

3.4.2 Dual-h CPM

The case $H = 2$ is more interesting in the sense that it is possible to find a closed-form expression for the FN when $\{K_0, K_1\}$ are relatively prime, and $K_0, K_1 > 1$, i.e.,

$$g(K_0, K_1) = K_0K_1 - K_0 - K_1. \tag{39}$$

Several examples of dual-h modulation schemes are considered in the following to illustrate the validity of earlier derived bounds on ζ. In Figures 7–9, the first $T_\gamma^{(2)}$ symbols of each element of the TSS are shown in the $V_0^{(\Gamma)}$-$V_1^{(\Gamma)}$ plane for three modulation schemes in which different bounds are achieved. Since ζ itself is independent of L and M, the only active parameters for these illustrations are K_0, K_1, and P. Note that the simplex in $\mathbb{R}^2$, represented by (27), is a line with slope $-\frac{K_0}{K_1}$, and axis intercepts, $\frac{mP-\Gamma}{K_0}$ and $\frac{mP-\Gamma}{K_1}$. Each of these figures contains several of these lines for distinct values of m and Γ. Lines with equal value of m are grouped together by shaded regions. Moreover, it can be observed that there are P TSS points each chosen from the set of non-negative lattice points, while meeting the criterion of minimum length for each Γ. Note that ζ is the maximum value taken by a coordinate of this set of TSS points. The $\|.\|_\infty$-norm balls, corresponding to derived bounds, are drawn to illustrate the tightness of the bounds.

The multi-h ARTM scheme is a quaternary 3-RC modulation with parameters $K_0 = 5$, $K_1 = 4$, $P = 16$, $M = 4$, and $L = 3$. In Fig. 7, 16 TSS points are shown that terminate all possible initial cumulative phase states. For example, the point $(1, 2)$ on the line for $\Gamma = 3$ and $m = 1$ indicates that additional symbols $U_N = 1$ and $U_{N+1} = 2$ are required to be appended to terminate the cumulative phase state $\Gamma = 3$. The largest coordinate value $\zeta = 3$ is achieved by 7 different TSS points. From $\zeta = 3$, (31), and (32), it can be implied that $T_\gamma^{(2)} = 2$ and $T^{(2)} = 5$. As shown in Fig. 7, the lattice points are arranged in a square, and $\zeta_{PL} = 3$ is achieved. However, $\zeta_{FL} = \frac{16}{9} \approx 1.7$ is not as tight, since quite a few of the first P lines do not contain a lattice point. Similarly, the upper bound $\zeta_{PU} = 15$ is too pessimistic for this modulation scheme, and is not shown in Fig. 7. Since K_0, K_1 are relatively prime, the FN exists, and is equal to $g(5, 4) = 11$, which implies that $\zeta_{FU} = \frac{27}{4} \approx 5.4$.

An extreme case for dual-h modulation schemes is defined such that $(K_0, K_1) = (P, P-1)$ for $P > 3$. In Fig. 8, the lattice points corresponding to the TSS are shown for this scheme when $P = 5$. Note that each value of m yields only one optimal TSS point. It can be shown that every solution has the form $(0, P - \Gamma)$, and the upper bound in *Theorem 2*, i.e., $\zeta_{PU} = P - 1$ is met for this combination of modulation indices. *Theorem 3* is also applicable as $(K_0, K_1) = (P, P - 1)$ are relatively prime, and the FN for these parameters is $g(P, P - 1) = P^2 - 3P + 1$, which implies that $\zeta_{FU} = \zeta_{PU} = \zeta = P - 1$.

Another case of interest is that of $(K_0, K_1) = (2, 1)$. It is special in the sense that every line (1-simplex) has an integer solution, and thus $m \leq 1$. ζ is either very close to or achieves the lower bound $\zeta_{FL} = \frac{P-1}{3}$. The bound is achieved when ζ_{FL} is an integer, i.e., P is of the form $3i + 1$, for $i \in \mathbb{Z}^+$. The TSS for this modulation scheme is illustrated in Fig. 9, when $P = 16$, and for this particular case, $\zeta = \zeta_{FL} = 5$. The upper bound ζ_{FU} is not applicable, since $K_0 = 1$, and the FN does not exist. However, $\zeta_{PU} = 15$ can be computed but is loose by a factor of 3. Closed balls corresponding

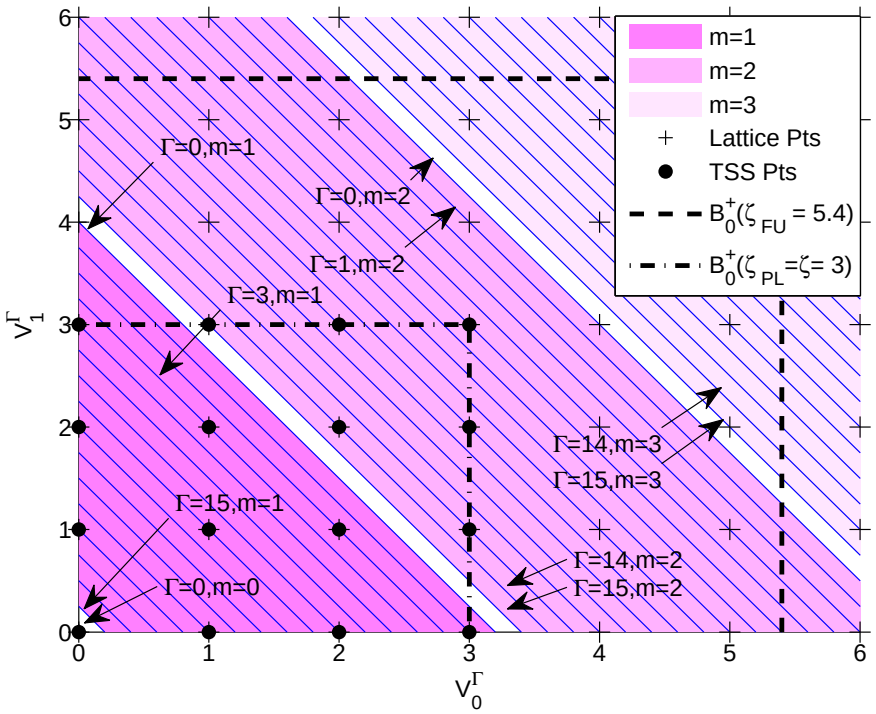

Figure 7: TSS and bounds on ζ for dual-h aeronautical telemetry (ARTM) Tier-2 waveform with parameters $H = 2, (K_0, K_1) = (5, 4)$, and $P = 16$.

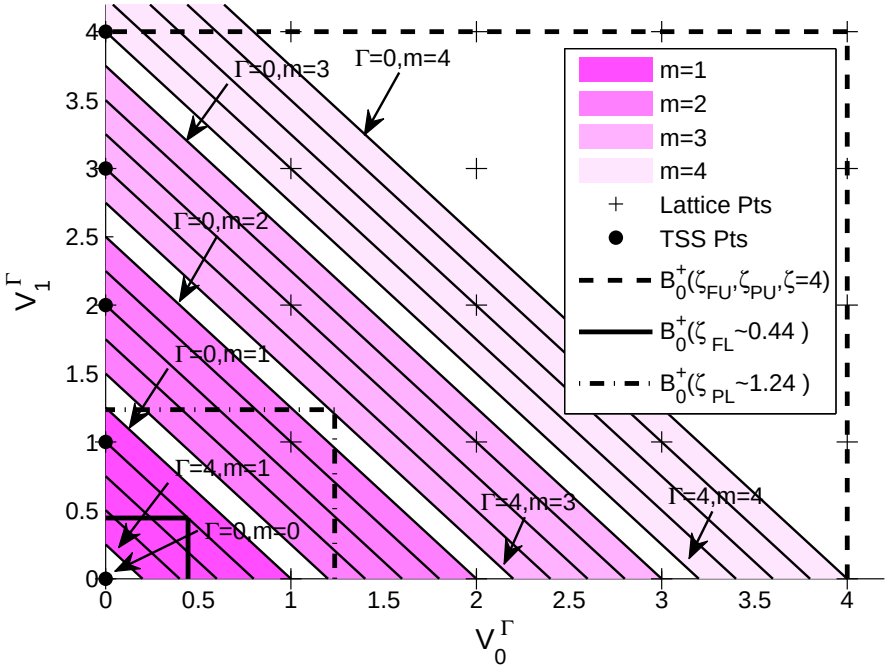

Figure 8: TSS and bounds on ζ for dual-h CPM with parameters $H = 2, (K_0, K_1) = (P, P - 1)$, and $P = 5$.

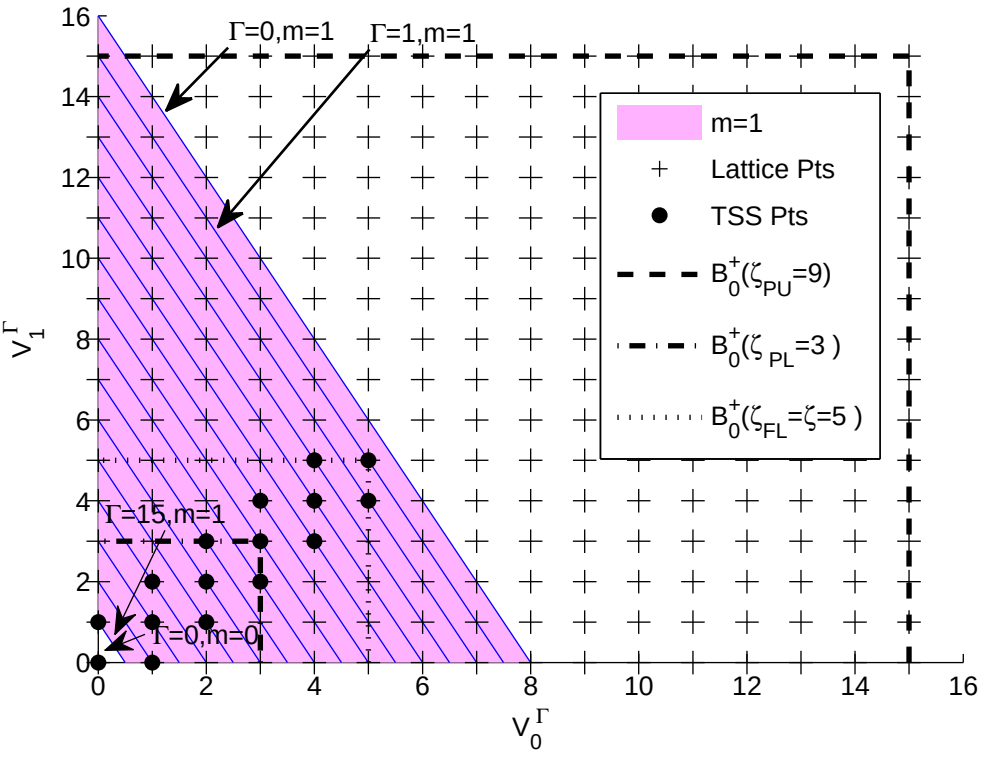

Figure 9: TSS and bounds on ζ for dual-h CPM with parameter values $H = 2, (K_0, K_1) = (2, 1),$ and $P = 16$.

to ζ, ζ_{PL}, ζ_{FL}, and ζ_{PU} are also shown in Fig. 9.

In Fig. 10, the average behaviour of ζ is considered, and earlier derived bounds on all admissible values of K_0 and K_1, for fixed P, are drawn. The admissible values of (K_0, K_1) are defined such that both $K_1 < K_0 \leq P$ and $\gcd(\mathrm{K_0}, \mathrm{K_1}) = 1$ hold, and thus all the bounds are defined. Note that ζ_{PL} and ζ_{PU} are independent of $\mathbb{K}$, and hence, do not require this averaging. As already observed in the examples above, all the bounds are relevant, since for each bound, there exist instance(s) of set $\mathbb{K}$ such that they can be achieved. This is corroborated in Fig. 10, since the deviation of ζ around its arithmetic mean is confined tightly by ζ_{PL} and ζ_{PU}.

The simulations that lead to Fig. 10 also facilitate in making a couple of general conjectures, as they include many dual-h schemes of practical interest. The worst case of $\zeta = \zeta_{PU} = P - 1$ occurs only for the case $(K_0, K_1) = (P, P - 1)$. Other

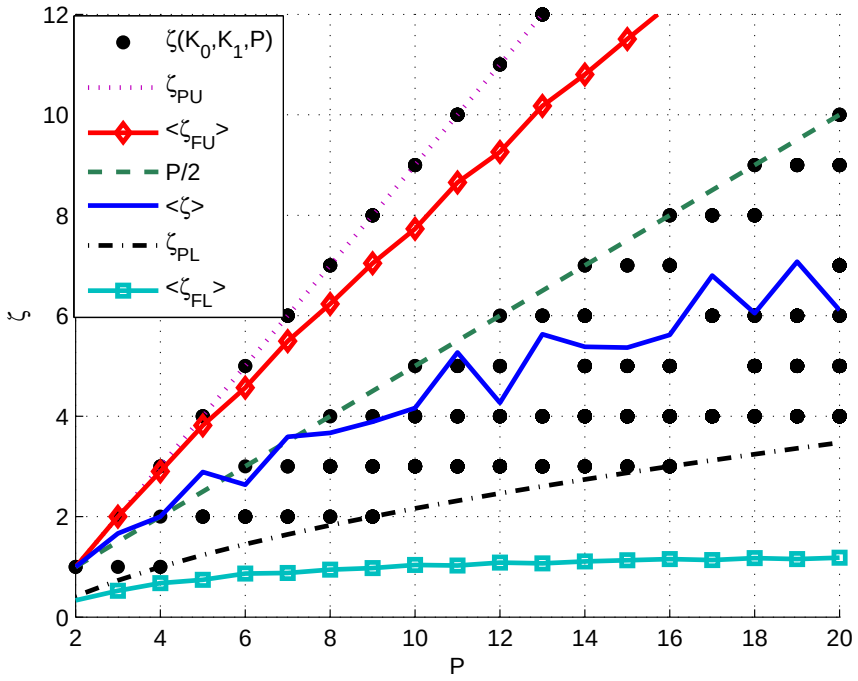

Figure 10: Plot of ζ, average value of ζ, and its bounds versus P, for $H = 2$. Averaging is done only over the admissible values of K_0 and K_1.

admissible pairs have $\zeta \leq \frac{P}{2}$. This is the reason for a big gap of ζ points between the lines corresponding to $P-1$ and $\frac{P}{2}$. In addition, it can be guessed that $\zeta = \lfloor \frac{P}{2} \rfloor$ is achieved if and only if $K_0 + K_1 = P$. The forward implication is easy to prove analytically. Although this figure allows for above-mentioned interesting observations, it must be mentioned that this is only an average behavior of the bounds, and may be misleading if extended to individual cases. For example, as can be see from Fig. 10, $<\zeta_{FL}> < \zeta_{PL}$ for all values of P, but for the case $(K_0, K_1, P) = (2, 1, 16)$, $\zeta_{FL} > \zeta_{PL}$.

3.4.3 H > 2

The minimal length TSS can be computed for these modulation schemes in a way similar to the earlier discussed examples for $H \leq 2$, and the bounds introduced in *Theorem 2* and *Theorem 3* will also apply. However, ζ_{FU} cannot be computed in

general, since a closed-form expression for the FN cannot be found for $H \geq 3$ [15]. The FN is however derived for some special cases, e.g., for a set $\mathbb{K}$ containing H consecutive positive integers [51],

$$g(K_0, K_0+1, ..., K_0+H-1) = \left(\left\lfloor \frac{K_0 - 2}{H-1} \right\rfloor + 1 \right) K_0 - 1. \tag{40}$$

Moreover, if there is no closed-form expression for $g(\mathbb{K})$, any upper bound may also be used for computing ζ_{FP} as mentioned in *Theorem 3*. Several bounds on the FN have been presented in literature, a concise reference of which is [15]. Tighter bounds on $g(\mathbb{K})$ will give a better estimate of ζ. However, a bound may be tight for a given set $\mathbb{K}$ and not as effective for others. Three bounds are included from [15] as examples.

1. $g(\mathbb{K}) \leq (min(\mathbb{K}) - 1)\,(max(\mathbb{K}) - 1) - 1.$

2. If $gcd(\mathbb{K}) = 1$, then

$$g(K_0, K_1, K_2) \leq \frac{K_0 K_1 K_2}{2} \sqrt{\frac{1}{K_0 K_1} + \frac{1}{K_1 K_2} + \frac{1}{K_2 K_0}} - \frac{(K_0 - K_1 - K_2)}{2}$$

3. An upper bound $G(\kappa)$ or an exact value of the FN $g(\kappa)$, evaluated for any subset κ of $\mathbb{K}$ can also serve as an upper bound for $g(\mathbb{K})$ itself. This is because $g(\mathbb{K}) \leq g(\kappa) \leq G(\kappa)$. For example, for a triplet $\mathbb{K} = \{K_0, K_1, K_2\}$, (39) is an upper bound.

In Fig. 11, TSS is shown for a triple-h modulation scheme, with parameters, $P = 8$, $\mathbb{K} = \{K_0, K_1, K_2\} = \{5, 4, 2\}$. For $H = 3$, (27) represents a plane for each value of m and Γ. These planes are parallel to each other, and may have no, unique, or multiple lattice points. For this example, TSS points occupy all the edges of the cube $B_0^+(1)$ and, thus, the bound ζ_{PL} is achieved.

The modulation schemes become increasingly impractical as one moves to higher values of H because of the rise in decoding complexity. The average value of ζ as a

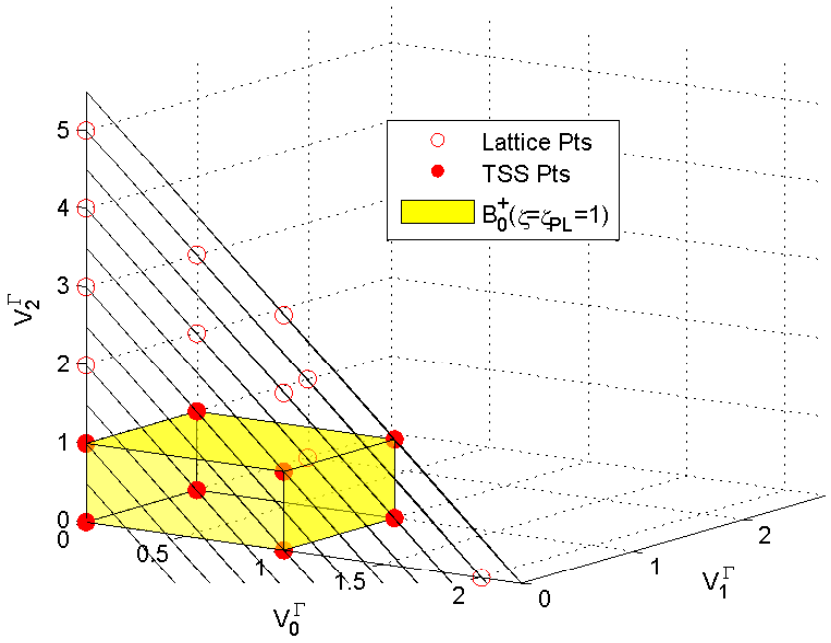

Figure 11: TSS and ζ for CPM with parameters $H = 3$, $(K_0, K_1, K_2) = (5, 4, 2)$, $P = 8$.

function of H decreases for these schemes as there is more choice among modulation indices. This is also evident from the expressions of bounds ζ_{PL}, ζ_{FL}, and ζ_{FU}. Thus, one may be tempted to use higher H modulation schemes to not only get better minimum distance properties but also shorter terminating sequences. However, as explained below, the average reduction in length of the TS is not significant enough to warrant an acceptable trade-off with increased receiver complexity.

In Fig. 12, $H<\zeta>$ is plotted as a function of P for different values of H, where the averaging is done over the admissible $H-$tuples $\mathbb{K}$. The admissible $\mathbb{K}$ are such that $\sup(\mathbb{K}) \leq P$. The quantity $H<\zeta>$ represents a measure of $T^{(H)}$ with L and M fixed. The average becomes smoother for higher values of H, as the number of admissible schemes become exponentially larger. Even though $<\zeta>$ drops appreciably with increasing H, the drop in $H<\zeta>$ is not significant. Moreover, the drop indicates a diminishing trend, as moving from $H = 3$ to $H = 4$ does not offer much advantage.

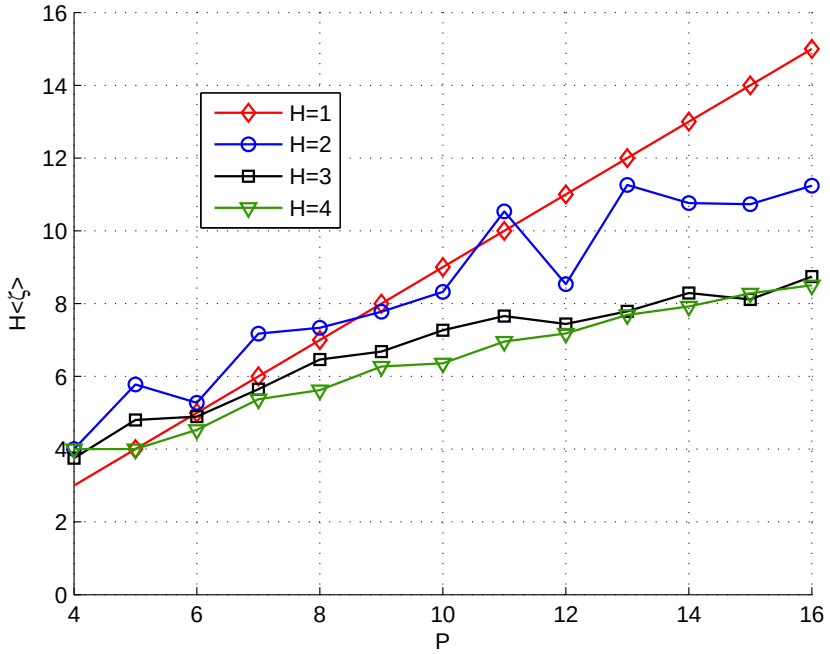

Figure 12: Plot of the average value of ζ versus P, for $H = 2, 3$, and 4. Averaging is done over all admissible H-tuples.

As observed for the dual-h case, $\zeta \leq \lfloor \frac{P}{2} \rfloor$, except when at least $H-1$ elements of $\mathbb{K}$ are positive multiples of P. In this case, the $H-1$ modulation indices are integers, and $\zeta = \zeta_{PU} = P-1$. Thus, schemes with integer modulation indices and large values of P may have significant overhead because of trellis termination.

3.5 Summary

In this Chapter, we proved the periodicity of multi-h CPM tilted-phase trellis, and a decomposition of the modulator as the cascade of a periodic recursive CPE and a phase modulator is presented. The problem of trellis termination was discussed in detail, and posed in terms of a classical number theory problem. The heuristic criterion of minimum length TS was translated to an analytical metric, which led to a convenient geometric interpretation. Various bounds on the length of the terminating sequence were also proposed and proven analytically. Some interesting examples for single-h and dual-h schemes were discussed, where an analytical expression for

the length of the terminating sequence can be computed. It is observed that multi-h schemes with integer modulation indices, and large P generally require long terminating sequences.

CHAPTER IV

INTRAFIX FOR FREQUENCY-DOMAIN EQUALIZATION OF MULTI-H CPM

In this chapter, our focus is on the problem of constructing a symbol block to generate a cyclic multi-h continuous phase modulated (CPM) signal so as to permit frequency-domain equalization (FDE) at the receiver. Like single-h CPM, the memory inherent in a multi-h CPM waveform requires the use of an additional segment, called an intrafix, in each transmitted block. The intrafix forces the transmitter state machine to regress to the state it had at the start of the block. The constraints on the symbols of the intrafix, which ensure above condition, are shown to be a set of linear Diophantine equations (LDEs). Three different methods are proposed for finding the symbols of the intrafix such that the length of the intrafix is minimized. The last two methods connect the problem of intrafix insertion to the problem of trellis termination of the tilted phase. This connection enables one to state and justify that existing bounds established on the length of the terminating sequence are effective for the length of the intrafix. It is observed that multi-h CPM schemes typically require a shorter intrafix as compared to single-h CPM schemes having similar modulation parameters. The proposed procedure is applied to a dual-h CPM scheme.

The rest of this chapter is organized as follows. The excess-phase and tilted-phase state vectors are defined in Section 4.1. The structure of the cyclic multi-h CPM block is discussed in Section 4.2, and three different methods to obtain the intrafix symbols are proposed in Section 4.3. A numerical example is presented in Section 4.4 to illustrate the theoretical results. Important results of this chapter are summarized in Section 4.5.

The multi-h CPM waveform and modulation parameters are described in Section 2.7, and the notation used in this chapter is defined in Section 2.6.

4.1 State Vector for Multi-h CPM

In this section, two different but equivalent state definitions for multi-h CPM are discussed. In the subsequent sections, these definitions will facilitate the formulation of different constraints on the structure of the transmitted block.

4.1.1 Excess-phase Representation

For $t \in [nT, (n+1)T]$, using the definition of $q(t)$ and $h_{(i)}$, (2) can be written as

$$\phi(t, \mathbf{x}) = \frac{\pi}{P} \sum_{i=0}^{n-L} K_{(i)_H} x_i + \frac{2\pi}{P} \sum_{i=n-L+1}^{n} K_{(i)_H} x_i q(t - iT). \tag{41}$$

A change of variable in the second summation results in

$$\phi(t, \mathbf{x}) = \frac{\pi}{P} \sum_{i=-\infty}^{n-L} K_{(i)_H} x_i + \frac{2\pi}{P} \sum_{i=0}^{L-1} K_{(n-i)_H} x_{n-i} q(t - (n-i)T). \tag{42}$$

Since only the principal (or reduced mod 2π) value of the phase $\phi(t, \mathbf{x})$ determines the signal in (1), it is easy to see that the first term in (42), called the cumulative excess phase, can assume $2P$ different values. In the special case, where the numerator of each modulation index is even, i.e, $2|K_i, \forall i \in \mathbb{N}_H$, we have only P effective values of this term. If

$$\mathcal{T}_n := \left(\sum_{i=-\infty}^{n} K_{(i)_H} x_i \right)_{2P}, \tag{43}$$

then the excess-phase state

$$\chi_n(x) := (\mathcal{T}_{n-L}, \mathbf{x}_{n-L+1}^{n-1}, (n)_H) \tag{44}$$

and the current symbol x_n completely determine the signal in (1) for $t \in [\, nT, (n+1)T \,]$. The $L-1$ symbols following $\mathcal{T}_{n-L}$ in the state vector are included because of their contribution to the second term of (42), and are called correlative excess symbols. Note that $(\mathcal{T}_{n-L}) \in \mathbb{N}_{2P}$, and the total number of excess phase states is $2PHM^{L-1}$. However, only PM^{L-1} of these states can be reached in a given symbol interval.

4.1.2 Tilted-phase Representation

Let

$$u_i := \frac{x_i + (M-1)}{2}, \tag{45}$$

be the non-negative symbols, such that $u_n \in \mathbb{N}_M$. Using this transformation in (42),

$$\begin{aligned}\phi(t, \mathbf{u}) = \frac{2\pi}{P} \sum_{i=-\infty}^{n-L} K_{(i)_H} u_i + \frac{4\pi}{P} \sum_{i=0}^{L-1} K_{(n-i)_H} u_{n-i} q(t-(n-i)T) \\ - \frac{2\pi(M-1)}{P} \sum_{i=0}^{L-1} K_{(n-i)_H} q(t-(n-i)T) - \frac{\pi(M-1)}{P} \sum_{i=-\infty}^{n-L} K_{(i)_H},\end{aligned} \tag{46}$$

where $\mathbf{u}$ denotes the sequence of symbols $\{u_n\}$. The first term in (46) can assume P unique values when reduced modulo 2π, and is called the cumulative tilted-phase state, while the second term contains the input term ($i = 0$) and the correlative tilted-phase state terms ($i \neq 0$). As defined in [52], the tilted phase $\psi(t, \mathbf{u})$ for $t \in [nT, (n+1)T]$ is related to the excess phase as

$$\psi(t, \mathbf{u}) = \phi(t, \mathbf{u}) + \frac{\pi(M-1)}{P} \sum_{i=-\infty}^{n-1} K_{(i)_H} + \frac{\pi(M-1) K_{(n)_H} (t - nT)}{PT}. \tag{47}$$

It was shown in [52] that the tilted phase defines a periodic phase trellis with period H, and its state vector can be defined as

$$\rho_n(u) := \left(\mathcal{I}_{n-L}, \mathbf{u}_{n-L+1}^{n-1}, (n)_H\right), \tag{48}$$

where $\mathcal{I}_n := \left(\sum_{i=-\infty}^{n} K_{(i)_H} u_i\right)_P$. In Chapter 3 and [52], the termination of $\rho_n(u)$ is discussed in detail, and bounds are computed on the minimum number of symbols required to reach an arbitrary state from a given state. However, for the excess phase in (46), $\rho_n(u)$ is not a complete state vector. The reason for this being the additional memory introduced by the second term in (47), which is also responsible for the period of excess phase trellis being $2H$ in general, instead of being H. This term has $\eta = 2P/(M-1, P)$ unique contributions to the principal value of the excess phase vector. In the special case of even numerators of all modulation indices,

$\eta = P/(M-1,P)$. Using the definition of $\mathcal{I}_n$, an alternate state vector representation for the excess phase state vector of (44) is obtained, i.e.,

$$\chi_n(u) := ((2\mathcal{I}_{n-L} - \mathcal{K}_{n-L})_{2P}, \mathbf{u}_{n-L+1}^{n-1}, (n)_H), \tag{49}$$

where $\mathcal{K}_n := \left((M-1)\sum_{i=-\infty}^{n} K_{(i)_H}\right)_{2P}$.

In the next section, a block structure is presented that ensures a cyclic excess phase, and hence, a cyclic multi-h CPM signal. The proposed structure will impose certain constraints on the state vector at a specific time instant in the block, and the state vector definitions presented in the current section will be used to interpret these constraints in terms of simple algebraic equations. The components $\mathcal{K}_{n-L}$ and $(n)_H$ of $\chi_n(u)$ are interesting in the sense that they are determined solely by the parameters of the modulation scheme and the current time index, and cannot be controlled by the input symbols. Thus reaching a certain state $\chi_n(u)$, from an arbitrary state, not only involves a cautious choice of the symbols from the alphabet $\mathbb{M}$ but also requires the satisfaction of a condition on the time index of the last symbol.

4.2 Block Structure for Cyclic Multi-h CPM Waveform

The construction of the transmitted block that enables FDE of single-h CPM has been considered in [11, 12, 24, 39]. The procedure proposed by [12] specifies that the minimum number of intrafix symbols is $\lceil \frac{P-1}{M-1} \rceil$. In this section, the notation of [12, 24] is used wherever possible, and the concepts presented therein for single-h CPM are extended to multi-h CPM. A block based communication system similar to those defined in these references is assumed in the following.

Consider a block of $N-F$ source symbols sampled from the alphabet $\mathbb{M}$, and split into two segments, $X_f^{(l)}$ and $X_s^{(l)}$, of lengths $N-F-N_{CP}$ and N_{CP}, respectively, where l denotes the index of the block. To make the signal cyclic with period N, as is done for memoryless modulation schemes, take $X_p^{(l)} = X_s^{(l)}$, and use it as the prefix to the original source block $[X_f^{(l)}, X_s^{(l)}]$, resulting in $[X_p^{(l)}, X_f^{(l)}, X_s^{(l)}]$. The length of

the cyclic prefix, N_{CP}, is assumed longer than the length of the discrete-time channel so as to avoid any interblock interference. The received signal corresponding to these symbols is discarded at the receiver. However, for a modulation signal with memory, such as CPM, the insertion of this cyclic prefix alone is insufficient. As identified in [11], and later on refined in [12, 24], an additional segment of length F symbols, called an intrafix or a tail sequence, is required. It is inserted between $X_f^{(l)}$ and $X_s^{(l)}$, and is denoted by $X_c^{(l)}$. The overall block has length $N_T = N + N_{CP}$ and is structured as $[X_p^{(l)}, X_f^{(l)}, X_c^{(l)}, X_s^{(l)}]$. All these segments and their relative positions in the block are shown in Fig. 13.

The choice of the symbols in the intrafix $X_c^{(l)}$, and their quantity F, is made so that the following cyclic condition is satisfied for all transmitted blocks:

$$\phi(\tau, x) \equiv \phi(\tau + NT, x) \mod (2\pi), \tag{50}$$

for $\tau \in [0, N_{CP}T]$, where $\tau := t - (l-1)N_T T$. The authors in [12] made an intriguing observation that the above condition can be achieved by ensuring that the state of the transmitter be identical at epochs $\tau = N_{CP}T$ and $\tau = N_T T$, i.e.,

$$\chi_{N_{CP}}^{(l)} = \chi_{N_T}^{(l)}, \tag{51}$$

where the superscript l is the index of the block, and subscript denotes the time index when this state is reached. The notation $x_n^{(l)} := x_{n+(l-1)N_T}$ is also used for the symbols of block l, and $K_{(n)_H}^{(l)} := K_{(n+(l-1)N_T)_H}$ for the corresponding modulation index. The approach introduced in [12] makes the selection of symbols in the intrafix independent of the previous blocks. For multi-h CPM signal, it follows from (44) that (51) translates into the following three constraints:

$$x_n^{(l)} = x_{n+N}^{(l)}, \forall n \in \{N_{CP} - (L-1), N_{CP} - 1\}, \tag{52}$$

$$(N_{CP})_H = (N_T)_H \ , \tag{53}$$

$$\mathcal{T}_{N_{CP}-L-1} = \mathcal{T}_{N_T-L-1} \ . \tag{54}$$

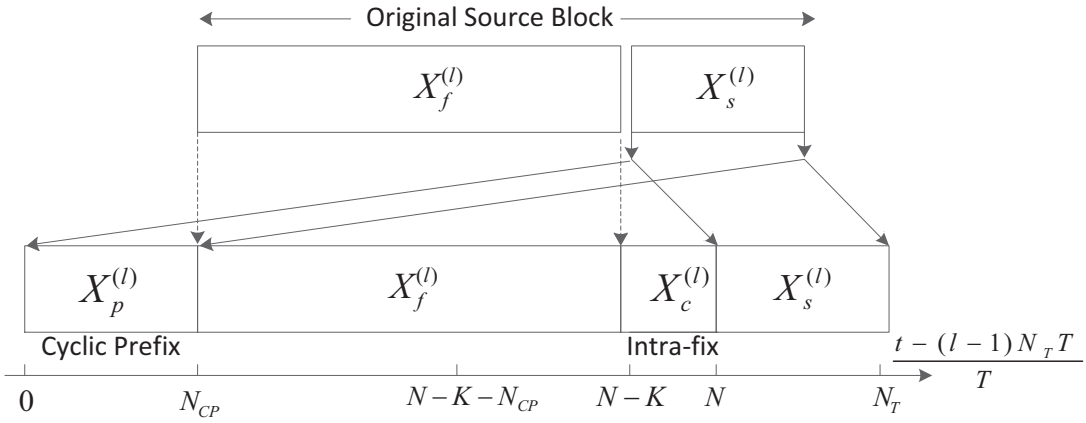

Figure 13: Structure of a cyclic transmitted block for multi-h CPM.

Prefixing of the transmitted block as defined above, i.e., $X_p^{(l)} = X_s^{(l)}$, ensures that (52) is satisfied. Typically, $N_{CP} \geq L$ (since $L < 4$ usually), which implies that (52) does not depend on the previous blocks. Since $N := N_T - N_{CP}$, and $((a)_H - (b)_H)_H = (a-b)_H$ for arbitrary integers a and b, it follows from (53) that

$$(N)_H = 0. \tag{55}$$

In addition to this constraint on N, it is also desirable to define N to be a positive integer power of 2, which enables efficient implementation of the $N-$point FFT algorithm used in the FDE portion of the receiver. Such a choice of N automatically satisfies (55) for dual-h CPM schemes. Now that both conditions (52) and (53) are satisfied, the last constraint (54) is satisfied by an appropriate choice of the symbols in the intrafix segment. It is easy to see that a symbol $x_n^{(l)}$ in the cyclic prefix $X_p^{(l)}$ has the same modulation index as the corresponding symbol in the segment $X_s^{(l)}$, i.e., $x_{n+N}^{(l)}$. This implies that their individual contributions to the cumulative excess phase are also equal. Using this fact, (54) can be extended as

$$\mathcal{T}_{N_{CP}-1} = \mathcal{T}_{N_T-1}, \tag{56}$$

or equivalently,

$$\left[\sum_{i=-\infty}^{(l-1)N_T-1} K_i x_i + \sum_{i=0}^{N_T-1} K_i x_i^{(l)}\right] - \left[\sum_{i=-\infty}^{(l-1)N_T-1} K_i x_i + \sum_{i=0}^{N_{CP}-1} K_i x_i^{(l)}\right] \equiv 0 \mod (2P). \tag{57}$$

After simplification, we get

$$\sum_{i=0}^{N_T-1} K_{(i)_H}^{(l)} x_i^{(l)} - \sum_{i=0}^{N_{CP}-1} K_{(i)_H}^{(l)} x_i^{(l)} \equiv 0 \mod (2P), \tag{58}$$

which can be rewritten as

$$\sum_{i=0}^{N-1} K_{(i)_H}^{(l)} x_i^{(l)} \equiv 0 \mod (2P). \tag{59}$$

If

$$\gamma_F := \left(\sum_{i=0}^{N-F-1} K_{(i)_H}^{(l)} x_i^{(l)}\right)_{2P}, \tag{60}$$

the sum in (59) can be split as

$$\sum_{i=N-F}^{N-1} K_{(i)_H}^{(l)} x_i^{(l)} + \gamma_F \equiv 0 \mod (2P). \tag{61}$$

Since all the constraints (52), (55), and (61) are independent of the previous blocks, the superscript (l) is dropped from here onwards (or equivalently assume $l = 0$). From the definition of γ_F, it appears that it may assume up to $2P$ unique values. However, irrespective of the set $\mathbb{K}$, γ_F will acquire only P distinct values for a fixed F. Let this set be denoted by Γ_F. The set Γ_F is described in the following for three cases:

1. If $2|K_j, \forall j \in \mathbb{N}_H$, the set $\Gamma_F = \{0, 2, ..., 2P-2\}$, whether F is even or odd. Note that P cannot take an even value in this case. In this situation, (61) can be re-written as

$$\sum_{i=N-F}^{N-1} \frac{K_{(i)_H}}{2} x_i + \bar{\gamma}_F \equiv 0 \mod (P), \tag{62}$$

where $\bar{\gamma}_F = \gamma_F/2$, and $\bar{\gamma}_F \in \mathbb{N}_P$. Thus in (61), both F and N can be either even or odd.

2. If $2 \nmid K_j, \forall j \in \mathbb{N}_H$, and whether P is even or odd,

$$\Gamma_F = \begin{cases} \{0, 2, \ldots, 2P-2\} \ , \ \text{if } (N-F)_2 = 0 \\ \{1, 3, \ldots, 2P-1\} \ , \ \text{if } (N-F)_2 = 1. \end{cases} \tag{63}$$

Now from (61) and its first term (similar to the definition of γ_F), $(N-F)_2 = (F)_2$, which implies that $(N)_2 = 0$ is required.

3. Now consider the general situation where some K_j's are even, and others are odd, where j belongs to some proper subset of $(N)_H$. Consider the running sum in (60). The accumulation starts from 0, and each subsequent step, i, adds $K_{(i)_H} x_i$, which is an odd (even) number if K_i is odd (even). If K_i is odd, the previous sum gets toggled from even to odd, and vice versa. However, for even $K_{(i)_H}$, this toggling does not occur. Let O_{N-F} be the number of symbol intervals for which $K_{(i)_H}$ was odd, for $0 \leq i \leq N-F-1$. Then,

$$\Gamma_F = \begin{cases} \{0, 2, \ldots, 2P-2\} \ , \ \text{if } (O_{N-F})_2 = 0 \\ \{1, 3, \ldots, 2P-1\} \ , \ \text{if } (O_{N-F})_2 = 1. \end{cases} \tag{64}$$

Let O_N be the number of symbol intervals for which $K_{(i)_H}$ is odd, for $0 \leq i \leq N-1$. Then, for (61) to hold, N must also satisfy

$$(O_N)_2 = 0. \tag{65}$$

Note that (61) is a linear Diophantine equation (LDE) [45] for each γ_F, with positive integer coefficients from the set $\mathbb{K}$, and odd integer variables $x_i \in \mathbb{M}$. The variables in (61) are the symbols of the intrafix segment $X_c^{(l)}$. Consider the following optimization problem:

$$\begin{aligned} &\text{minimize} \quad F \\ &\text{subject to } (61) \text{ holds } \forall \gamma_F \in \Gamma_F, x_i \in \mathbb{M}. \end{aligned} \tag{66}$$

This section is concluded with the following definition:

$$J_F^{(j)} := \{ i \in \mathbb{N} | N - F \leq i \leq N-1 \wedge (i)_H = j \}, \tag{67}$$

and $\mathbf{J}_F := (|J_F^{(0)}|, |J_F^{(1)}|, ..., |J_F^{(H-1)}|)$, where sum of elements of $\mathbf{J}_F$ is equal to F.

4.3 Optimal Solution for Linear Diophantine Constraints

In this section, three different procedures are proposed to solve the optimization problem in (66); one working directly on the excess phase symbols x_i, and the other two based on the tilted-phase or unipolar symbols u_i.

4.3.1 Excess-phase based Solution

If the intrafix symbols corresponding to each modulation index are combined in a separate variable, (61) becomes

$$\sum_{j=0}^{H-1} K_j V_j^{(\gamma)} + \gamma_F \equiv 0 \mod (2P), \tag{68}$$

where

$$V_j^{(\gamma)} := \sum_{i \in J_F^{(j)}} x_i \tag{69}$$

are components of $\mathbf{V}^{(\gamma)} := \left(V_0^{(\gamma)}, V_1^{(\gamma)}, \ldots, V_{H-1}^{(\gamma)}\right)$. Note that an integer $V \in \mathbb{Z}$ can always be written as a sum of odd numbers from $\mathbb{M}$. Given an arbitrary integer V, the minimum number of symbols $x_i \in \mathbb{M}$ required to express V as in (69) is a function of M and V, and can be shown to be equal to

$$\mu(M,V) = \left\lfloor \frac{|V|}{M-1} \right\rfloor + \Big(2 - (\eta(M,V))_2\Big) I(\eta(M,V) \neq 0) \ , \tag{70}$$

where $\eta(M,V) := (|V|)_{M-1}$ and $I(\ \cdot\ )$ is an indicator function. The indicator function takes a statement as an argument, and is defined as identity if the statement is true, and zero otherwise. Note that μ is a function of the absolute value of V. Consider the following claim about μ:

Lemma 1: $\mu(M,V)$, as defined by (70), satisfies the following conditions:

1. $\mu(2,V)$ is a strictly increasing function of $|V|$, specifically, $\mu(2,V) = |V|$.

2. For a fixed M, $\mu(M,V)$ is a non-decreasing function of $|V|$, i.e., for $a,b \in \mathbb{Z}$, $|a| > |b|$ implies $\mu(M,a) \geq \mu(M,b)$, unless $(a-b) \leq M-1$ and $(|a|-|b|)$ is an odd integer.

Proof: See Appendix D.

The minimal expansion of an integer V in terms of the elements of $\mathbb{M}$ is not unique, and one of such expansions is,

$$y_\mu(V) = \begin{cases} \text{sign}(V)(M-1)\mathbf{1}_\mu & \text{if } \eta = 0, \\ \text{sign}(V)((M-1)\mathbf{1}_{\mu-1}, \eta) & \text{if } (\eta)_2 = 1, \\ \text{sign}(V)((M-1)\mathbf{1}_{\mu-2}, \eta-1, 1) & \text{otherwise.} \end{cases} \tag{71}$$

Note that this expansion is not unique, and the order of the symbols in the vector $y_\mu(V)$ is not important. The set of all $V \in \mathbb{Z}$ that can be written as a sum of $Q \in \mathbb{N}$, M-ary source symbols (with Q minimal such number) defines an equivalence class on the set of integers, and is denoted by $[Q]$, i.e.,

$$[Q] := \{V \in \mathbb{Z} | \mu(M,V) = Q\}, \tag{72}$$

It can be observed that

$$[Q] = \begin{cases} \{0\} & \text{if } Q = 0 \\ \mathbb{M} & \text{if } Q = 1 \\ \pm\{(Q-2)(M-1)+2, (Q-2)(M-1)+4, \ldots, Q(M-1)\} & \text{for } Q > 1, \end{cases} \tag{73}$$

and

$$|[Q]| = \begin{cases} 1 & \text{if } Q = 0 \\ M & \text{if } Q = 1 \\ 2(M-1) & \text{if } Q > 1. \end{cases} \tag{74}$$

Note that an integer V can only be expressed as a sum of $\mu(M,V)+2i$ number of symbols from $\mathbb{M}$, where $i \in \mathbb{N}$. One such decomposition for V is

$$z_{\mu+2i}(V) = (y_\mu(V), (+c,-c) \otimes \mathbf{1}_i), \tag{75}$$

for any $c \in \mathbb{M}$, where $\otimes$ denotes the Kronecker product of the two vectors. The set of all integers that can be expressed by at most Q symbols from $\mathbb{M}$ can be written as

$$\mathsf{d}(Q) = \bigcup_{i=0}^{\lfloor \frac{Q}{2} \rfloor} [2i + (Q)_2]. \tag{76}$$

Also, equivalently,

$$\mathsf{d}(Q) = \{V \in \mathbb{Z} | \mu(M,V) \leq Q \wedge (\mu(M,V) - Q)_2 = 0\}. \tag{77}$$

Since the individual sets in (76) are disjoint, it can be inferred from (74) that

$$|\mathsf{d}(Q)| = Q\,(M-1) + 1. \tag{78}$$

Finally, consider the H-tuple: $\mathbf{Q} = (Q_0, Q_1, \ldots, Q_{H-1})$. Define the set of points $\mathsf{D}(\mathbf{Q}) \subset \mathbb{Z}^H$ by the following Cartesian product:

$$\mathsf{D}(\mathbf{Q}) = \prod_{j \in \mathbb{N}_H} d\,(Q_j)\,. \tag{79}$$

Using this notation, the following result can be stated:

Theorem 4

1. *The optimization problem defined in* (66) *is equivalent to*

$$\begin{aligned} &\textit{minimize} \quad F \\ &\textit{subject to } (68) \textit{ holds } \forall \gamma_F \in \Gamma_F, \mathbf{V}^{(\gamma)} \in \mathsf{D}(\mathbf{J}_F). \end{aligned} \tag{80}$$

2. *Moreover, if F is restricted to be an even/odd multiple of H, then the above optimization problem can be written as*

$$\begin{aligned} &\textit{minimize } ||\mathbf{V}^{(\gamma)}||_\infty \\ &\textit{subject to } (68) \textit{ holds } \forall \gamma_F \in \Gamma_F, \mathbf{V}^{(\gamma)} \in \mathsf{D}((F/H)\mathbf{1}_H). \end{aligned} \tag{81}$$

3. *For binary modulation schemes ($M = 2$), F can be any multiple of H for the equivalence of* (66) *and* (81).

4. *If* (61) *is satisfied for a value of* F *(for all* $\gamma_F \in \Gamma_F$*), then it is also satisfied by* $F+1$ *(for all values of* $\gamma_{F+1} \in \Gamma_{F+1}$*).*

Proof: See Appendix E.

The difference between the two optimization problems in Theorem 4 is that first has P dependent constraints, while the second is in fact composed of P decoupled subproblems with independent constraints.

To interpret the results of this theorem, it is helpful to consider a geometric perspective. The sets $\mathsf{D}(\mathbf{J}_F)$ are constructed such that each member is a feasible vector for F intrafix symbols. So, the equivalence of (66) and(80) is established by the fact that the cost function F is same, and the new constraints (68), in terms of the vector $\mathbf{V}^{(\gamma)}$, are also equal to (61). Only the feasible set has changed from $\mathbb{M}$ to $\mathsf{D}(\mathbf{J}_F)$ because of the variable transformation from x_i to $\mathbf{V}_j^{(\gamma)}$. The advantage in performing this transformation is that unlike (66), in solving (80), the number of optimization variables is known to be H. The feasible sets are plotted for dual-h ($H=2$) schemes in Fig. 14 and Fig. 15, for $M=2$ and $M=4$, respectively. It can be observed that in both cases, the first four sets $\mathsf{D}(0,0), \mathsf{D}(0,1), \mathsf{D}(1,1)$, and $\mathsf{D}(1,2)$ (corresponding to values of F from 0 to 3, respectively), are disjoint. However, these sets are contained in $\mathsf{D}(2,2)$, $\mathsf{D}(2,3)$, $\mathsf{D}(3,3)$, and $\mathsf{D}(3,4)$, respectively. In general, it can be inferred that a feasible vector for F is also feasible for $F+2H$. For the second part of *Theorem 4*, based upon the sets $\mathsf{D}(0,0)$, $\mathsf{D}(1,1)$, $\mathsf{D}(2,2)$, and $\mathsf{D}(3,3)$, it can be concluded that for any feasible vector, the cost $||.||_\infty$ is equivalent to F under the stated conditions. For example, for $M=2$, every element $\mathbf{V}^{(\gamma)} \in \mathsf{D}(\kappa_1 \mathbf{1}_H) \backslash \mathsf{D}(\kappa_2 \mathbf{1}_H)$, $\mathbf{W}^{(\gamma)} \in \mathsf{D}(\kappa_2 \mathbf{1}_H)$, given that $\kappa_1 > \kappa_2$ implies that $||\mathbf{V}^{(\gamma)}||_\infty > ||\mathbf{W}^{(\gamma)}||_\infty$. However, for $M>2$, this may not hold when $\kappa_1 = \kappa_2 + 1$, and hence we have to further restrict F to be either even or odd multiples of H.

Using this theorem, a heuristic algorithm can be developed for finding an optimal value of F, i.e., F_{opt}. Start with $F = \Omega H$, where Ω is the smallest integer such that

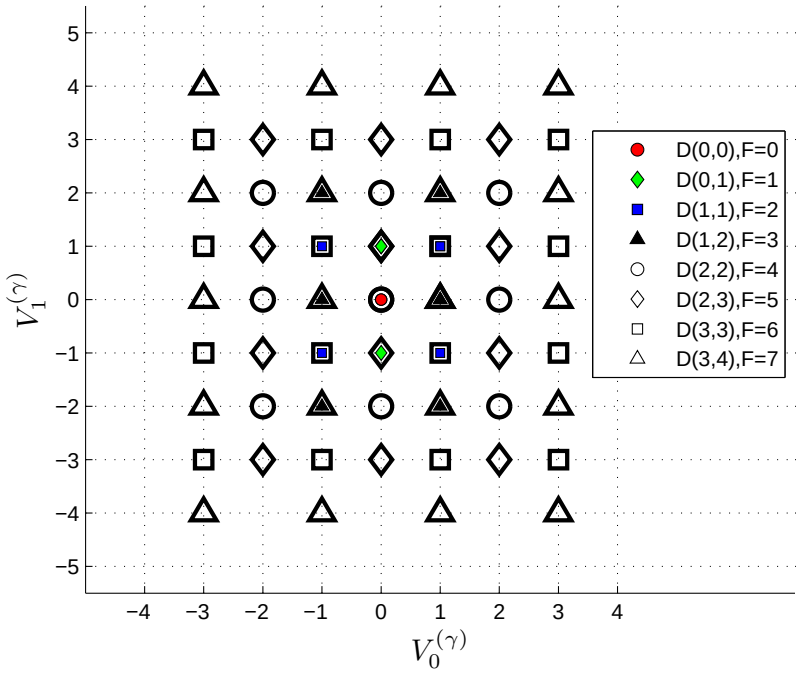

Figure 14: Feasible sets $\mathsf{D}(\mathbf{J}_F)$ corresponding to different values of F for dual-h ($H = 2$) binary ($M = 2$) modulation schemes.

$|\mathsf{D}(\mathbf{J}_F)| \geq P$. If P points satisfying the P constraints in (68) are not found, proceed to $F = (\Omega + 2)H$, and try again. The advantage of jumping forward by a step of 2 is that all the solutions $\mathbf{V}^{(\gamma)}$ found for $F = \Omega H$ are also valid for $F = (\Omega + 2)H$, and need not be found again. This follows from the subset property described above. Also, we notice that if $\mathbf{V}^{(\gamma)}$ solves (68) for some $\gamma_F \in \Gamma_F$, then $-\mathbf{V}^{(\gamma)}$ is the solution for $2P - \gamma_F$.

At some stage, a value of Ω is found such that $F = (\Omega - 2)H$ does not satisfy all of the P equations, while $F = \Omega H$ does. Now, check for $F = (\Omega - 1)H$. In this way, the smallest value Ω_{opt} can be reached, such that $F = \Omega_{opt} H$ satisfies all of the P constraints. Now, consider the fact that if all the constraints in (61) for $\gamma_F \in \Gamma_F$ are satisfied, then the symbol x_{N-F-1} can be chosen such that the constraints (61) can be met for each $\gamma_{F+1} \in \Gamma_{F+1}$. In other words, if a valid intrafix of length F has been found, it is possible to construct one of length $F + 1$. Thus,

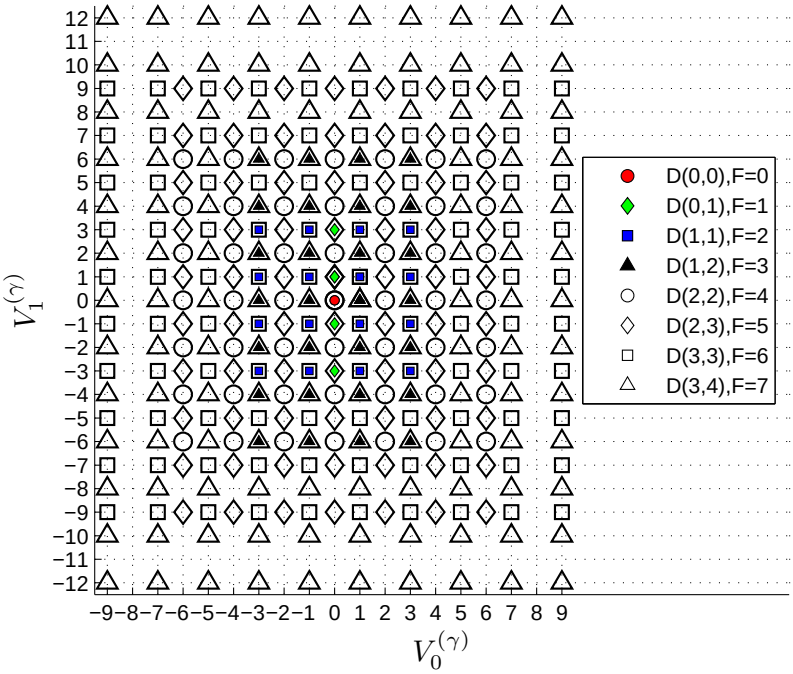

Figure 15: Feasible sets $\mathsf{D}(\mathbf{J}_F)$ corresponding to different values of F for dual-h ($H = 2$) quaternary ($M = 4$) modulation schemes.

$(\Omega_{opt} - 1)H < F_{opt} \leq \Omega_{opt} H$. F_{opt} can be reached by repeated binary partitions of this interval. However, while working in this interval, all the sets $\mathsf{D}(\mathbf{J}_F)$ are disjoint, and solutions for each succeeding value of F need to be started from scratch. Once F_{opt} and optimal vectors $\mathbf{V}^{(\gamma)}$ are found, they can be converted to the desired intrafix symbols x_i by making the following assignment:

$$\mathbf{x}(J_F^{(j)}) := z_{|J_F^{(j)}|}(V_j^{(\gamma)}), \forall j \in \mathbb{N}_H, \tag{82}$$

where $\mathbf{x}(J_F^{(j)})$ is a vector formed by collecting the intrafix symbols x_i corresponding to the j-th modulation index. This section is concluded with the following theorem, which specifies bounds on the length of the intrafix F.

Theorem 5 *If $H|F$, then the intrafix length F_{opt} satisfies the following bounds:*

$$\frac{\sqrt[H]{P} - 1}{M - 1} \leq \frac{F_{opt}}{H} \leq \left\lceil \frac{P - 1}{M - 1} \right\rceil. \tag{83}$$

Proof is omitted because of space limitations. A similar theorem was presented in [52] for the length of tilted-phase terminating sequence (TS). The upper bound is achieved only if all modulation indices except one, are integer valued, and $\min(\mathbb{K}) = P - 1$. Also, the upper bound is achieved for $H = 1$, and is the reported length of the intrafix for single-h modulation schemes [12].

4.3.2 Tilted-phase Approaches

In this section, two additional methods are presented to solve the problem of finding and minimizing the number of intrafix symbols, F. Both these methods work by reposing the problem either in terms of the tilted-phase state vector (48) or by transforming the symbols using (45).

Second Method (A Bad Idea): To motivate this procedure, observe that the first components of the state vectors in (49) and (48) differ by the term $\mathcal{K}_{n-L}$. If this term can be eliminated, then the approach developed in [52] for termination of the tilted-phase vector in (48) can be applied to satisfy the cyclic constraints on excess phase state in (51). Using the relationship $\mathcal{T}_{n-L} \equiv [2\mathcal{I}_{n-L} - \mathcal{K}_{n-L}] \bmod (2P)$, the condition (54) can be posed in terms of I_{n-L} alone, if

$$(M-1)\sum_{i=0}^{N-1} K_{(i)_H} \equiv 0 \bmod (2P). \tag{84}$$

This together with (55) requires that

$$(N)_G = 0, \tag{85}$$

where $G := \operatorname{lcm}\left\{H, 2PH/\gcd\{2PH, (M-1)\sum_{i=0}^{H-1} K_i\}\right\}$. Although this condition simplifies the problem to one of tilted-phase termination, the constraint on the size of the block can be very strict for some parameter values, and its further discussion is not considered for this reason.

Third Method (A better Idea): This method works in the domain of unipolar symbols u_n, and does not impose any stringent constraint on the block size. The details of this procedure are similar to the one based on excess phase, and analogous definitions and notations are used. As explained in the following, it is a more elegant technique than the latter, and leads to simpler feasible sets.

Substituting for x_i according to (45) in (61),

$$2\sum_{i=N-F}^{N-1} K_{(i)_H} u_i - (M-1)\sum_{i=N-F}^{N-1} K_{(i)_H} + \gamma_F \equiv 0 \mod (2P). \tag{86}$$

Let

$$\hat{\gamma} := \frac{\gamma_F - (M-1)\sum_{i=N-F}^{N-1} K_{(i)_H}}{2} \mod (P). \tag{87}$$

This transformation from γ_F to $\hat{\gamma}$ is a bijective function from Γ_F to $\mathbb{N}_P$, if N and Γ_F are chosen complying with (55), (64), and (65). Thus, using (87), (86) can be rewritten as

$$\sum_{i=N-F}^{N-1} K_{(i)_H} u_i + \hat{\gamma} \equiv 0 \mod (P). \tag{88}$$

Note that (88) is a linear Diophantine equation (LDE) [45] for each $\hat{\gamma}$, with positive integer coefficients from the set $\mathbb{K}$, and non-negative integer variables $u_i \in \mathbb{N}_M$. u_i are the transformed symbols of the intrafix segment $X_c^{(l)}$. If the symbols u_i corresponding to each modulation index are combined into a separate variable, (88) becomes

$$\sum_{j=0}^{H-1} K_j U_j^{(\hat{\gamma})} + \hat{\gamma} \equiv 0 \mod (P), \tag{89}$$

where

$$U_j^{(\hat{\gamma})} := \sum_{i \in J_F^{(j)}} u_i, \tag{90}$$

are components of $\mathbf{U}^{(\hat{\gamma})} := \left(U_0^{(\hat{\gamma})}, U_1^{(\hat{\gamma})}, \ldots, U_{H-1}^{(\hat{\gamma})}\right)$. Note that any integer $U \in \mathbb{N}$ can always be written as a sum of elements from $\mathbb{N}_M$. Given an arbitrary non-negative integer U, the minimum number of symbols $u_i \in \mathbb{N}_M$, required to express U as in (90) are

$$\hat{\mu}(M,U) = \left\lceil \frac{U}{M-1} \right\rceil \ . \tag{91}$$

Note that $\hat{\mu}(M,V)$ is a non-decreasing (increasing) function of U for a fixed M (for $M=2$), respectively. The expansion of an integer U in terms of the elements of $\mathbb{N}_M$ is not unique, and can be expressed as

$$\hat{y}_{\hat{\mu}(U)} = \begin{cases} (M-1)\mathbf{1}_{\hat{\mu}} & , \text{ if } (U)_{M-1} = 0 \\ ((M-1)\mathbf{1}_{\hat{\mu}-1}, (U)_{M-1}) & , \text{ if } (U)_{M-1} \neq 0 \end{cases}. \tag{92}$$

Note that this expansion is not unique, and the order of the symbols in the vector $y_\mu(U)$ is immaterial. The set of all $U \in \mathbb{N}$ that can be written as a sum of $\hat{Q} \in \mathbb{N}$ symbols from the set $\mathbb{N}_M$ (with $\hat{Q}$ minimal such number) define an equivalence class on the set of non-negative integers:

$$[\hat{Q}] := \left\{ U \in \mathbb{N} | \hat{\mu}(M,U) = \hat{Q} \right\}, \tag{93}$$

It is easy to see that,

$$[\hat{Q}] = \begin{cases} \{0\} & , \text{ if } \hat{Q} = 0, \\ \left\{ \left(\hat{Q}-1\right)(M-1)+1, \ldots, \hat{Q}\,(M-1) \right\} & , \text{ if } \hat{Q} > 1, \end{cases} \tag{94}$$

and

$$\left| [\hat{Q}] \right| = \begin{cases} 1 & , \text{ if } \hat{Q} = 0 \\ M-1 & , \text{ if } \hat{Q} > 0 \end{cases}. \tag{95}$$

Note that an integer U can only be expressed as a sum of $\hat{\mu}(M,U)+i$ symbols from $\mathbb{N}_M$, where $i \in \mathbb{N}$. One such decomposition for U is

$$\hat{z}_{\hat{\mu}+i}(U) = (\hat{y}_{\hat{\mu}}(U), \mathbf{0}_i), \tag{96}$$

where $\mathbf{0}_i$ is an i-dimensional null vector. The set of all integers which can be expressed by at most $\hat{Q}$ symbols from $\mathbb{N}_M$ can be written as

$$\hat{\mathsf{d}}(\hat{Q}) = \bigcup_{i=0}^{\hat{Q}} [\hat{Q}]. \tag{97}$$

Also, equivalently,

$$\mathsf{d}(Q) = \{ U \in \mathbb{N} | \mu(M,U) \leq Q \}. \tag{98}$$

Since the individual sets in (97) are disjoint, from (95),

$$\left|\hat{\mathsf{d}}(\hat{Q})\right| = \hat{Q}\,(M-1)+1. \tag{99}$$

Finally, consider the H-tuple, $\hat{\mathbf{Q}} = \left(\hat{Q}_0, \hat{Q}_1, \ldots, \hat{Q}_{H-1}\right)$. Define $\hat{\mathsf{D}}(\hat{\mathbf{Q}}) \subset \mathbb{N}^H$ as the following Cartesian product,

$$\hat{\mathsf{D}}(\hat{\mathbf{Q}}) = \prod_{j \in \mathbb{N}_H} \hat{d}\left(\hat{Q}_j\right). \tag{100}$$

Using this notation, the following result can be stated:

Theorem 6

1. *The optimization problem defined in* (66) *is equivalent to:*

$$\begin{aligned} &\textit{minimize} \quad F \\ &\textit{subject to } (89) \textit{ holds } \forall \hat{\gamma} \in \mathbb{N}_P, \mathbf{U}^{(\hat{\gamma})} \in \hat{\mathsf{D}}(\mathbf{J}_F). \end{aligned} \tag{101}$$

2. *Moreover, if F is restricted to be a multiple of H, then the optimization problem can be written as,*

$$\begin{aligned} &\textit{minimize} \quad ||\mathbf{U}^{(\hat{\gamma})}||_\infty \\ &\textit{subject to } (89) \textit{ holds } \forall \hat{\gamma} \in \mathbb{N}_P, \mathbf{U}^{(\hat{\gamma})} \in \mathbb{N}^H. \end{aligned} \tag{102}$$

3. *If* (88) *is satisfied for a value of F (for all $\hat{\gamma} \in \mathbb{N}_P$), then it is also satisfied by $F+1$.*

The proof for this theorem builds on ideas analogous to those used for proof of Theorem 4.

Based upon this theorem, a procedure can be posed for finding the optimal length F of the intrafix for a given modulation scheme. Before proceeding, consider the feasible set $\hat{\mathsf{D}}(\mathbf{J}_F)$ in (101). These sets, corresponding to different values of F, are

shown in Fig. 16, for $M = 4$. For example, for $F = 3$, $\mathbf{J}_3 = \{1, 2\}$ and $\hat{\mathsf{D}}(1, 2) := \hat{\mathsf{d}}(1) \times \hat{\mathsf{d}}(2)$, where $\hat{\mathsf{d}}(0) = \{0\}$, $\hat{\mathsf{d}}(1) = \mathbb{N}_4$, and $\hat{\mathsf{d}}(2) = \mathbb{N}_7$ by (97), and $\times$ denotes the Cartesian product of the two sets. Note that the sequence of sets of feasible integer vectors, indexed by F, form a nested family of sets, i.e., $\hat{\mathsf{D}}(0, 0) \subset \hat{\mathsf{D}}(0, 1) \subset \hat{\mathsf{D}}(1, 1) \subset \hat{\mathsf{D}}(1, 2)$, and so on. Thus the optimization problem in *Theorem 6* can be solved by starting with $F = 0$, and looking for integer solutions to (68). If solutions are not found for all $\hat{\gamma}$, F is incremented by one, and the procedure is repeated. If a solution for (76) is found for certain value of $\hat{\gamma}$, in a given step, it remains valid for all larger values of F; since the feasible sets contain the solutions corresponding to smaller values of F. A value of F is considered final when an integer vector $\mathbf{U}^{(\hat{\gamma})}$ is found for all $\hat{\gamma} \in \mathbb{N}_P$. This value of F is optimal and is the minimum required length of the intrafix for a given modulation scheme. The optimal vectors $\mathbf{U}^{(\hat{\gamma})}$ can now be converted to the desired intrafix symbols x_i by making the following assignment:

$$\mathbf{x}(J_F^{(j)}) := 2\hat{z}_{|J_F^{(j)}|}(U_j^{(\hat{\gamma})}) - (M - 1), \forall j \in \mathbb{N}_H. \tag{103}$$

The following theorem states bounds on optimal length of intrafix F_{opt}.

Theorem 7 *If $H|F$, $\gcd\{\mathbb{K}\} = 1$, and the Diophantine Frobenius number $g(\mathbb{K})$ (see [52, 15]) exists, then*

$$\frac{P - 1}{(M - 1)\sum_{k=0}^{H-1} K_k} \leq \frac{F_{opt}}{H} \leq \left\lceil \frac{g(\mathbb{K}) + P}{(M - 1)\min_k K_k} \right\rceil \quad . \tag{104}$$

The bounds stated in *Theorem 5* and *Theorem 7* were derived in [52] for the number of symbols required to reach an arbitrary cumulative phase state in the tilted-phase trellis. The length of the intrafix can be viewed as a special case of that problem, and these bounds are also applicable here. Although the intrafix computing approaches based upon excess or tilted-phase state vectors result in different feasible sets, both the approaches are equivalent in the sense that they solve the same optimization problem (66). Moreover, the resulting intrafix length for a given modulation scheme

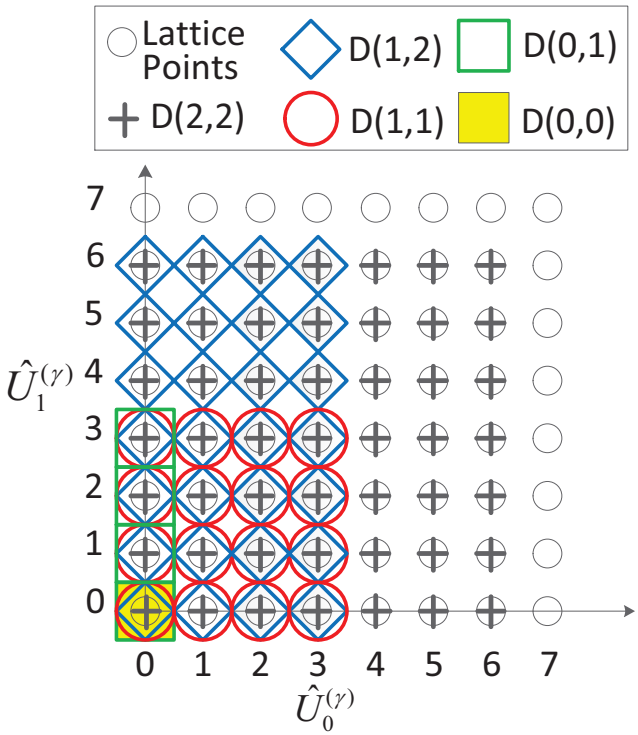

Figure 16: Feasible sets $\hat{\mathsf{D}}(\mathbf{J}_F)$ corresponding to different values of F for dual-h ($H = 2$) quaternary ($M = 4$) modulation schemes.

is the minimum possible for each method, and the bounds proposed in *Theorem 5* and *Theorem 7* are applicable.

4.4 Numerical Example

In this section, intrafix symbols are computed for the Tier-2 aeronautical telemetry waveform called ARTM CPM in IRIG-106 standard [6]. It is a quaternary ($M = 4$), dual-h ($H = 2$) CPM scheme with modulation index set $h = \left\{\frac{4}{16}, \frac{5}{16}\right\}$, i.e., $\mathbb{K} = \{4, 5\}$, and $P = 16$. For the purpose of this example, it is assumed that $K_0 = 4$ and $K_1 = 5$. Since one element of $\mathbb{K}$ is odd and other is even, the situation falls under Case (3) in Section 4.2. The condition on the FFT block length N requires an even number of symbol intervals corresponding to the index with odd numerator 5, implying that either $(N)_4 = 0$ or $(N)_4 = 1$. However, (55) specifies that N should be even. Thus a choice of N such that $4|N$ simultaneously satisfies both conditions. This is not a

very binding restriction; since it is automatically met if N is defined to be an integer power of 2 for an efficient FFT implementation. Now, the methods discussed in the previous section are applied to compute the intrafix symbols.

For the procedure based upon excess phase, (68) becomes

$$4V_0^{(\gamma)} + 5V_1^{(\gamma)} + \gamma_F = 32m, \tag{105}$$

where $m \in \mathbb{Z}$. The choice of F is made such that (105) has integer solutions for all $\gamma_F \in \Gamma_F$. This equation is plotted for various values of m and $\gamma \in \{0, 1, 2, ..., 31\}$ in Fig. 17. First, consider $F = 1$. Since $(N - F)_4 = 3$, $(O_{N-F})_2 = 1$. Hence, $\Gamma_1 = \{1, 3, ..., 31\}$ by (64). Note that for $M = 4$, $\mathsf{D}(0, 1) = \{(0, -3), (0, -1), (0, 1), (0, 3)\}$. Since $|\mathsf{D}(0, 1)| = 4 < P$, a larger value of F is required. Although the four lattice points are insufficient to satisfy 16 LDEs in (68), 4 of them are satisfied, i.e., $\mathbf{V}^{(15)} = (0, -3)$,$\mathbf{V}^{(5)} = (0, -1)$,$\mathbf{V}^{(27)} = (0, 1)$, and $\mathbf{V}^{(17)} = (0, 3)$.

Now increment to $F = 2$, which is a multiple of $H = 2$. Since $(N - F)_4 = 2$, and $(O_{N-F})_2 = 1$, hence, $\Gamma_2 = \{1, 3, ..., 31\}$ by (64). Moreover, for $M = 4$, $\mathbf{J}_2 = (1, 1)$, $\mathsf{d}(1) = \mathbb{M}$, and $\mathsf{D}(1, 1) = \mathbb{M} \times \mathbb{M}$. Note that $\mathsf{D}(1, 1)$ is disjoint with the feasible set $\mathsf{D}(0, 1)$ for $F = 1$, and the 4 integer solutions found in the previous step cannot be used. Since $|\mathsf{D}(1, 1)| = M^2 = P$, $F = 2$ can be the length of the intrafix only if each vector in $\mathsf{D}(1, 1)$ represents a solution to LDEs of (68) for a distinct value of Γ_F. This indeed happens for this example, as the vectors $\mathbf{V}^{(\gamma)}$ are shown in Fig. 17 corresponding to the γ_2 for which an LDE is satisfied. If the intrafix symbols are defined as $(x_{N-1}, x_N) := \mathbf{V}^{(\gamma)}$, one per modulation index, it can be concluded that the intrafix has minimum length $F_{opt} = 2$ for the ARTM scheme. Compare this to $\lceil \frac{P-1}{M-1} \rceil = 5$ symbols required for any single-h CPM with $P = 16$ [12].

For the second method, based upon tilted-phase termination, the constraint (85) on the FFT-length N, requires that N be a multiple of 64. The problem with this approach is that it imposes this stringent condition without offering any reduction in the number of intrafix symbols F. This was the reason for introducing it as a 'bad

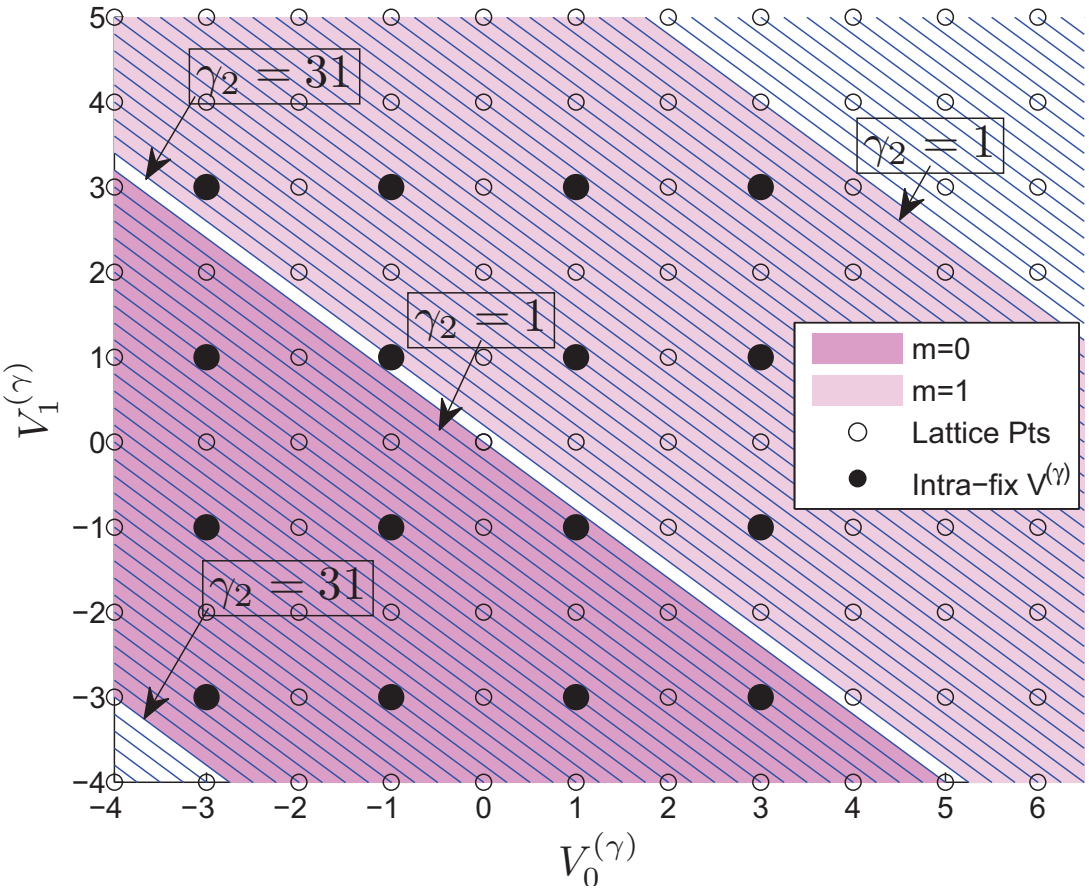

Figure 17: Optimum intrafix symbols obtained for the ARTM CPM modulation scheme using Method 1.

idea'. On the other hand, the third method was presented as a 'better idea' as it does not impose this additional constraint (85) of second method, and also provides an elegant solution to the problem when compared with first method.

The third approach computes the transformed unipolar symbols u_i corresponding to each $\hat{\gamma}$. In the first method, the set Γ_F had to be predetermined for each value of F, and the set of constraints changed on each step. The advantage of the third method is that the values of $\hat{\gamma} \in \mathbb{N}_P$ are independent of F. Moreover, because of the nesting of the family of feasible sets, the solutions $\mathbf{U}^{(\hat{\gamma})}$, found for a value of F remain valid for all larger values. For any $m \in \mathbb{N}$, (89) for the third method can be written as

$$4U_0^{(\hat{\gamma})} + 5U_1^{(\hat{\gamma})} + \hat{\gamma} = 16m \ . \tag{106}$$

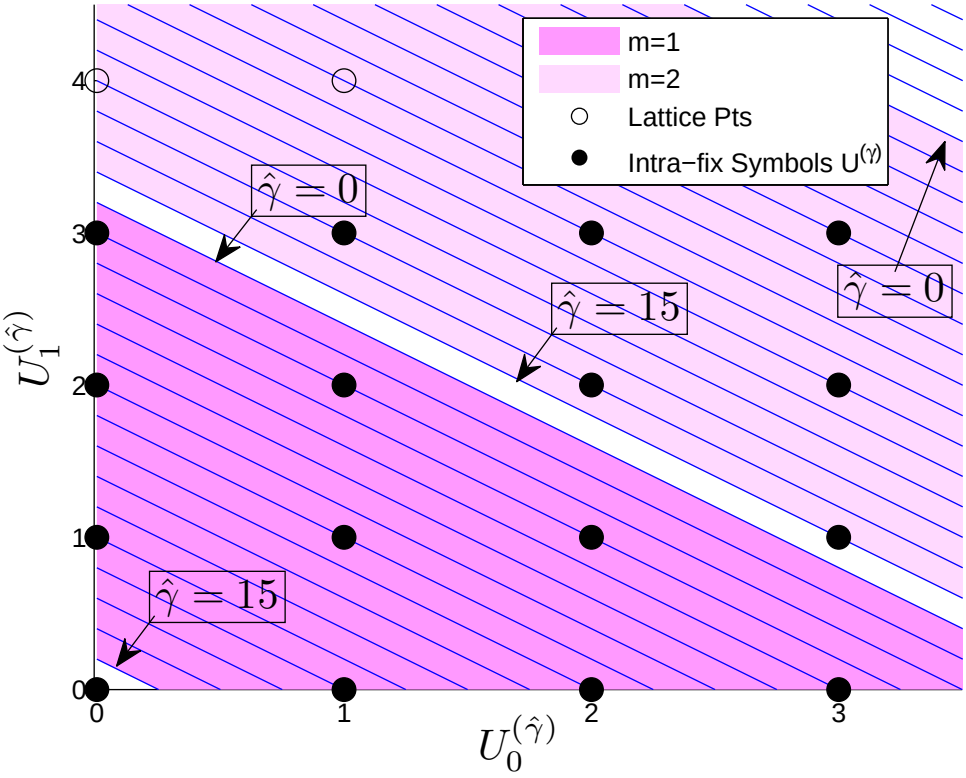

Figure 18: Optimum intrafix symbols obtained for the ARTM CPM modulation scheme using Method 3.

The lines corresponding to these equations are shown for different values of m and $\hat{\gamma}$ in Fig. 18. Non-negative integer lattice points are also shown. Starting from $F = 0$, the feasible set is $\hat{\mathsf{D}}(0,0) = \{(0,0)\}$, which is a solution for $\hat{\gamma} = 0$. Incrementing to $F = 1$, the feasible set $\hat{\mathsf{D}}(0,1)$ now contains three additional solutions for $\hat{\gamma} \in \{11, 6, 1\}$. For $F = 2$, the feasible set $\hat{\mathsf{D}}(1,1)$ contains 12 new lattice points, which correspond to solutions of (106) for rest of the values of $\hat{\gamma}$, as shown in Fig. 18. So, $F_{opt} = 2$ for the ARTM CPM modulation scheme. The intrafix symbols can be determined by using the transformations (87) and (103).

This example also serves to verify the equivalence of approaches based upon excess phase and tilted phase, as the optimal vectors, $\mathbf{V}^{(\gamma)}$ and $\mathbf{U}^{(\hat{\gamma})}$, are listed in Table 2 for both approaches. Note that for each pair of γ_2 and $\hat{\gamma}$, the optimal vectors are related by $+V_j^{(\gamma)} = 2U_j^{(\gamma)} - (M-1)$, for $j = \{0, 1\}$, the transformation in (45). The intrafix

Table 2: Intrafix symbols for ARTM CPM scheme computed using Method 1 and Method 3.

$\gamma_2 \in \Gamma_2$	$\mathbf{V}^{(\gamma)}$	$\hat{\gamma} \in \mathbb{N}_{16}$	$\mathbf{U}^{(\hat{\gamma})}$
1	$(+1,-1)$	3	$(2,1)$
3	$(+3,-3)$	4	$(3,0)$
5	$(+3,+3)$	5	$(3,3)$
7	$(-3,+1)$	6	$(0,2)$
9	$(-1,-1)$	7	$(1,1)$
11	$(+1,-3)$	8	$(2,0)$
13	$(+1,+3)$	9	$(2,3)$
15	$(+3,+1)$	10	$(3,2)$
17	$(-3,-1)$	11	$(0,1)$
19	$(-1,-3)$	12	$(1,0)$
21	$(-1,+3)$	13	$(1,3)$
23	$(+1,+1)$	14	$(2,2)$
25	$(+3,-1)$	15	$(3,1)$
27	$(-3,-3)$	0	$(0,0)$
29	$(-3,+3)$	1	$(0,3)$
31	$(-1,+1)$	2	$(1,2)$

length, $F_{opt} = 2$, also meets the lower bound in Theorem 5.

In Fig. 19, the phase of the CPM signal is shown corresponding to one block of symbols. The phase signal is unwrapped, and it can be seen that phase replicates itself in the cyclic-prefix zone (shown in green) except by a multliple of 2π. The red portion of the plot corresponds to the phase generated by the intrafix symbols, which form only a small fraction of total symbols in the block. Fig. 20 shows the in-phase component of the CPM complex envelope, and it can be seen that the exact replica of the signal is repeated in the cyclic-prefix zone.

In Fig. 21, the periodograms for this ARTM modulation scheme are illustrated for three different scenarios. The periodogram for standard multi-h CPM without cyclicity and intrafix is consistent with the one presented in [6]. The second curve is provided for the case of a cyclic block with $N = 256$, $N_{CP} = 32$, and $F = 0$. Note that skipping the intrafix altogether will result in a phase discontinuity once per block. For this reason, a considerable out-of-band energy is present in this situation.

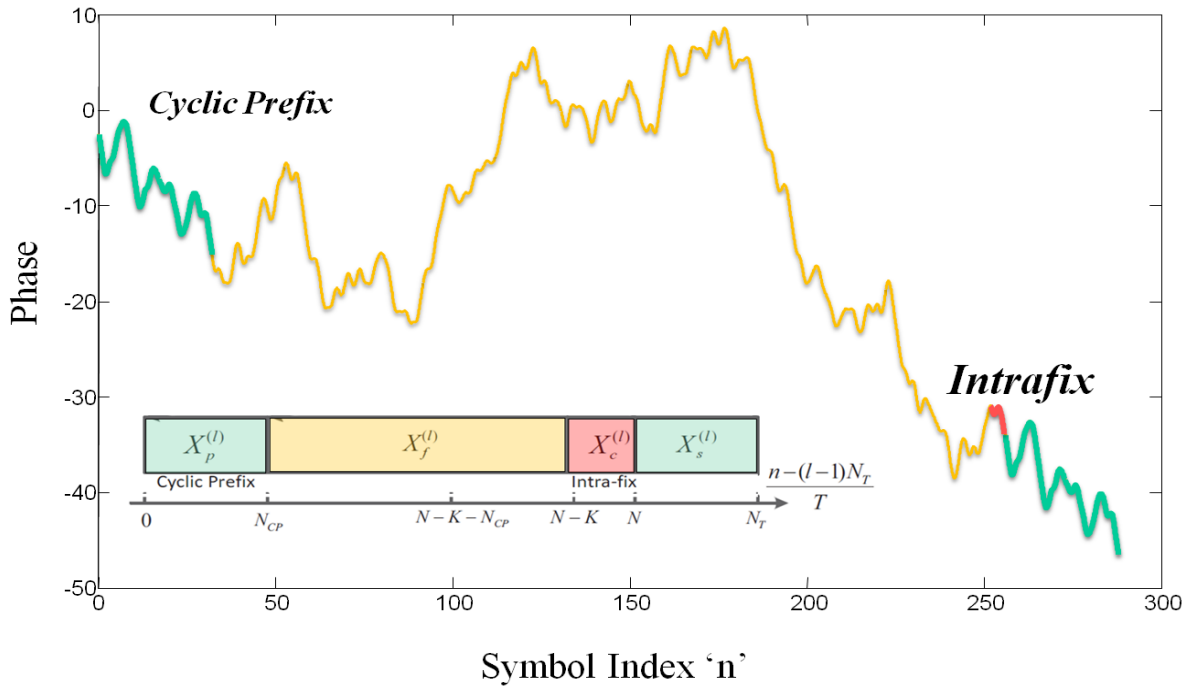

Figure 19: Phase (unwrapped) of the dual-h CPM signal generated by the cylic transmitted block. The principal value of the phase repeats exactly in the cyclic-prefix zone (shown in green).

The third curve is for the periodogram of cyclic multi-h CPM with intrafix inserted. The parameters are $N = 256$, $N_{CP} = 32$, and $F = 2$. The intrafix helps achieve the cyclicity and continuity of the excess phase simultaneously at the cost of two information symbols per block.

The Power Spectral Density (PSD) is almost the same for the case of standard multi-h CPM, and the intrafix-utilizing cyclic multi-h CPM. It is clear from Fig. 21 that under the cyclic constraint, the intrafix helps retain the spectral efficiency of multi-h CPM.

4.5 Summary

This section proposed efficient procedures to construct a cyclic symbol block for multi-h CPM signal. They ensure insertion of minimum possible number of intrafix symbols per block. The algebraic constraints on the structure of the block and the intrafix

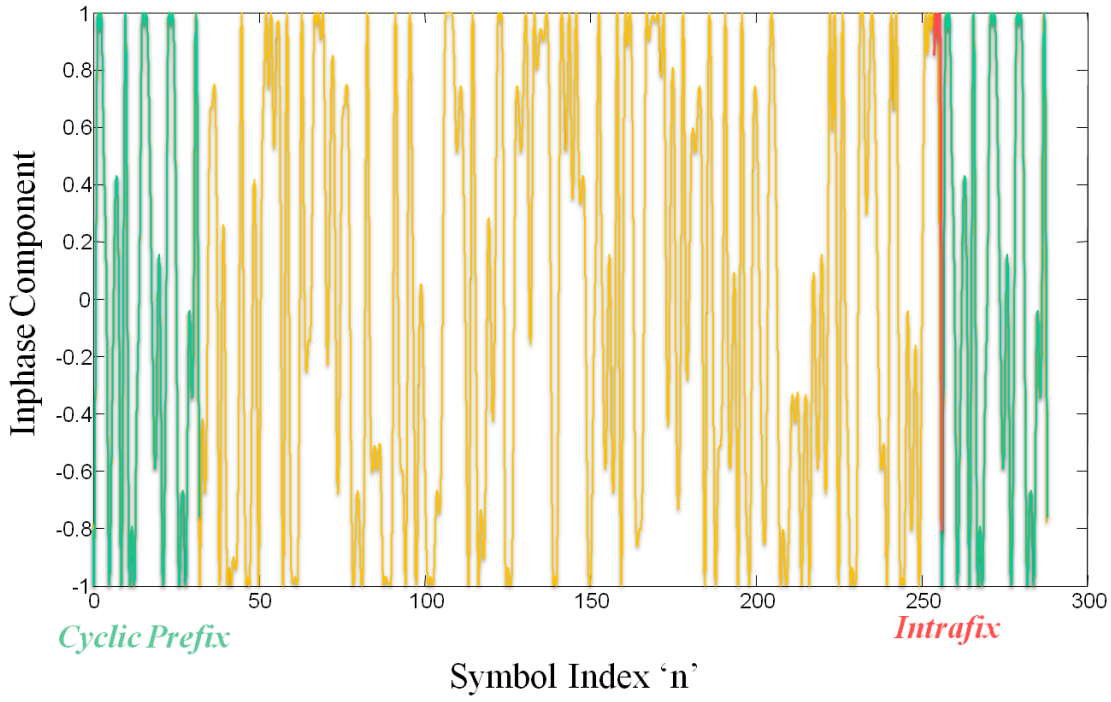

Figure 20: Inphase component of the CPM signal generated by a cyclic transmitted block. The signal replicates exactly in the cyclic-prefix zone (shown in green).

symbols were identified. The former is a function of the number of modulation indices, and the latter depends upon the rational modulation indices and the number of bits per symbol of the modulation scheme. The intrafix length for multi-h CPM is usually less when compared to similar single-h CPM schemes. An example of dual-h scheme was discussed to illustrate the proposed approach. It is observed that schemes with integer modulation indices and larger P generally require the longest intrafix. Finally, under a cyclic constraint, the intrafix helps retain the spectral efficiency of multi-h CPM.

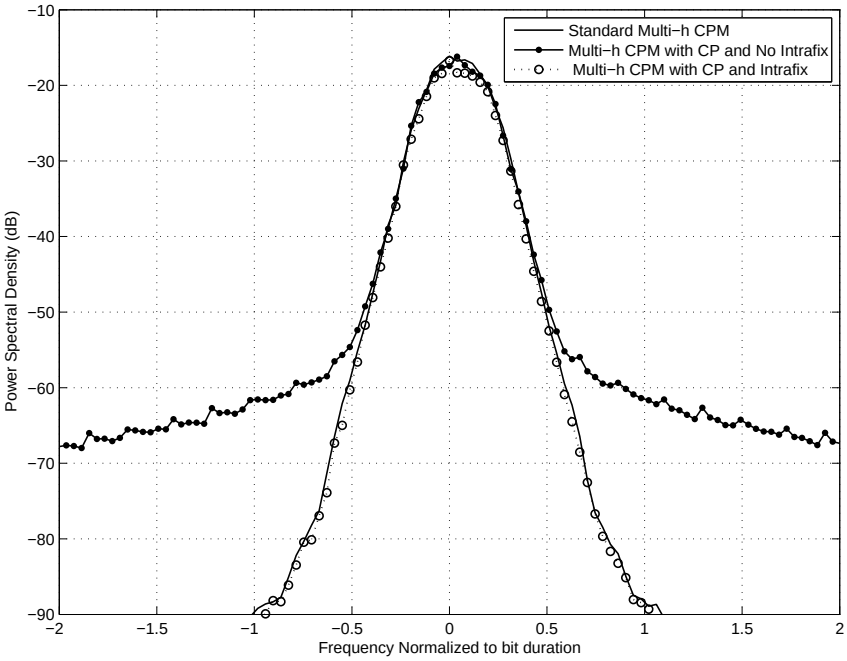

Figure 21: Power spectral density for ARTM multi-h CPM.

CHAPTER V

LOW-COMPLEXITY FREQUENCY-DOMAIN EQUALIZATION TECHNIQUES FOR MULTI-H CPM

For single-carrier modulation schemes, frequency-domain equalization (FDE) is a relatively low-complexity approach to mitigate the intersymbol interference introduced by propagation over a frequency-selective channel. In this chapter, we present two receiver architectures for FDE of multi-h continuous phase modulation (CPM). In the first approach, the receiver front end is a matched-filter bank, which is derived from Laurent decomposition of the signal. A circulant-matrix model derived for the samples of the matched filter (MF) is used to perform the equalization in frequency domain. The second technique employs a receiver with a simple front end consisting of a low-pass filter followed by a fractional sampler. We also develop a circulant matrix model for the latter approach, which relates the Laurent pseudo-symbols to each polyphase component of the output of the sampler. Using this model, a linear frequency-domain equalizer is designed. In addition to providing the details of these approaches, we propose simplifications applicable to each of the two cases, and provide a detailed discussion on the performance/complexity trade-off. Bit-error rate (BER) results are presented for the IRIG-106 aeronautical telemetry dual-h CPM waveform. We make following contributions towards frequency-domain equalization of multi-h CPM.

- We present a new interpretation of the Laurent decomposition for multi-h CPM signals that suppresses the periodicity of the Laurent pulses. This is achieved by merely re-labelling the Laurent pulses and their pseudo-symbols. However, this

seemingly naive step enables visualizing multi-h CPM as essentially a higher-order single-h CPM, thus paving the way for extension of techniques available for single-h CPM and making them available to multi-h CPM.

- We propose two FDE receiver architectures for multi-h CPM; one that uses a matched-filter front end and the other that uses a single low-pass (anti-aliasing) filter followed by a sampler. For both schemes, we show that the sampled output of the receiver filter(s) satisfies a circulant matrix model for general multi-h CPM waveforms given that the transmitted signal is cyclic for the duration of the block. The effect of the memory of the modulator and that of the frequency-selective channel is isolated by the models. This isolation enables the equalizer to eliminate exclusively the effect of the channel, while a trellis-based AWGN demodulator can then follow the equalizer to recover the data symbols.

- The reduction in the complexity of the receiver using MF front end is proposed by dropping the MFs and the FDE branches corresponding to low-energy Laurent pulses. It is observed that the loss in performance is acceptable even when a few significant branches are considered. Similarly, further complexity reduction can be forced for sampling-based approach by partially truncating the auto-correlation matrix of the multi-h CPM signal.

- Simulation results are obtained for the IRIG-106 Tier-2 dual-h CPM waveform. The channel model used to perform these simulations is the wideband aeronautical telemetry channel.

The remainder of this chapter is organized as follows. Section 5.1 briefly reviews earlier discussed process of cyclic-block construction. In Section 5.2, we introduce the matched filter front end receiver, and discuss the equalizer design for this architecture. In Section 5.3, we discuss the sampling-based receiver design. Section 5.4 analyzes and compares the complexity of these two receiver architectures, while Section 5.5 contains

the simulation results for the aeronautical telemetry channel model. A summary of this chapter is presented in Section 5.6.

The multi-h CPM waveform and modulation parameters are described in Section 2.7, and the notation used in this chapter is defined in Section 2.6.

5.0.1 An Alternate Interpretation of Laurent Decomposition

It can be observed from (4) that Laurent pulses appear periodically and the total number of unique pulses are in fact $\overline{Q} = HQ$. To facilitate the development of a matrix model for the received signal, we propose to re-label the Laurent pulses in a manner that eliminates the periodicity and increases the symbol duration to $\overline{T} = HT$. The new set of indices (k, m) are bijectively related to the original indices (q, i) in the Laurent expansion, i.e.,

$$(q, i) \rightleftharpoons (k, m). \tag{107}$$

The forward transformation is defined as

$$(k, m) := \left(q + (i)_H Q, \lfloor i/H \rfloor\right), k \in \mathbb{N}_{\overline{Q}}, m \in \mathbb{Z}, \tag{108}$$

and the reverse transformation is

$$(q, i) = \left((k)_Q, mH + \left\lfloor \frac{k}{Q} \right\rfloor\right). \tag{109}$$

The re-labelled set of pulses are defined as

$$\bar{g}_k(t) := g_{(k)_Q, \lfloor k/Q \rfloor}\left(t - \lfloor k/Q \rfloor T\right), \tag{110}$$

and the corresponding pseudo-symbols are

$$b_{k,m} := a_{(k)_Q, mH + \lfloor k/Q \rfloor}. \tag{111}$$

The re-labeled pulses are plotted in Fig. 22 for Tier-2 IRIG-106 dual-h CPM waveform. For this waveform, $Q = 48$ and $H = 2$. Note how the pulses numbered $0 - 47$

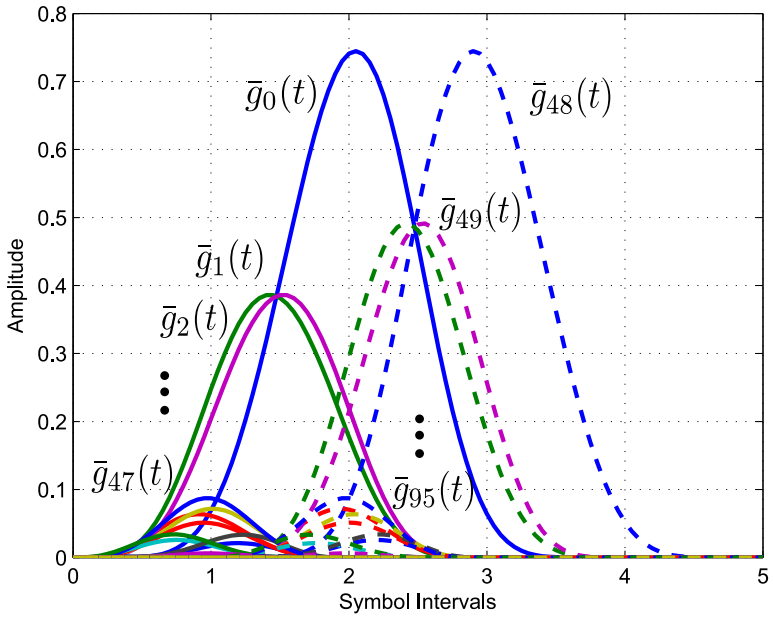

Figure 22: Re-labeled set of Laurent pulses for IRIG-106 dual-h CPM waveform.

corresponding to even symbol intervals appear as in Fig. 3, while the pulses numbered $48-95$ corresponding to odd symbol intervals (see Fig. 4) are delayed. Laurent decomposition in (4) can now be expressed as

$$s(t,\mathbf{x}) = \sum_{m=-\infty}^{\lceil n/H \rceil} \sum_{k=0}^{\overline{Q}-1} b_{k,m}\bar{g}_k(t-m\overline{T}), \quad t \leq nT. \tag{112}$$

In this work, we assume that the receiver is synchronized and has perfect information of the channel. For a frequency-selective channel, the received signal is the sum of the linear convolution of impulse response of the channel $c(t)$ and the transmitted signal $s(t)$ and the additive noise $\eta(t)$, i.e.,

$$r(t) = c(t) \star s(t,\mathbf{x}) + \eta(t). \tag{113}$$

The complex noise process $\eta(t)$ is assumed to be circularly-symmetric, white, and Gaussian, with two-sided spectral density equal to $N_o/2$. Block diagrams for the transmitter and the channel are shown in Fig. 23 and Fig. 24, respectively. The sub-components of transmitter will be explained in next section.

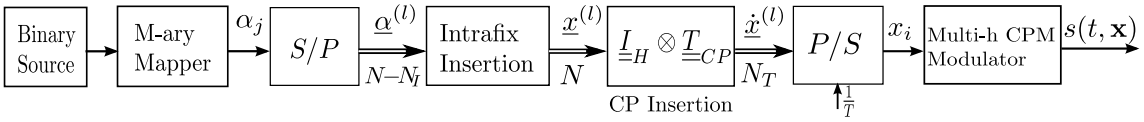

Figure 23: Block diagram of a cyclic multi-h CPM transmitter. Double-lined connections between the blocks represent a vector. The label of the vector is mentioned on the top of the connection and its dimension is specified on the bottom. S/P and P/S denote serial-to-parallel and parallel-to-serial converters, respectively.

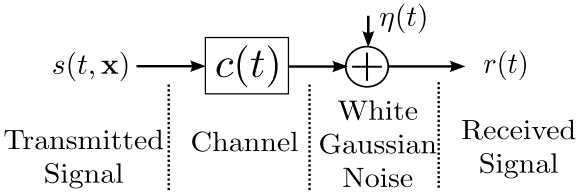

Figure 24: Block diagram of the frequency-selective channel with additive white Guassian noise.

5.1 Cyclic Signal Generation

We consider a block-based transmission system with the block length N_T chosen such that $c(t)$ remains invariant for the l-th block. To use the efficient Fast Fourier transform (FFT) algorithms in the FDE at the receiver, this linear convolution is forced to be equal to the circular convolution. The length of cyclic prefix N_P has to be greater than the combined memory of the channel (L_c) and that of the modulator (L). The equality of linear and circular convolution is achieved by imposing the following cyclic constraint on the transmitted signal corresponding to the l-th block, i.e.,

$$s(t, \mathbf{x}) = s(t + NT, \mathbf{x}), \forall t \in [lN_T T, (lN_T + N_P)T], \tag{114}$$

where N and N_P are the FFT-length and cyclic-prefix length, respectively, and are chosen such that $(N)_H = 0$ and $(N_P)_H = 0$. The constraint in (114) can be satisfied by following the procedure below (for details, see [53] and Fig. 25):

For each block, choose $N - N_I$ M-ary source symbols $\alpha_j^{(l)} \in \mathbb{M}$ for $j \in \mathbb{N}_{N-N_I}$.

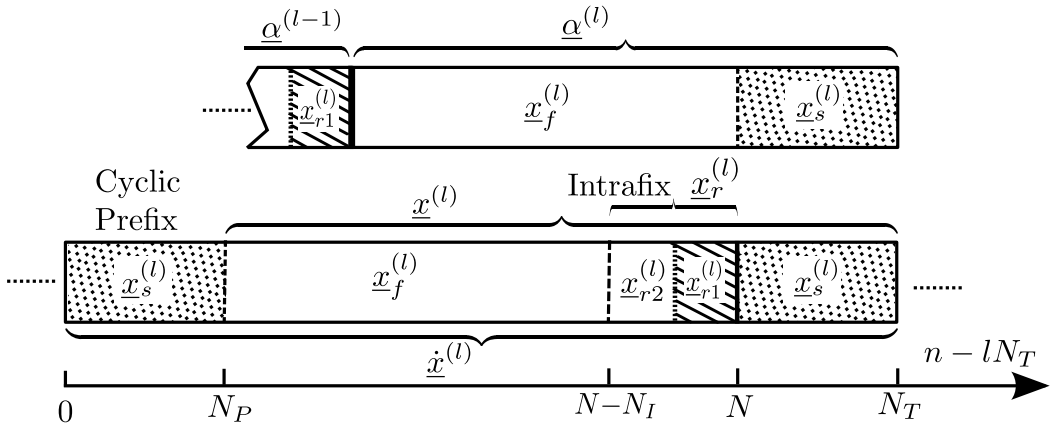

Figure 25: Proposed block structure that generates a cyclic multi-h CPM signal. Intrafix and cyclic prefix ensure the required cyclic constraints.

Construct the intermediate N-length block as follows:

$$\underline{x}^{(l)} := \left[\underline{x}_f^{(l)}; \underline{x}_r^{(l)}; \underline{x}_s^{(l)}\right],$$

where $\underline{x}_f^{(l)} := \left[\alpha_0^{(l)}, \ldots, \alpha_{N-N_P-N_I-1}^{(l)}\right]^T$, and $\underline{x}_s^{(l)} := \left[\alpha_{N-N_P-N_I}^{(l)}, \ldots, \alpha_{N-N_I-1}^{(l)}\right]^T$. The intrafix segment $\underline{x}_r^{(l)}$ itself can be further divided into two sub-segments such that

$$\underline{x}_{r1}^{(l)} := \left[\alpha_{N-N_I-L+1}^{(l-1)}, \ldots, \alpha_{N-N_I-1}^{(l-1)}\right]^T,$$

and now $\underline{x}_{r2}^{(l)}$ is selected such that

$$\left[K_{(lN_T+N_P)_H}, \ldots, K_{((l+1)N_T-1)_H}\right] \underline{x}^{(l)} \equiv 0 \bmod 2\mathrm{P},$$

is satisfied. The intrafix for l-th block is now defined as

$$\underline{x}_r^{(l)} := \left[\underline{x}_{r2}^{(l)}; \underline{x}_{r1}^{(l)}\right].$$

Finally, the N_T-length cyclic block is composed as follows.

$$\begin{aligned}\dot{\underline{x}}^{(l)} &:= \left[\underline{x}_s^{(l)}; \underline{x}^{(l)}\right], \\ &= \left[\underline{x}_s^{(l)}; \underline{x}_f^{(l)}; \underline{x}_{r2}^{(l)}; \underline{x}_{r1}^{(l)}; \underline{x}_s^{(l)}\right]. \end{aligned} \tag{115}$$

The resulting signal $s(t, \mathbf{x})$ satisfies the cyclic constraint in (114). These steps are also shown in the transmitter block diagram of Fig. 23.

5.1.1 Vector of Laurent Pseudo-symbols

Although CPM is a non-linear modulation scheme (in the sense that the transmitted CPM signal is a non-linear function of the source symbols $\alpha_j^{(l)}$), but the Laurent decomposition lumps all the non-linearity in the transformation from source symbols $\alpha_j^{(l)}$ to the psuedo-coefficients $b_{k,m}$. This decomposition allows the rest of the operations in the modulator (except intrafix insertion) and a linear receiver (such as MMSE equalizer) to be expressed as a series of matrix operations on the vector of pseudo-symbols, which is defined in the following. The k-th pseudo-symbols $b_{k,l\overline{N}+m}$ corresponding to the l-th block $\underline{x}^{(l)}$ (which includes the intrafix symbols) can be expressed as a vector of dimension $\overline{N} \times 1$,

$$\underline{b}_k^{(l)} := \left[b_{k,l\overline{N}} \;\; b_{k,l\overline{N}+1} \;\; \ldots b_{k,(l+1)\overline{N}-1} \right]^T. \tag{116}$$

The vector of k-th pseudo-symbols corresponding to the cyclically extended block $\underline{\dot{x}}^{(l)}$ can be related by the following linear transformation:

$$\underline{\dot{b}}_k^{(l)} := \underline{\underline{T}}_{CP} \underline{b}_k^{(l)}, \tag{117}$$

where

$$\underline{\underline{T}}_{CP} := \left[\underline{\underline{0}}_{\overline{N}_P \times \overline{N} - \overline{N}_P}, \underline{\underline{I}}_{\overline{N}_P}; \underline{\underline{I}}_{\overline{N}} \right].$$

The vector containing all the $\overline{Q}$ pseudo-symbols for the l-th block can be constructed by appending all $\underline{b}_k^{(l)}$ for $0 \leq k \leq \overline{Q} - 1$ as

$$\underline{b}^{(l)} := \left[\underline{b}_0^{(l)}; \;\; \underline{b}_1^{(l)}; \;\; \ldots; \;\; \underline{b}_{\overline{Q}-1}^{(l)} \right], \tag{118}$$

and using the transformation in (117), and the definition in (118), we get

$$\underline{\dot{b}}^{(l)} := \left[\underline{\dot{b}}_0^{(l)}; \;\; \underline{\dot{b}}_1^{(l)}; \;\; \ldots; \;\; \underline{\dot{b}}_{\overline{Q}-1}^{(l)} \right] = \left(\underline{\underline{I}}_{\overline{Q}} \otimes \underline{\underline{T}}_{CP} \right) \underline{b}^{(l)}. \tag{119}$$

In the next two sections, we develop linear models for both receiver architectures with the vector $\underline{b}^{(l)}$ acting as the input to the model.

5.2 Receiver Design with Matched-Filter (MF) Front end

We consider a receiver that uses a MF front end with one filter matched to each of the $\overline{Q}$ Laurent pulses $\bar{g}_k(t)$. The MF bank is shown in Fig. 26. We assume a quasi-static $\overline{T}$-spaced channel model such that (113) can be expressed as

$$r(t) = \sum_{\nu=0}^{\overline{L}_c} c_\nu s(t - \nu\overline{T}) + \eta(t), \tag{120}$$

where $\overline{L}_c := \lceil L_c/H \rceil$. The MF-based receiver ([11, 22]) correlates the received signal with the current Laurent pulses to generate the following statistics for symbol detection:

$$\sigma_{q,i} := \int r(t) g_{q,(i)_H}(t - iT)dt. \tag{121}$$

Correlation of the received signal with the re-labelled Laurent pulses, i.e.,

$$r_{k,m} := \int r(t)\bar{g}_k(t - m\overline{T})dt, \tag{122}$$

also result in exactly the same statistics. For example, if (k, m) and (q, i) are related by (108), then $r_{k,m} = \sigma_{q,i}$. Using (120), (122) can be written as

$$r_{k,m} = \int \sum_{\nu=0}^{\overline{L}_c} c_\nu s(t - \nu\overline{T})\bar{g}_k(t - m\overline{T})dt + \eta_{k,m}, \tag{123}$$

where $\eta_{k,m} := \int n(t)\bar{g}_k(t - m\overline{T})dt$. Using the Laurent expansion in (112), (123) becomes

$$r_{k,m} = \sum_{\nu=0}^{\overline{L}_c} c_\nu \sum_{\acute{m}} \sum_{\acute{k}=0}^{\overline{Q}-1} b_{\acute{k},\acute{m}} \int \bar{g}_{\acute{k}}\big(t-(\acute{m}+\nu)\overline{T}\big)\bar{g}_k(t-m\overline{T})dt + \eta_{k,m}$$

If we define the cross-correlation between Laurent pulses as

$$\omega_{\acute{k},m_0}(k) := \int \bar{g}_{\acute{k}}(t + m_0\overline{T})\bar{g}_k(t)dt, \tag{124}$$

then the output of the MFs can be expressed as the following linear convolution:

$$\begin{aligned} r_{k,m} &= \sum_{\acute{k}=0}^{\overline{Q}-1} \sum_{\acute{m}} \sum_{\nu=0}^{L_c} c_\nu b_{\acute{k},\acute{m}} \omega_{\acute{k},m-\acute{m}-\nu}(k) + \eta_{k,m}, \\ &= \sum_{\acute{k}=0}^{\overline{Q}-1} c_m \star \omega_{\acute{k},m}(k) \star b_{\acute{k},m} + \eta_{k,m}. \end{aligned} \tag{125}$$

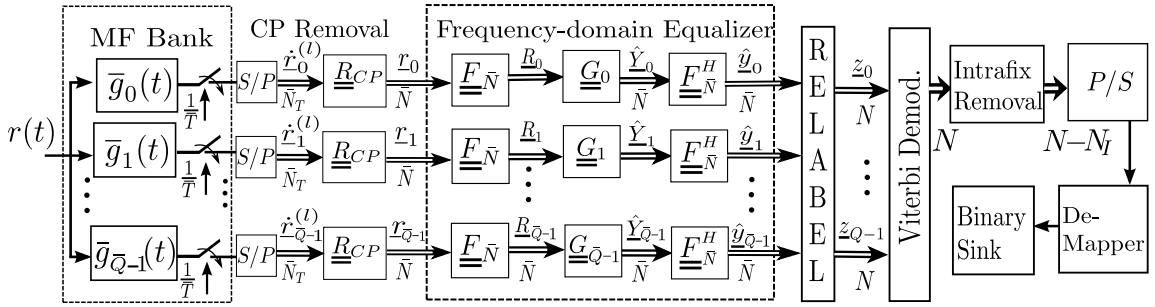

Figure 26: Block diagram of the proposed MF-based FDE receiver. Double-lined connections between the blocks represent a vector. The label of the vector is mentioned on the top of the connection and its dimension is specified on the bottom. S/P and P/S denote serial-to-parallel and parallel-to-serial converters, respectively.

In the next section, we use the cyclic construction of the transmit-block to show that this linear convolution can be re-interpreted as an equivalent circular convolution for the duration of the block.

5.2.1 Time-domain Matrix Model for MF Technique

The outputs of k-th MF corresponding to the l-th block can be represented by a column vector:

$$\underline{\dot{r}}_k^{(l)} \triangleq [r_{l\overline{N}_T,k} \;\; r_{l\overline{N}_T+1,k} \;\; \dots r_{(l+1)\overline{N}_T-1,k}]^T.$$

In the following, we use the assumption that the channel is quasi-static (it is constant for each transmitted block but fades independently from one block to other). Using (125), and similar analysis as [25], this vector $\underline{\dot{r}}_k^{(l)}$ can be expressed as the following matrix equation:

$$\begin{aligned}\underline{\dot{r}}_k^{(l)} &= \underline{\underline{c}}_0^{(l)}[\underline{\underline{\omega}}_{0,0}^k \;\; \underline{\underline{\omega}}_{1,0}^k \;\; \dots \underline{\underline{\omega}}_{\overline{Q}-1,0}^k](\underline{\underline{I}}_{\overline{Q}} \otimes \underline{\underline{T}}_{CP})\underline{b}^{(l)} \\ &+ \underline{\underline{c}}_1^{(l)}[\underline{\underline{\omega}}_{0,1}^k \;\; \underline{\underline{\omega}}_{1,1}^k \;\; \dots \underline{\underline{\omega}}_{\overline{Q}-1,1}^k](\underline{\underline{I}}_{\overline{Q}} \otimes \underline{\underline{T}}_{CP})\underline{b}^{(l-1)} + \underline{\dot{\eta}}_k^{(l)}, \end{aligned} \tag{126}$$

where the matrices are defined in terms of pulse correlations (see (124)) and channel coefficients as follows:

$$\begin{aligned}
[\underline{\underline{\omega}}^{k}_{\acute{k},0}]_{(n,m)} &:= \omega_{\acute{k},n-m}(k), \\
[\underline{\underline{\omega}}^{k}_{\acute{k},1}]_{(n,m)} &:= \omega_{\acute{k},\overline{N}_T+n-m}(k), \\
[\underline{\underline{c}}^{(l)}_{0}]_{(n,m)} &:= c^{(l)}_{n-m}, \\
[\underline{\underline{c}}^{(l)}_{1}]_{(n,m)} &:= c^{(l-1)}_{\overline{N}_T+n-m},
\end{aligned}$$

and $\dot{\underline{\eta}}^{(l)}_{k} := [\eta_{l\overline{N}_T,k},\, \eta_{l\overline{N}_T+1,k},\, \ldots\, \eta_{(l+1)\overline{N}_T-1,k}]^T$, where $\forall k, \acute{k} \in \mathbb{N}_{\overline{Q}}$ and $\forall n, m \in \mathbb{N}_{\overline{N}_T}$. Note that the l-th received vector (in (126)) has a term representing the inter-block interference (IBI), which depends upon the pseudo-symbols of $(l-1)$-th block, i.e., $\underline{b}^{(l-1)}$. Also, note that owing to the block-fading channel, the channel convolution in this IBI term is with the impulse response of the channel realized in the previous block.

Removal of the cyclic prefix at the receiver removes the inter-block interference (IBI), and can be represented by the matrix $\underline{\underline{R}}_{CP} := [\underline{\underline{0}}_{\overline{N}\times\overline{N}_P}, \underline{\underline{I}}_{\overline{N}}]$. Applying $\underline{\underline{R}}_{CP}$ to $\dot{\underline{r}}_k$ results in the following vector:

$$\begin{aligned}
\underline{r}^{(l)}_{k} &:= \underline{\underline{R}}_{CP}\dot{\underline{r}}^{(l)}_{k}, \\
&= \underline{\underline{R}}_{CP}\underline{\underline{c}}^{(l)}_{0}[\underline{\underline{\omega}}^{k}_{0,0}\ \underline{\underline{\omega}}^{k}_{1,0}\ \cdots \underline{\underline{\omega}}^{k}_{\overline{Q}-1,0}](\underline{\underline{I}}_{\overline{Q}} \otimes \underline{\underline{T}}_{CP})\underline{b}^{(l)} + 0 + \underline{\underline{R}}_{CP}\dot{\underline{\eta}}^{(l)}_{k}, \\
\underline{r}_{k} &= \underline{\underline{R}}_{CP}\underline{\underline{c}}\left[\underline{\underline{\omega}}^{k}_{0}\underline{\underline{T}}_{CP}\ \underline{\underline{\omega}}^{k}_{1}\underline{\underline{T}}_{CP}\ \cdots \underline{\underline{\omega}}^{k}_{\overline{Q}-1}\underline{\underline{T}}_{CP}\right]\underline{b} + \underline{\eta}_{k}, \qquad (127)
\end{aligned}$$

where $\underline{\eta}_{k} := \underline{\underline{R}}_{CP}\dot{\underline{\eta}}_{k}$. Note that we have removed the block index l and the extra sub-script of the sub-matrices from the notation to indicate the independence of $\underline{r}_k$ from the previous block. Choosing $N_P > L_C + L$, it can be shown that

$$\underline{\underline{R}}_{CP}\underline{\underline{c}}\ \underline{\underline{\omega}}^{k}_{\acute{k}}\ \underline{\underline{T}}_{CP} = \underline{\underline{R}}_{CP}\underline{\underline{c}}\ \underline{\underline{T}}_{CP}\underline{\underline{R}}_{CP}\ \underline{\underline{\omega}}^{k}_{\acute{k}}\ \underline{\underline{T}}_{CP},$$

which implies that

$$\underline{r}_{k} = \underline{\underline{R}}_{CP}\underline{\underline{c}}\ \underline{\underline{T}}_{CP}[\underline{\underline{R}}_{CP}\underline{\underline{\omega}}^{k}_{0}\underline{\underline{T}}_{CP},\ \underline{\underline{R}}_{CP}\underline{\underline{\omega}}^{k}_{1}\underline{\underline{T}}_{CP}, \cdots,\ \underline{\underline{R}}_{CP}\underline{\underline{\omega}}^{k}_{\overline{Q}-1}\underline{\underline{T}}_{CP}]\underline{b} + \underline{\eta}_{k}, \qquad (128)$$

and can be further written as

$$\underline{r}_k = \underline{\underline{\dot{c}}}[\underline{\underline{\dot{\omega}}}_0^k \;\; \underline{\underline{\dot{\omega}}}_1^k \cdots \underline{\underline{\dot{\omega}}}_{\bar{Q}-1}^k]\underline{b} + \underline{\eta}_k,$$

where for all matrices $\underline{\underline{x}}$,

$$\underline{\underline{\dot{x}}} := \underline{\underline{R}}_{CP}\underline{\underline{x}}\,\underline{\underline{T}}_{CP},$$

and it is a circulant matrix, with entries $[\underline{\underline{\dot{x}}}]_{(n,m)} = [\underline{\underline{x}}]_{(n-m)_{\overline{N}},1}$ [13]. Now, $\underline{r}_k$ can be expressed compactly as

$$\underline{r}_k = \underline{\underline{\dot{c}}}\,\underline{\underline{\omega}}_k\,\underline{b} + \underline{\eta}_k, \tag{129}$$

while

$$\underline{\underline{\omega}}_k := [\underline{\underline{\dot{\omega}}}_0^k,\;\; \underline{\underline{\dot{\omega}}}_1^k, \cdots, \underline{\underline{\dot{\omega}}}_{\bar{Q}-1}^k],$$

is the correlation matrix for k-th Laurent pulse. Each sub-matrix in (129) has the desired circulant property. To illustrate the structure of the matrices in (129), we present a visual description in Fig. 27. Note that the correlation matrices has $\bar{N} \times \bar{N}$ sub-matrices, all of which are circulant. By concatenating all the vectors $\underline{r}_k$, $\forall k \in \mathbb{N}_{\bar{Q}}$, in a single vector, we can define

$$\underline{r} := [\underline{r}_0;\; \underline{r}_1; \cdots \underline{r}_{\bar{Q}-1}], \tag{130}$$

and use (129) to arrive at

$$\underline{r} = \underline{\underline{c}}_{\bar{Q}}\underline{\underline{\omega}}\,\underline{b} + \underline{\eta}, \tag{131}$$

where $\underline{\underline{\omega}} := [\underline{\underline{\omega}}_0;\; \underline{\underline{\omega}}_1; \cdots ; \underline{\underline{\omega}}_{\bar{Q}-1}]$, $\underline{\eta} := [\underline{\eta}_0;\; \underline{\eta}_1; \cdots \underline{\eta}_{\bar{Q}-1}]$, and $\underline{\underline{c}}_{\bar{Q}} := \underline{\underline{I}}_{\bar{Q}} \otimes \underline{\underline{\dot{c}}}$. So far, we have obtained a time-domain matrix model of (129) and (131), which expresses the vector $\underline{r}$, containing all the outputs of the MF bank for a given block, in terms of the vector of pseudo-symbols $\underline{b}$. The matrices appearing in the model, i.e., $\underline{\underline{\omega}}$ and $\underline{\underline{c}}_{\bar{Q}}$ have the desired structure, i.e., the sub-matrices of size $\bar{N} \times \bar{N}$ are circulant.

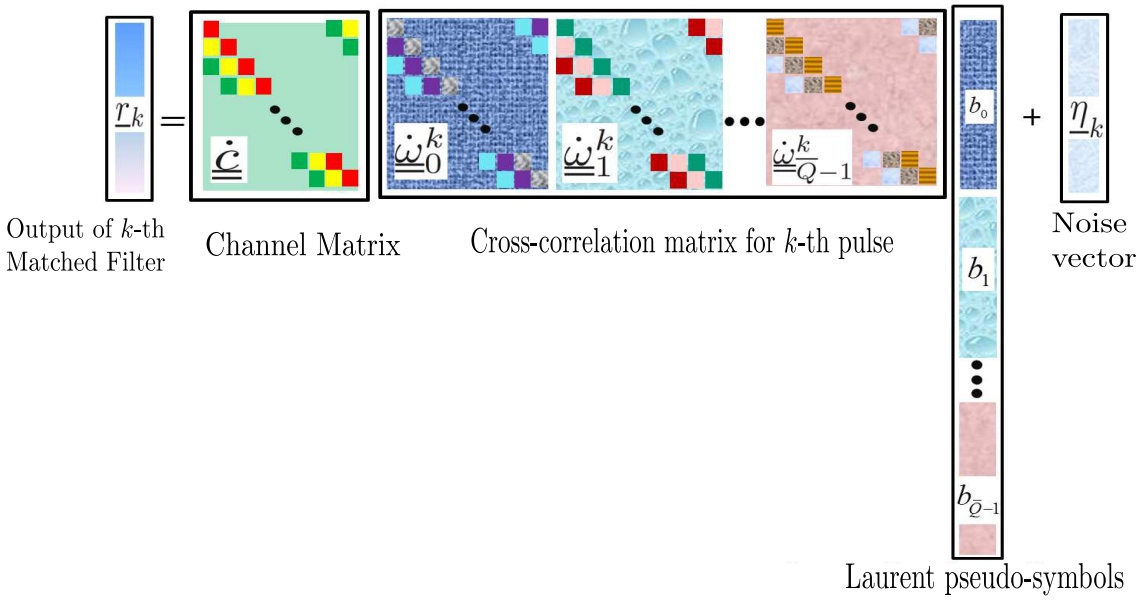

Figure 27: A visual representation of the matrix model for matched-filter(MF) front end given by (129). Distinctly colored blocks of the cross-correlation matrix denote $\bar{N} \times \bar{N}$ sub-matrices.

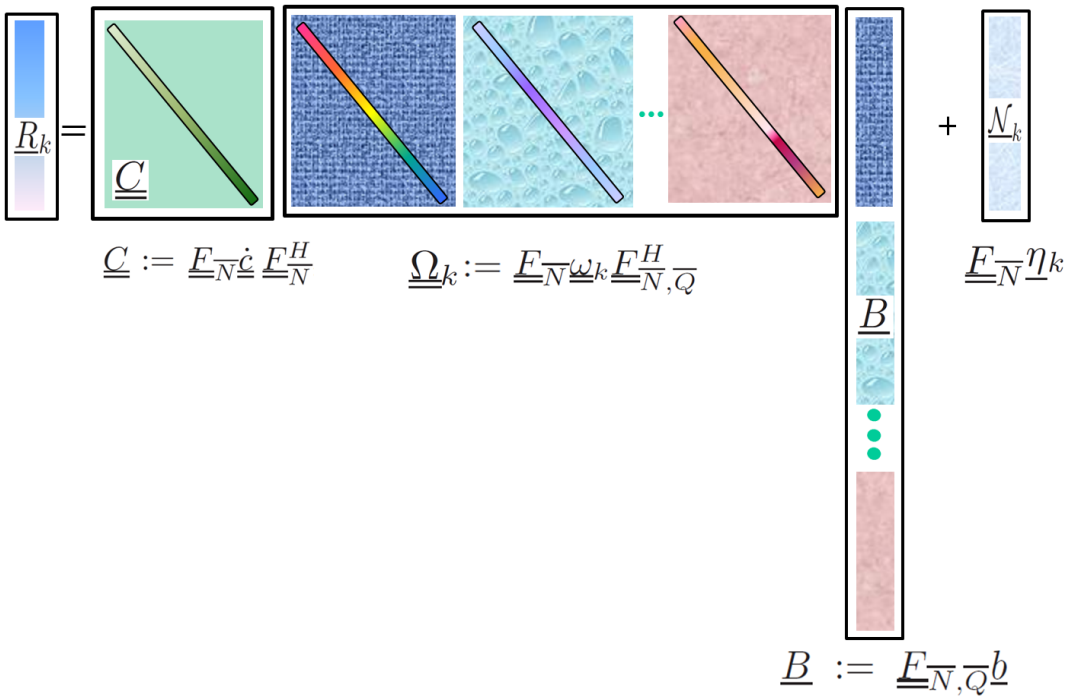

Figure 28: Frequency-domain model for the matched-filter (MF) front end receiver. In the frequency-domain, all the sub-matrices are diagonal, which is very desirable in computation of the FDE.

5.2.2 Frequency-domain Model for MF Technique

In this section, we convert the time-domain matrix model, in (129) and (131) to the frequency domain. For this purpose, we use the fact that a circulant matrix is diagonalized by the FFT-matrix, i.e., for any circulant matrix $\underline{\underline{\dot{x}}}$,

$$\underline{\underline{X}} := \underline{\underline{F}}_{\overline{N}} \underline{\underline{\dot{x}}} \, \underline{\underline{F}}_{\overline{N}}^{H}, \tag{132}$$

is a diagonal matrix, where

$$[F_{\overline{N}}]_{(m,n)} := \frac{1}{\sqrt{\overline{N}}} \exp\left(\frac{-j2\pi mn}{\overline{N}}\right), \forall m, n \in \mathbb{N}_{\overline{N}}.$$

We also make the following definition:

$$\underline{\underline{F}}_{\overline{N},\overline{Q}} := \underline{\underline{I}}_{\overline{Q}} \otimes \underline{\underline{F}}_{\overline{N}}.$$

The matrix model in (129) can then be expressed in the frequency domain as follows:

$$\begin{aligned} \underline{R}_k : &= \underline{\underline{F}}_{\overline{N}} \underline{r}_k, \\ &= \underline{\underline{C}} \, \underline{\underline{\Omega}}_k \, \underline{B} + \underline{\mathcal{N}}_k, \end{aligned} \tag{133}$$

where

$$\underline{\underline{C}} := \underline{\underline{F}}_{\overline{N}} \underline{\underline{\dot{c}}} \, \underline{\underline{F}}_{\overline{N}}^{H},$$

is a diagonal $\overline{N} \times \overline{N}$ matrix, and

$$\underline{\underline{\Omega}}_k := \underline{\underline{F}}_{\overline{N}} \underline{\underline{\omega}}_k \underline{\underline{F}}_{\overline{N},\overline{Q}}^{H}, \tag{134}$$

is a matrix with one diagonal block corresponding to each circulant sub-matrix in $\underline{\underline{\omega}}_k$. Also, $\underline{B} := \underline{\underline{F}}_{\overline{N},\overline{Q}} \underline{b}$ and $\underline{\mathcal{N}}_k := \underline{\underline{F}}_{\overline{N}} \underline{\eta}_k$ are the column vectors of all the pseudo-symbols and noise in the frequency domain, respectively. The consolidated model for all the pulses can be obtained by defining

$$\underline{R} := [\underline{R}_0; \, \underline{R}_1; \cdots \underline{R}_{\overline{Q}-1}], \tag{135}$$

and it can be seen that

$$\underline{R} = \underline{\underline{F}}_{\overline{N},\overline{Q}}\underline{r}, \tag{136}$$

$$= \underline{\underline{C}}_{\overline{Q}}\underline{\underline{\Omega}}\,\underline{B} + \underline{\mathcal{N}}, \tag{137}$$

where $\underline{\underline{C}}_{\overline{Q}} := \underline{\underline{I}}_{\overline{Q}} \otimes \underline{\underline{C}}$, $\underline{\mathcal{N}} := \underline{\underline{F}}_{\overline{N},\overline{Q}}\underline{\eta}$, and

$$\underline{\underline{\Omega}} := \underline{\underline{F}}_{\overline{N},\overline{Q}}\,\underline{\underline{\omega}}\,\underline{\underline{F}}^{H}_{\overline{N},\overline{Q}},$$

$$= [\underline{\underline{\Omega}}_0;\ \underline{\underline{\Omega}}_1; \cdots ; \underline{\underline{\Omega}}_{\overline{Q}-1}]. \tag{138}$$

5.2.3 Frequency-domain Equalizer for MF Technique

The matrix model derived in the previous sub-section relates the output of the MF-bank with the pseudo-symbols corresponding to the current block. This model has a special property that it isolates the transformation of the channel (i.e., $\underline{\underline{C}}$) and the combined effect of the modulator and the MF-bank (i.e., $\underline{\underline{\Omega}}_k$) on the pseudo-symbols $\underline{B}$. A similar model was derived in [25] for single-h CPM, and two approaches were discussed for equalizer/receiver design. The first one, equalizes the product $\underline{\underline{C}}\,\underline{\underline{\Omega}}_k$ and the demodulator detects the sequence of psuedo-symbols. The second approach equalizes only the channel $\underline{\underline{C}}$ in the frequency domain and the correlation between the Laurent pulses is passed to the demodulator for sequence detection. We follow the latter approach, and define $\underline{Y}_k := \underline{\underline{\Omega}}_k\,\underline{B}$, then (133) becomes

$$\underline{R}_k = \underline{\underline{C}}\,\underline{Y}_k + \underline{\mathcal{N}}_k \tag{139}$$

Using this model, the zero-forcing (ZF) equalizer can be defined as

$$\underline{\underline{G}}^{ZF}_k = \left[\underline{\underline{C}}^{H}\underline{\underline{C}}\right]^{-1}\underline{\underline{C}}^{H}, \tag{140}$$

and the MMSE equalizer is given by

$$\underline{\underline{G}}_k := \underline{\underline{\mathfrak{R}}}^{(k)}_{YY}\underline{\underline{C}}^{H}[\underline{\underline{C}}\,\underline{\underline{\mathfrak{R}}}^{(k)}_{YY}\underline{\underline{C}}^{H} + \underline{\underline{\mathfrak{R}}}^{(k)}_{\mathcal{N}\mathcal{N}}]^{-1}, \tag{141}$$

where

$$\underline{\underline{\mathfrak{R}}}_{YY}^{(k)} := \mathbf{E}[\underline{Y}_k \underline{Y}_k^H], \tag{142}$$

is the correlation matrix for $\underline{Y}_k$, and

$$\underline{\underline{\mathfrak{R}}}_{\mathcal{N}\mathcal{N}}^{(k)} := \mathbf{E}[\underline{\mathcal{N}}_k \underline{\mathcal{N}}_k^H],$$

is the correlation matrix for $\underline{\mathcal{N}}_k$. These correlation matrices can be computed off-line from the correlation between pseudo-symbols and the Laurent pulses, respectively. For details, see [21]. An application of the matrix inversion lemma to (141), results in an alternate expression for the MMSE equalzier:

$$\underline{\underline{G}}_k = [\underline{\underline{\mathfrak{R}}}_{YY}^{(k)\,-1} + \underline{\underline{C}}^H \underline{\underline{\mathfrak{R}}}_{\mathcal{N}\mathcal{N}}^{(k)\,-1} \underline{\underline{C}}]^{-1} \underline{\underline{C}}^H \underline{\underline{\mathfrak{R}}}_{\mathcal{N}\mathcal{N}}^{(k)\,-1}. \tag{143}$$

The output of the FDE is given by

$$\underline{\hat{Y}}_k = \underline{\underline{G}}_k \underline{R}_k, \quad \forall k \in \mathbb{N}_{\overline{Q}}. \tag{144}$$

After FDE, $\underline{\hat{Y}}_k$ is converted to the time domain by an $\overline{N}$-point IFFT, for each $k \in \mathbb{N}_{\overline{Q}}$, i.e., we get

$$\underline{\hat{y}}_k = \underline{\underline{F}}_N^H \underline{\hat{Y}}_k. \tag{145}$$

Using the transformation (108), we re-label the computed statistics as follows:

$$z_{q,i} = \hat{y}_{k,m}, \forall k \in \mathbb{N}_{\overline{Q}}, m \in \mathbb{N}_{\overline{N}}, q \in \mathbb{N}_Q, \text{and } i \in \mathbb{N}_N. \tag{146}$$

Note that the outputs $z_{q,i}$ are obtained after ISI removal by the FDE and correspond to ones at the output of the MF for an AWGN channel. Thus, we can now utilize the Viterbi demodulator for multi-h CPM, proposed by [22]. The j-th branch metric, with Laurent pseudo-symbol hypothesis $\check{a}_{q,(i)_H}^{*(j)}$, for each time instant i is computed as

$$\lambda_i^{(j)} := \mathrm{Re}\left(\sum_{q=0}^{Q-1} z_{q,i} \check{a}_{q,(i)_H}^{*(j)} \right), \tag{147}$$

and the path corresponding to maximum cumulative metric determines the detected sequence of symbols $\check{x}_n^{(l)}$. All the receiver operations described above are shown in Fig. 26. We discuss the computational complexity of different operations in the MF receiver in Section 5.4, while the performance results, simulated for an aeronautical telemetry model, are presented in Section 5.5.

5.3 Receiver Design with Sampling-based Front end

In the last section, we presented a detailed discussion on FDE design in the situation when a matched-filter front end is utilized. We observed that a matrix model with a circulant sub-structure leads to much simplification in the computation of FDE. However, we observed that one FDE branch (an FFT-IFFT pair and equalization filter) is required for each Laurent pulse. In this section, we develop another receiver architecture which gets rid of the large number of filters in the MF-bank and the equalizer. This architecture makes use of the observation that for most of the CPM modulation schemes, the power-spectrum is very compact, and there is little energy beyond $1/T$ Hz. Thus a front end consisting of an anti-aliasing low-pass filter $\psi_r(t)$ and a fractional sampler can be used instead of a whole bank of matched filters. We name this architecture as the sampling filter(SF)-based FDE design.

Some of the details in the development of SF matrix model are very similar to those used in the previous section on MF-based design. Hence, many quantities (matrices, vectors, signals) analogous to those found in MF-based approach appear here. Whenever possible, we use similar notation for such quantities except that, for distinction and comparison, we use a $\tilde{(.)}$ (super-script) in this section.

In this section also, we assume that the received signal $r(t)$ is given by (113), i.e., the transmitted signal $s(t, \mathbf{x})$ is filtered by a frequency-selective channel $c(t)$, and the white Guassian noise $\eta(t)$ is added to the result. This channel model is also depicted in Fig. 24.

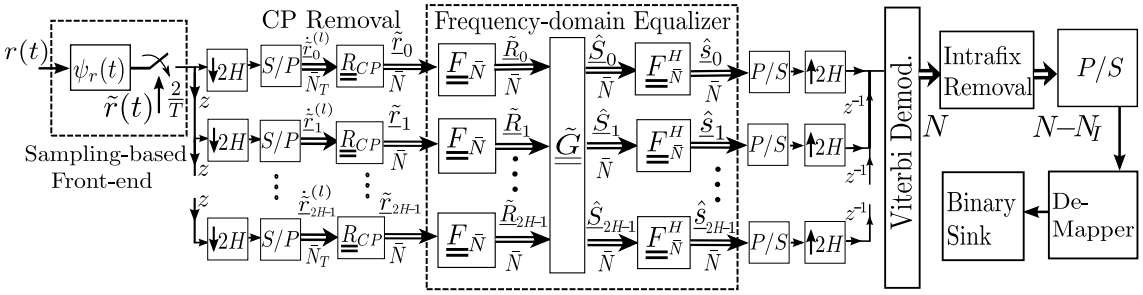

Figure 29: Block diagram of the proposed SF-based FDE receiver. A double-lined connection between the blocks represents a vector. The label of the vector is mentioned above the connection and the dimension of the vector is specified below the connection.

For this SF-based architecture, the received signal $r(t)$ is passed through a low-pass filter $\psi_r(t)$ and sampled at twice the symbol rate $1/T$. The overall impulse response of the channel and the receiver filter can be defined as $\tilde{c}(t) := c(t) \star \psi_r(t)$. A detailed block diagram of the SF-based receiver architecture is shown in Fig. 29.

Since all the processing following the front end is performed at the fractional rate of $2/T$, we assume that the overall response $\tilde{c}(t)$ can be equivalently expressed by $T/2$-spaced samples. Thus, $\tilde{r}(t)$ can be written as

$$\tilde{r}(t) = \sum_{\nu} \tilde{s}_\nu \tilde{c}(t - \nu T/2) + \tilde{\eta}(t), \tag{148}$$

where $\tilde{\eta}(t) := \eta(t) \star \psi_r(t)$ is the noise term, and the fractionally sampled CPM signal $\tilde{s}_n$ is defined as

$$\tilde{s}_n := s(t, \mathbf{x})|_{t=\frac{nT}{2}}, \tag{149}$$

$$= \sum_{k=0}^{\overline{Q}-1} \sum_{m} b_{k,m} \tilde{g}_{k,n-2mH}, \tag{150}$$

where $\tilde{g}_{k,n} := \bar{g}_k(t)|_{t=\frac{nT}{2}}$, are the fractional samples of re-labelled Laurent pulses, and $b_{k,m}$ are the pseudo-symbols (see (112)).

Now, we utilize the polyphase decomposition of the sampled signal, and try to express it as a discrete linear convolution. For a modulation scheme with H modulation indices, the sampled received signal is decomposed into $2H$ polyphase components

(see Fig. 29). The sequence of i-th polyphase component is defined as

$$\tilde{r}_n^i := \tilde{r}(t)|_{t=(2nH+i)\frac{T}{2}}, \tag{151}$$

and by using (148) and (149), it can be written as

$$\begin{aligned}\tilde{r}_n^i &= \sum_{\nu} \tilde{s}_\nu \tilde{c}\left((2nH+i-\nu)\,T/2\right) + \tilde{\eta}_n^i, \\ &= \sum_{\nu} \tilde{s}_\nu \tilde{c}_{2nH+i-\nu} + \tilde{\eta}_n^i,\end{aligned} \tag{152}$$

where $\tilde{c}_n := \tilde{c}(t)|_{t=\frac{nT}{2}}$ is the sequence of samples of overall channel impulse response, and $\tilde{\eta}_n^i := \tilde{\eta}(t)|_{t=(2nH+i)\frac{T}{2}}$ is the i-th polyphase component of the filtered noise process.

To write $\tilde{r}_n^i$ as a linear convolution, we define new variables $j := (\nu)_{2H}$ and $m := \lfloor \nu/2H \rfloor$, and use them to split the single summation in (152) into two as follows:

$$\begin{aligned}\tilde{r}_n^i &:= \sum_{j\in\mathbb{N}_{2H}} \sum_{m} \tilde{s}_m^j \tilde{c}_{2nH+i-(2mH+j)} + \tilde{\eta}_n^i, \\ &= \sum_{j\in\mathbb{N}_{2H}} \sum_{m} \tilde{s}_m^j \tilde{c}_{n-m}^{i-j} + \tilde{\eta}_n^i,\end{aligned} \tag{153}$$

where $\tilde{s}_m^j$ is the j-th polyphase component of the sampled multi-h CPM signal, i.e.,

$$\tilde{s}_m^j := \tilde{s}_{2mH+j} = \sum_{k=0}^{\overline{Q}-1} \sum_{\acute{n}} b_{k,\acute{n}} \tilde{g}_{k,m-\acute{n}}^j. \tag{154}$$

The second equality follows from (112) and the definition $\tilde{g}_{k,m}^j := \tilde{g}_{k,2mH+j}$. Now using (154), (153) becomes

$$\begin{aligned}\tilde{r}_n^i &= \sum_{j\in\mathbb{N}_{2H}} \sum_{m} \sum_{k=0}^{\overline{Q}-1} \sum_{\acute{n}} b_{k,\acute{n}} \tilde{g}_{k,m-\acute{n}}^j \tilde{c}_{n-m}^{i-j} + \tilde{\eta}_n^i, \\ &= \sum_{j\in\mathbb{N}_{2H}} \tilde{c}_n^{i-j} \star \left(\sum_{k=0}^{\overline{Q}-1} b_{k,n} \star \tilde{g}_{k,n}^j \right) + \tilde{\eta}_n^i; i,j \in \mathbb{N}_{2H}.\end{aligned} \tag{155}$$

So far, we have expressed the the i-th polyphase component of the output of the receiver front end as the repeated convolution of pseudo-symbols, with the polyphase components of the sampled Laurent pulses and the polyphase components of the

overall-impulse response (i.e., channel and receiver filter), and the polyphase component of the noise. In the next sub-section, we use the cyclic properties of the transmitted block (as discussed in Section 5.1) to interpret these linear convolutions as circular for the duration of the block.

5.3.1 Time-domain Matrix Model for SF-based Technique

The i-th polyphase component for the l-th block can be represented by a column vector: $\dot{\underline{\tilde{r}}}_i^{(l)} := \left[\tilde{r}^i_{l\overline{N}_T}\ \tilde{r}^i_{l\overline{N}_T+1}\ \cdots\ \tilde{r}^i_{(l+1)\overline{N}_T-1}\right]^T$. Using (155), and similar analysis as [25], this vector $\dot{\underline{\tilde{r}}}_i^{(l)}$ can be expressed as the following matrix equation:

$$\begin{aligned}\dot{\underline{\tilde{r}}}^{(l)} := \begin{bmatrix}\dot{\underline{\tilde{r}}}_0^{(l)}\\ \vdots \\ \dot{\underline{\tilde{r}}}_i^{(l)}\\ \vdots \\ \dot{\underline{\tilde{r}}}_{2H-1}^{(l)}\end{bmatrix} = \begin{bmatrix}\underline{\underline{\tilde{c}}}_0^{(0,l)}, \cdots, \underline{\underline{\tilde{c}}}_0^{(-2H+1,l)} \\ \ddots \\ \underline{\underline{\tilde{c}}}_0^{(i-j,l)} \\ \ddots \\ \underline{\underline{\tilde{c}}}_0^{(2H-1,l)}, \cdots, \underline{\underline{\tilde{c}}}_0^{(0,l)}\end{bmatrix}\begin{bmatrix}\underline{\underline{\tilde{g}}}_{0,0}^{(0)}, \cdots, \underline{\underline{\tilde{g}}}_{\overline{Q}-1,0}^{(0)} \\ \ddots \\ \underline{\underline{\tilde{g}}}_{k,0}^{(j)} \\ \ddots \\ \underline{\underline{\tilde{g}}}_{0,0}^{(2H-1)}, \cdots, \underline{\underline{\tilde{g}}}_{\overline{Q}-1,0}^{(2H-1)}\end{bmatrix}(\underline{\underline{I}}_{\overline{Q}} \otimes \underline{\underline{T}}_{CP})\underline{b}^{(l)} \\ + \begin{bmatrix}\underline{\underline{\tilde{c}}}_1^{(0,l)}, \cdots, \underline{\underline{\tilde{c}}}_1^{(-2H+1,l)} \\ \ddots \\ \underline{\underline{\tilde{c}}}_1^{(i-j,l)} \\ \ddots \\ \underline{\underline{\tilde{c}}}_1^{(2H-1,l)}, \cdots, \underline{\underline{\tilde{c}}}_1^{(0,l)}\end{bmatrix}\begin{bmatrix}\underline{\underline{\tilde{g}}}_{0,1}^{(0)}, \cdots, \underline{\underline{\tilde{g}}}_{\overline{Q}-1,1}^{(0)} \\ \ddots \\ \underline{\underline{\tilde{g}}}_{k,1}^{(j)} \\ \ddots \\ \underline{\underline{\tilde{g}}}_{0,1}^{(2H-1)}, \cdots, \underline{\underline{\tilde{g}}}_{\overline{Q}-1,1}^{(2H-1)}\end{bmatrix}(\underline{\underline{I}}_{\overline{Q}} \otimes \underline{\underline{T}}_{CP})\underline{b}^{(l-1)} + \begin{bmatrix}\dot{\underline{\tilde{\eta}}}_0^{(l)}\\ \vdots \\ \dot{\underline{\tilde{\eta}}}_i^{(l)}\\ \vdots \\ \dot{\underline{\tilde{\eta}}}_{2H-1}^{(l)}\end{bmatrix}, \end{aligned} \quad (156)$$

where the $\overline{N}_T \times \overline{N}_T$ sub-matrices are the convolution matrices of the polyphase components, and are defined as follows:

$$\begin{aligned}[\underline{\underline{\tilde{g}}}_{k,0}^{(j)}]_{(n,m)} &:= \tilde{g}^j_{k,n-m}, \\ [\underline{\underline{\tilde{g}}}_{k,1}^{(j)}]_{(n,m)} &:= \tilde{g}_{k,\overline{N}_T+n-m}, \\ [\underline{\underline{\tilde{c}}}_0^{(i-j,l)}]_{(n,m)} &:= \tilde{c}^{(i-j,l)}_{n-m}, \\ [\underline{\underline{\tilde{c}}}_1^{(i-j,l)}]_{(n,m)} &:= \tilde{c}^{(i-j,l-1)}_{\overline{N}_T+n-m}, \end{aligned} \quad (157)$$

$\forall i, j \in \mathbb{N}_{2H}$, $\forall n, m \in \mathbb{N}_{\overline{N}_T}$, and $\forall k \in \mathbb{N}_{\overline{Q}}$. The i-th polyphase component of noise for the l-th block is represented by the vector, $\underline{\dot{\tilde{\eta}}}_i^{(l)} := [\tilde{\eta}^i_{l\overline{N}_T},\ \tilde{\eta}^i_{l\overline{N}_T+1},\ \ldots,\ \tilde{\eta}^i_{(l+1)\overline{N}_T-1}]^T$. The second term in (156) represents the IBI. Both the first and second term represent a series of linear operations (i.e., cyclic prefix insertion, modulation by the Laurent pulses, and the convolution with the channel) on the vector of pseudo-symbols. All the non-linear operations (i.e, phase modulation and intrafix insertion) are concealed in the construction of the vector of pseudo-symbols. The third term in (156) is the contribution of filtered noise.

When written compactly, the i-th polyphase compact in (156) can be equivalently expressed as

$$\underline{\dot{\tilde{r}}}_i^{(l)} = \sum_{j=0}^{2H-1} \underline{\underline{\tilde{c}}}_0^{(i-j,l)} \sum_{k=0}^{\overline{Q}-1} \underline{\underline{\tilde{g}}}_{k,0}^{(j)} \underline{\underline{T}}_{CP} \underline{b}_k^{(l)} + \sum_{j=0}^{2H-1} \underline{\underline{\tilde{c}}}_1^{(i-j,l)} \sum_{k=0}^{\overline{Q}-1} \underline{\underline{\tilde{g}}}_{k,1}^{(j)} \underline{\underline{T}}_{CP} \underline{b}_k^{(l-1)} + \underline{\dot{\tilde{\eta}}}_i^{(l)}, \forall i \in \mathbb{N}_{2H}. \tag{158}$$

Removal of the cyclic prefix at the receiver is equivalent to pre-multiplication of each polyphase component by the matrix $\underline{\underline{R}}_{CP}$, and we define the result as

$$\underline{\tilde{r}}_i^{(l)} := \underline{\underline{R}}_{CP} \underline{\dot{\tilde{r}}}_i^{(l)}, \forall i \in \mathbb{N}_{2H}. \tag{159}$$

Using (158), and defining $\underline{\tilde{\eta}}_i^{(l)} := \underline{\underline{R}}_{CP} \underline{\dot{\tilde{\eta}}}_i^{(l)}$, we can write $\forall i \in \mathbb{N}_{2H}$,

$$\begin{aligned} \underline{\tilde{r}}_i^{(l)} &= \sum_{j=0}^{2H-1} \underline{\underline{R}}_{CP} \underline{\underline{\tilde{c}}}_0^{(i-j,l)} \sum_{k=0}^{\overline{Q}-1} \underline{\underline{\tilde{g}}}_{k,0}^{(j)} \underline{\underline{T}}_{CP} \underline{b}_k^{(l)} + \sum_{j=0}^{2H-1} \underline{\underline{R}}_{CP} \underline{\underline{\tilde{c}}}_1^{(i-j,l)} \sum_{k=0}^{\overline{Q}-1} \underline{\underline{\tilde{g}}}_{k,1}^{(j)} \underline{\underline{T}}_{CP} \underline{b}_k^{(l-1)} + \underline{\tilde{\eta}}_i^{(l)}, \\ &= \sum_{j=0}^{2H-1} \sum_{k=0}^{\overline{Q}-1} \underline{\underline{R}}_{CP} \underline{\underline{\tilde{c}}}_0^{(i-j,l)} \underline{\underline{\tilde{g}}}_{k,0}^{(j)} \underline{\underline{T}}_{CP} \underline{b}_k^{(l)} + \sum_{j=0}^{2H-1} \sum_{k=0}^{\overline{Q}-1} \underline{\underline{R}}_{CP} \underline{\underline{\tilde{c}}}_1^{(i-j,l)} \underline{\underline{\tilde{g}}}_{k,1}^{(j)} \underline{\underline{T}}_{CP} \underline{b}_k^{(l-1)} + \underline{\tilde{\eta}}_i^{(l)}. \end{aligned} \tag{160}$$

Removing the cyclic prefix elimintes the IBI term (and assuming $N_{CP} > L_c + L + L_r$, where $L_r T$ is the support of $\psi_r(t)$), and the equation above simplifies:

$$\underline{\tilde{r}}_i^{(l)} = \sum_{j=0}^{2H-1} \sum_{k=0}^{\overline{Q}-1} \underline{\underline{R}}_{CP} \underline{\underline{\tilde{c}}}_0^{(i-j,l)} \underline{\underline{T}}_{CP} \underline{\underline{R}}_{CP} \underline{\underline{\tilde{g}}}_{k,0}^{j} \underline{\underline{T}}_{CP} \underline{b}_k^{(l)} + 0 + \underline{\tilde{\eta}}_i^{(l)}, \tag{161}$$

Since the dependence on the previous block and impulse response is now removed, we can drop the block index l and extra sub-script to get

$$\begin{aligned}\tilde{\underline{r}}_i &= \sum_{j=0}^{2H-1}\sum_{k=0}^{\overline{Q}-1} \underline{\underline{R}}_{CP}\tilde{\underline{\underline{c}}}^{(i-j)}\underline{\underline{T}}_{CP}\underline{\underline{R}}_{CP}\tilde{\underline{\underline{g}}}_k^{(j)}\underline{\underline{T}}_{CP}\underline{b}_k + \tilde{\underline{\eta}}_i, \\ &= \sum_{j=0}^{2H-1}\sum_{k=0}^{\overline{Q}-1} \dot{\underline{\underline{c}}}^{(i-j)}\dot{\underline{\underline{g}}}_k^{(j)}\underline{b}_k + \tilde{\underline{\eta}}_i. \end{aligned} \tag{162}$$

In the second equality, we are using the idea that a circulant matrix $\underline{\underline{\dot{x}}}$ is obtained from a pre- and post-multiplication of a convolution matrix $\underline{\underline{\dot{x}}}$ by $\underline{\underline{R}}_{CP}$ and $\underline{\underline{T}}_{CP}$, respectively [13].

Finally, collecting all the $2H$ polyphase components of (162) in a single vector, we obtain the desired matrix model:

$$\begin{aligned}\tilde{\underline{r}} &:= \left[\tilde{\underline{r}}_0; \cdots; \tilde{\underline{r}}_i, \cdots; \tilde{\underline{r}}_{2H-1}\right], \\ &= \left(\underline{\underline{I}}_{2H} \otimes \underline{\underline{R}}_{CP}\right)\dot{\tilde{\underline{r}}}^{(l)}, \end{aligned} \tag{163}$$

$$\underbrace{\begin{bmatrix} \tilde{\underline{r}}_0 \\ \vdots \\ \tilde{\underline{r}}_k \\ \vdots \\ \tilde{\underline{r}}_{\overline{Q}-1} \end{bmatrix}}_{\tilde{\underline{r}}} = \underbrace{\begin{bmatrix} \dot{\underline{\underline{c}}}^{(0)} & \cdots & \dot{\underline{\underline{c}}}^{(-2H+1)} \\ & \ddots & \\ & \dot{\underline{\underline{c}}}^{(i-j)} & \\ & \ddots & \\ \dot{\underline{\underline{c}}}^{(2H-1)} & \cdots & \dot{\underline{\underline{c}}}^{(0)} \end{bmatrix}}_{\dot{\tilde{\underline{\underline{c}}}}} \underbrace{\begin{bmatrix} \dot{\underline{\underline{g}}}_0^{(0)} & \cdots & \dot{\underline{\underline{g}}}_{\overline{Q}-1}^{(0)} \\ & \ddots & \\ & \dot{\underline{\underline{g}}}_k^{(j)} & \\ & \ddots & \\ \dot{\underline{\underline{g}}}_0^{(2H-1)} & \cdots & \dot{\underline{\underline{g}}}_{\overline{Q}-1}^{(2H-1)} \end{bmatrix}}_{\dot{\tilde{\underline{\underline{g}}}}} \underbrace{\begin{bmatrix} \underline{b}_0 \\ \vdots \\ \underline{b}_k \\ \vdots \\ \underline{b}_{\overline{Q}-1} \end{bmatrix}}_{\underline{b}} + \underbrace{\begin{bmatrix} \tilde{\underline{\eta}}_0 \\ \vdots \\ \tilde{\underline{\eta}}_k \\ \vdots \\ \tilde{\underline{\eta}}_{\overline{Q}-1} \end{bmatrix}}_{\tilde{\underline{\eta}}}$$

Using the above matrix definitions, we can write

$$\tilde{\underline{r}} = \dot{\tilde{\underline{\underline{c}}}}\,\dot{\tilde{\underline{\underline{g}}}}\,\underline{b} + \tilde{\underline{\eta}}. \tag{164}$$

A visual representation of this time-domain matrix model that emphasizes the circulant structure of the $\bar{N} \times \bar{N}$-sized sub-matrices of $\dot{\tilde{\underline{\underline{c}}}}$ and $\dot{\tilde{\underline{\underline{g}}}}$ is made in Fig. 30 for dual-h modulation schemes.

5.3.2 Frequency-domain Matrix Model for SF-based Technique

In this section, we transform the matrix model (164) developed in the previous section to the frequency domain. This transforms the circulant sub-matrices in the model to

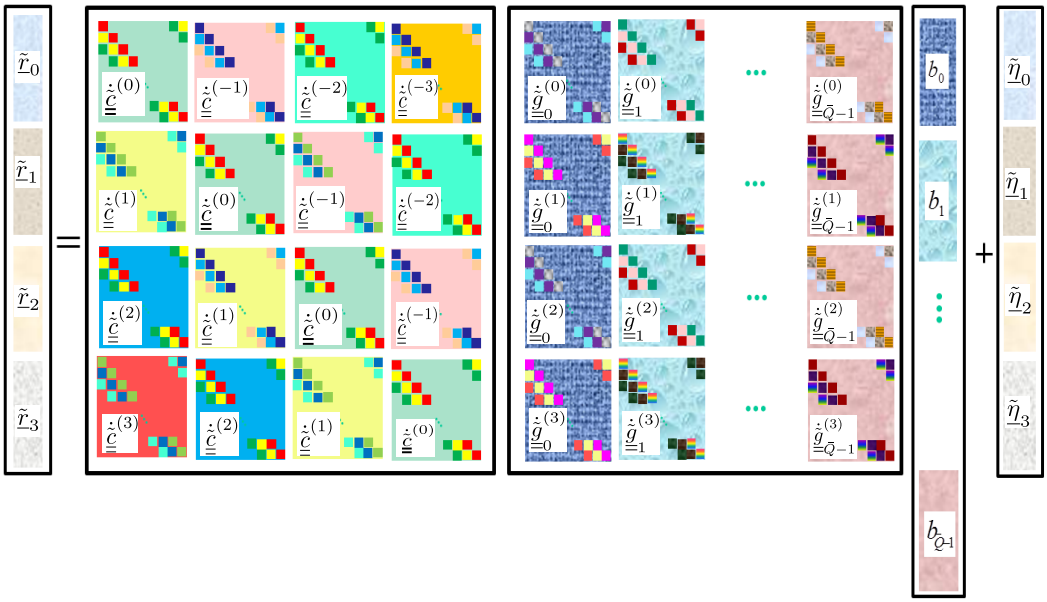

Figure 30: Time-domain matrix model for the polyphase components of a dual-h CPM modulation scheme.

diagonal matrices. Definitions and properties of FFT matrices from Section 5.2.2 are utitlized in this section.

We define the $\bar{N}$-point FFT of each polyphase component $\underline{\tilde{r}}_i$, as follows:

$$\underline{\tilde{R}}_i := \underline{\underline{F}}_{\bar{N}} \underline{\tilde{r}}_i, \forall i \in \mathbb{N}_{2H}. \tag{165}$$

A single vector obtained by concatenating all these frequency-transformed components $\underline{\tilde{R}}_i$ can be written as

$$\begin{aligned} \underline{\tilde{R}} &:= \left[\underline{\tilde{R}}_0; \cdots \underline{\tilde{R}}_i; \cdots ; \underline{\tilde{R}}_{2H-1}\right], \\ &= \left[\underline{\underline{F}}_{\bar{N}} \underline{\tilde{r}}_0; \cdots \underline{\underline{F}}_{\bar{N}} \underline{\tilde{r}}_i; \cdots ; \underline{\underline{F}}_{\bar{N}} \underline{\tilde{r}}_{2H-1}\right], \\ &= \underline{\underline{F}}_{\bar{N},2H} \underline{\tilde{r}}, \\ &= \underline{\underline{\tilde{C}}} \underline{\underline{\tilde{\Omega}}} \underline{B} + \underline{\tilde{\mathcal{N}}}, \end{aligned} \tag{166}$$

where $\underline{\underline{\tilde{C}}} := \underline{\underline{F}}_{\bar{N},2H} \dot{\underline{\underline{\tilde{c}}}} \underline{\underline{F}}^H_{\bar{N},2H}$, $\underline{\underline{\tilde{\Omega}}} := \underline{\underline{F}}_{\bar{N},2H} \dot{\underline{\underline{\tilde{g}}}} \underline{\underline{F}}^H_{\bar{N},\bar{Q}}$, $\underline{B} := \underline{\underline{F}}_{\bar{N},\bar{Q}} \underline{b}$, and $\underline{\tilde{\mathcal{N}}} := \underline{\underline{F}}_{\bar{N},2H} \underline{\tilde{\eta}}$. The structure of this model is very similar to that shown in Fig. 30 except that all the circulant $\bar{N} \times \bar{N}$ sub-matrices are now transformed to diagonal matrices. To

study the similarities and the differences between the two receiver architecture approaches presented in this chapter, this matrix model can be compared with MF-based frequency-domain model in (136).

5.3.3 Frequency-domain Equalizer for SF-based Technqiue

In this section, we use the frequency-domain matrix model (166) to derive linear equalizers for the sampling-based receiver architecture. This model also has the same property of separation of the effect of modulation and that of the channel on the pseudo-symbols. We define the equalizers to mitigate the effect of the channel. For this purpose, we define: $\underline{S} := \underline{\underline{\tilde{\Omega}}}\underline{B}$, then

$$\underline{\tilde{R}} := \underline{\underline{\tilde{C}}}\underline{S} + \underline{\tilde{\mathcal{N}}}. \tag{167}$$

The zero-forcing equalizer is given by

$$\underline{\underline{\tilde{G}}}^{ZF} = \left[\underline{\underline{\tilde{C}}}^H \underline{\underline{\tilde{C}}}\right]^{-1} \underline{\underline{\tilde{C}}}^H, \tag{168}$$

and the MMSE equalizer is expressed as

$$\underline{\underline{\tilde{G}}} := \underline{\underline{\mathfrak{R}}}_{SS}\underline{\underline{\tilde{C}}}^H[\underline{\underline{\tilde{C}}}\,\underline{\underline{\mathfrak{R}}}_{SS}\underline{\underline{\tilde{C}}}^H + \underline{\underline{\mathfrak{R}}}_{\tilde{\mathcal{N}}\tilde{\mathcal{N}}}]^{-1}, \tag{169}$$

where

$$\underline{\underline{\mathfrak{R}}}_{SS} := \mathbf{E}[\underline{S}\underline{S}^H], \tag{170}$$

is the correlation matrix for $\underline{S}$, and

$$\underline{\underline{\mathfrak{R}}}_{\tilde{\mathcal{N}}\tilde{\mathcal{N}}} := \mathbf{E}[\underline{\tilde{\mathcal{N}}}\underline{\tilde{\mathcal{N}}}^H],$$

is the correlation matrix for $\underline{\tilde{\mathcal{N}}}$. These correlation matrices can be computed off-line using the correlation between pseudo-symbols [21], and the impulse response $\psi_r(t)$, respectively. Applying the matrix inversion lemma to (169), we get

$$\underline{\underline{\tilde{G}}} = \left[\underline{\underline{\mathfrak{R}}}_{SS}^{-1} + \underline{\underline{\tilde{C}}}^H \underline{\underline{\mathfrak{R}}}_{\tilde{\mathcal{N}}\tilde{\mathcal{N}}}^{-1}\underline{\underline{\tilde{C}}}\right]^{-1} \underline{\underline{\tilde{C}}}^H \underline{\underline{\mathfrak{R}}}_{\tilde{\mathcal{N}}\tilde{\mathcal{N}}}^{-1}. \tag{171}$$

The output of the FDE is given by

$$\left[\hat{\underline{S}}_0; \hat{\underline{S}}_1; \cdots; \hat{\underline{S}}_{2H-1}\right] := \tilde{\underline{\underline{G}}}\tilde{\underline{R}}, \tag{172}$$

which is converted back to the time domain as follows:

$$\hat{\underline{s}}_i := \underline{\underline{F}}_{\bar{N}}^{H} \hat{\underline{S}}_i, \forall i \in \mathbb{N}_{2H}. \tag{173}$$

All these receiver operations are shown in Fig. 29. The vectors $\hat{\underline{s}}_i$ are the polyphase components of the equalized version of the sampled CPM signal (149). These polyphase components are combined by a polyphase expander [54], as shown in Fig. 29, to obtain $\hat{\underline{s}}$. The demodulation is now performed in the time domain to recover the CPM symbols. The metric to be maximized in the demodulator is given by

$$\tilde{\Lambda} := \check{\underline{s}}^{H} \hat{\underline{s}}. \tag{174}$$

where for l-th candidate block of symbols, i.e., $\underline{x}^{(l)}$, $\check{\underline{s}} := [\check{s}_{l\bar{N}_T}; \check{s}_{l\bar{N}_T+1}; \cdots; \check{s}_{(l+1)\bar{N}_T-1}]$ contains the samples of the corresponding CPM signal (149). The viterbi algorithm can be used to detect the sequence of symbols. For this purpose, we enumerate all branches (combinations of states and inputs), i.e., $(\chi_n, \alpha_i)^{(j)}$, for $j \in \mathbb{N}_{N_b}$, where $N_b = N_s.M$, and N_s being the number of states in the trellis for the particular multi-h CPM modulation under consideration. The branch metric at i-th symbol interval is computed for each branch j as follows:

$$\tilde{\lambda}_i^{(j)} := [\check{\underline{s}}^{(j)}]^H [\hat{s}_{2i}; \hat{s}_{2i+1}], \tag{175}$$

where $\check{\underline{s}}^{(j)} := \left[\check{s}_0^{(j)}; \check{s}_1^{(j)}\right]$ are the corresponding signal samples for j-th branch hypothesis $(\chi_n, \alpha_i)^{(j)}$. At the output of the demodulator, we get a sequence of M-ary PAM symbols, $\underline{x}^{(l)}$, from which we remove the inserted intrafix symbols. The result is then de-mapped from M-ary PAM to get the detected binary data.

This completes our discussion of various operations performed on the received signal in the SF-based FDE technique. In the next section, we discuss how the

complexity of computation of the MMSE equalizer (given by (171)) can be reduced by making an approximation. In Section 5.4, we will assess how much reduction in complexity is obtained by this approximation, while in Section 5.5, we determine the resulting loss in performance.

5.3.4 Further Complexity Reduction in SF-based Technique

It can be readily identified that a major source of complexity involved in the sampling-based receiver architecture is the computation of the inverse in (171), i.e.,

$$\left[\underline{\underline{\mathfrak{R}}}_{SS}^{-1} + \underline{\underline{\tilde{C}}}^H \underline{\underline{\mathfrak{R}}}_{\tilde{\mathcal{N}}\tilde{\mathcal{N}}}^{-1} \underline{\underline{\tilde{C}}}\right]^{-1}.$$

Although $\underline{\underline{\mathfrak{R}}}_{SS}^{-1}$ and $\underline{\underline{\mathfrak{R}}}_{\tilde{\mathcal{N}}\tilde{\mathcal{N}}}^{-1}$ can be computed off-line, but for each new realiazation of the channel impulse response, the overall inverse needs to be computed again. The sampling-based technique for FDE of single-h CPM was presented in [25], and a lower-complexity approximation to the inverse involved in the computation of the MMSE equalizer was suggested. We follow the same spirit, except that the structure of our matrix that needs to be inverted is slightly more involved. To get an approximation of the MMSE equalizer in (171), we define the following permutation matrix:

$$\underline{\underline{P}} := \left[\underline{\underline{I}}_{\bar{N}} \otimes \underline{e}_1, \;\; \underline{\underline{I}}_{\bar{N}} \otimes \underline{e}_2, \;\; \cdots, \;\; \underline{\underline{I}}_{\bar{N}} \otimes \underline{e}_{2H}\right], \tag{176}$$

where $\underline{e}_i$ is the i-th column of $\underline{\underline{I}}_{2H}$. Note that $\underline{\underline{P}}^{-1} = \underline{\underline{P}}^H$, and if we define

$$\underline{\underline{\tilde{C}}}_P := \underline{\underline{P}}\, \underline{\underline{\tilde{C}}}\, \underline{\underline{P}}^H,$$

$$\underline{\underline{\mathfrak{R}}}_{SS,P}^{-1} := \underline{\underline{P}}\, \underline{\underline{\mathfrak{R}}}_{SS}^{-1}\, \underline{\underline{P}}^H,$$

$$\underline{\underline{\mathfrak{R}}}_{\tilde{\mathcal{N}}\tilde{\mathcal{N}},P}^{-1} := \underline{\underline{P}}\, \underline{\underline{\mathfrak{R}}}_{\tilde{\mathcal{N}}\tilde{\mathcal{N}}}^{-1}\, \underline{\underline{P}}^H,$$

then the MMSE equalizer in (171) can equivalently be written as

$$\underline{\underline{\tilde{G}}} = \underline{\underline{P}}^H \left[\underline{\underline{\mathfrak{R}}}_{SS,P}^{-1} + \underline{\underline{\tilde{C}}}_P^H \underline{\underline{\mathfrak{R}}}_{\tilde{\mathcal{N}}\tilde{\mathcal{N}},P}^{-1} \underline{\underline{\tilde{C}}}_P\right]^{-1} \underline{\underline{\tilde{C}}}_P^H \underline{\underline{\mathfrak{R}}}_{\tilde{\mathcal{N}}\tilde{\mathcal{N}},P}^{-1} \underline{\underline{P}}. \tag{177}$$

The matrix to be inverted in the above equation, i.e.,

$$\underline{\underline{D}} := \left[\underline{\underline{\mathfrak{R}}}^{-1}_{SS,P} + \underline{\underline{\tilde{C}}}^{H}_{P}\underline{\underline{\mathfrak{R}}}^{-1}_{\tilde{\mathcal{N}}\tilde{\mathcal{N}},P}\underline{\underline{\tilde{C}}}_{P}\right], \tag{178}$$

has almost a block diagonal structure. Most of the energy is concentrated in blocks of size $2H \times 2H$ on the diagonal. Thus, a very good approximation to $\underline{\underline{D}}$ can be made as follows:

$$\underline{\underline{D}} \approx \underline{\underline{D}} \odot \left(\underline{\underline{I}}_{\bar{N}} \otimes \underline{\underline{J}}_{2H}\right), \tag{179}$$

where $\odot$ denotes the Hadamard (or entrywise) product of two matrices, and $\underline{\underline{J}}_{2H}$ is an all-ones square matrix of dimension $2H$. Now, instead of computing the exact inverse of D, as required by (177), we can approximate it by using (179). This approximate inverse of D involves inversion of $\bar{N}$ matrices, each of dimension $2H$. To distinguish it from SF-based FDE architecture, we call the technique presented in this section as the simplified sampling filter (SSF)-based FDE.

5.4 Computational Complexity

In this chapter, we have so far presented two different receiver architectures for the FDE of multi-h CPM, i.e., MF-based FDE (see Section 5.2) technique and SF-based FDE (see Section 5.3) technique. Moreover, we have derived a low-complexity approximate version of the latter, namely SSF-based FDE receiver (see Section 5.3.4). We observed that these architectures share many processing steps, but at the same time there are significant differences. In this section, we intend to perform a comparative analysis of these techniques and make an assessment of the computational burden posed by various components in each of these architectures.

It is pertinent to mention here that all the sub-optimal low-complexity techniques applicable to the multi-h CPM demodulator design for AWGN channel, which result in a substantial reduction of the number of states [22], are applicable here. In general, we assume that a receiver may employ a demodulator that only considers $K \leq Q$

most significant Laurent pulses, and as a result, the number of states in the decoding trellis $S_Q := PM^L$ are reduced, to say S_K.

To perform a comparison of these techniques, we identify that the receiver complexity mainly arises from the number of front end filters, the number of FFT/IFFT pairs, the computation of the equalizer filter, and the equalization itself. We discuss the complexity arising from these sources one by one in the following, and report the results comparing different receiver techniques in Table 3. The results are given in terms of the approximate number of floating-point operations (FLOPs) and hardware requirements.

- *Front end filters*: In the MF-based receiver, the size of the matched-filter bank is equal to the number of Laurent pulses. This can be a significant source of complexity, especially for non-binary and partial-response schemes. Laurent pulses, however, have the advantage that they are real-valued, and not all the pulses have a significant amount of energy. So, the MF-bank dimension is reduced, to say $K \leq Q$, by ignoring smaller pulses. On the other hand, for SF-based and SSF-based receivers, only one anti-aliasing filter is employed. These techniques definitely hold advantage over MF-based technique in this metric of complexity.

- *FFT/IFFT Pairs*: The number of FFT/IFFT paris in MF-based technique are H times the size of MF-bank, i.e., KH. Each FFT/IFFT is of size $\bar{N} = N/H$, which implies that the approximate number of FLOPs required for KH-pairs are $2KN \log_2 N/H$. The advantage of SF-based (and SSF-based) receiver is that the complexity of FFT/IFFT is independent of the number of Laurent pulses. One FDE branch is required for each polyphase component, so the number of FLOPS required for $2H$ FFT/IFFT pairs, each of size $\bar{N}$, is given by $4N \log_2 N/H$. This aspect of the complexity of the receiver techniques is almost

similar for modulation schemes where a small values of K could be used.

- *Equalizer Computation*: The equalizer computation for MF-based technique is relatively simple because of the diagonal structure of the matrix to be inverted (see (143)). However, we need to compute KH such equalizers for each block. The number of FLOPS are approximately given by KN. For SF-based technique, computing the equalizer involves inverse of a $2N \times 2N$ matrix (see (171)), and if the inverse is performed without considering the sparsity of this matrix, we need approximately $8N^3$ FLOPs. SSF-based technique proposed in Section 5.3.4 reduces the complexity of inversion by identifying the structure in $\underline{\underline{D}}$ (see (179)) and approximating it by a block diagonal matrix. Using this approximation, the inverse can be computing by inverting $\bar{N}$ matrices, each of size $2H \times 2H$. The number of FLOPs required in this case are roughly $4HN$. This analysis highlights the huge complexity of SF-based technique, which is a major disadvantage for this scheme. However, SSF-based techniques competes well with MF-based FDE, the complexity for both is linear in N, and their relative complexity is determined by the values of K and H being used.

- *Equalization*: In MF-based receiver, applying FDE to the frequency-transformed signal is equivalent to computing a dot product of two vectors of dimension $\bar{N}$, since the equalizer itself is diagonal. As there are KH equalizers to be applied, the process requires approximately $2KN$ FLOPs. SF-based FDE requires multiplication of a square matrix of size $2N \times 2N$ to a vector, which involves approximately $4N^2$ FLOPs. For SSF-based FDE, we need to perform $\bar{N}$ matrix to vector multiplications, with matrix size being $2H \times 2H$. This process amounts to roughly $8HN$ FLOPs. Again, we have linear complexity in N for both MF-based and SSF-based FDE schemes. On the other hand, SF-based receiver has a quadratic dependence on N.

- *Viterbi Algorithm for Demodulation*: For all three receiver types, we assume that a reduced-state trellis can be used in the demodulator. If the trellis is reduced to S_K states per symbol, the complexity of the Viterbi-based demodulation is given by $\mathcal{O}(S_K MN)$ FLOPs [24].

From this analysis, it is clear that the MF-based receiver has a reasonable complexity when a small value of K could be selected for the given modulation scheme. Otherwise, the size of the MF-bank and the number of FLOPs in other processes will increase considerably. Nevertheless, for all processes, the complexity is only a linear function of block size N. SF-based FDE has a simple front end, consisting of a single filter, and the number of FDE branches is also limited to the number of polyphase components. However, in its original form, the computation of MMSE equalizer is very involved, and the usual advantage of FDE, being low-complexity compared to MLSD and time-domain equalizer, is partially lost. SSF-based FDE overcomes the excessive complexity problem of SF-based FDE by simplifying the inversion problem, and as is the case for MF-based technique, the complexity of all the processes in the receiver is a linear function of block size N.

In the next section, we present simulation results for equalization of a dual-h modulation scheme, using the techniques presented in this chapter, and make observations regarding trade-off between performance and complexity.

5.5 Performance Evaluation

In this section, we apply the proposed FDE techniques to the dual-h CPM waveform defined in the IRIG-106 Aeronautical Telemetry standard. The parameters of the waveform are listed in Table 1. For detailed description, power spectrum, and its performance in AWGN, refer to [6] and [21]. The number of intrafix symbols required for this modulation scheme is $N_I = 4$ [53]. We assume an FFT-length of $N = 256$ symbols, and a cyclic prefix of $N_P = 32$ symbols. Using these parameters, the cyclic

Table 3: Complexity comparison for the proposed FDE architectures.

Receiver Techniques	Number of FLOPs per block				Front end Filters
	FFT/IFFT Pairs	Equalizer Calculation	Equalization	Viterbi Decoding	
MF-based FDE	$2KN\log_2(N/H)$	$\mathcal{O}(KN)$	$\mathcal{O}(KN)$	$\mathcal{O}(S_K MN)$	K
SF-based FDE	$4N\log_2(N/H)$	$\mathcal{O}(N^3)$	$\mathcal{O}(N^2)$	$\mathcal{O}(S_K MN)$	1
SSF-based FDE	$4N\log_2(N/H)$	$\mathcal{O}(HN)$	$\mathcal{O}(HN)$	$\mathcal{O}(S_K MN)$	1

block shown in Fig. 25 can be generated. Laurent decomposition for this waveform is shown to have $Q = 48$ pulses corresponding to each of the even and odd symbol intervals [22]. The longest pulse has a duration of $L + 1 = 4$ symbol intervals, while only 12 of the 48 Laurent pulses have any significant energy and a duration at least 2 symbol intervals. Simplified receivers may only use a fraction of these pulses and still achieve an acceptable performance [22].

For numerical simulations, we use the wideband aeronautical telemetry model proposed by Rice *et al.* [7], which is frequently used by the telemetry community. Multipath fading effects are modeled by a three-ray propagation model in most en-route scenarios. The exact parameters of the model, however, depend upon whether the flight is over-water/terrestrial, high/low altitude, etc. To accommodate for this variation, we define the following power-delay profile representing typical values of the path-gains and delays: The relative gains and delays are defined as $[1, 0.5, 0.03]$ and $[0, 100, 800]$ nsec, respectively. The rate of transmission is selected as 1 Mbps.

Performance curves for this simulation setup are shown in Fig. 31– 33 for MF-based FDE, SF-based FDE, and SSF-based FDE, respectively. The bit-energy-to-noise ratio (E_b/N_o) is on the horizontal axis, and the corresponding bit error rate (BER) is on

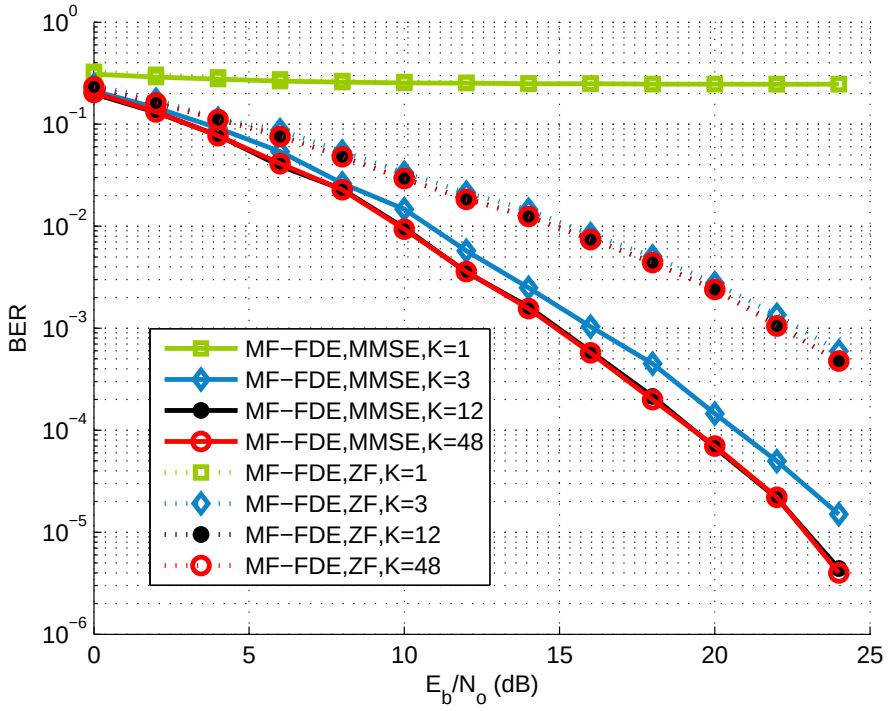

Figure 31: BER performance for the IRIG-106 dual-h CPM waveform with the MF-based FDE receiver.

the vertical axis. Results are presented for both zero forcing (ZF) and minimum mean-square error (MMSE) criterion. The parameter K represents the number of Laurent pulses used in the demodulator. For MF-based FDE receiver, this value of K also specifies the number of filters in the MF-bank and number of FDE branches (FFT/IFFT pair and the FDE) in the receiver. The branch metric defined in (147) was modified for the case $K \neq Q$ to account for the bias caused by the variation in the envelope of the estimated signal [22]. Each curve, in these figures, is labelled by the FDE type, error criterion, and the value of K employed. For example, 'MF-FDE,MMSE,K=12' indicates that the curve is for a MF-based FDE receiver, where the equalizer(s) use MMSE criterion and the 12 most significant Laurent pulses are used in the demodulator, MF-bank and the equalizer.

Following information can be gleaned from these figures:

- For all techniques (MF,SF,SSF-based FDE), performance for MMSE criterion

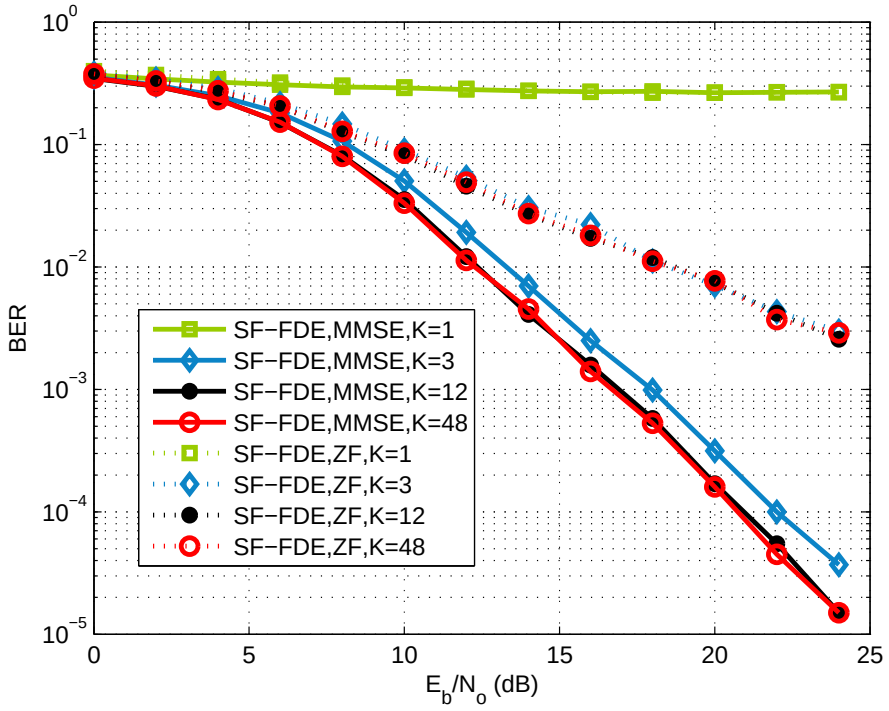

Figure 32: BER performance for the IRIG-106 dual-h CPM waveform with the SF-based FDE receiver.

is much better than in the case of ZF criterion. For example, in case of the MF-based FDE scheme in Fig. 31, a penalty of about 6dB is experienced, at the BER of 10^{-3}, for using ZF instead of the MMSE equalizer. The difference in the complexity of ZF and MMSE is not significant to justify this performance loss.

- For all techniques, in case of a ZF-forcing equalizer, as long as we use more than one pulse (i.e., $K = 1$), the performance is almost independent of K.

- For all techniques, in case of MMSE criterion, BER performance is almost same for $K = 12$ and $K = 48$. The performance curve for $K = 3$ shows a relative penalty of about $1 - 2$ dB.

- Using only a single Laurent pulse (i.e., $K = 1$) is futile. This observation is consistent with the one in the AWGN channel [22].

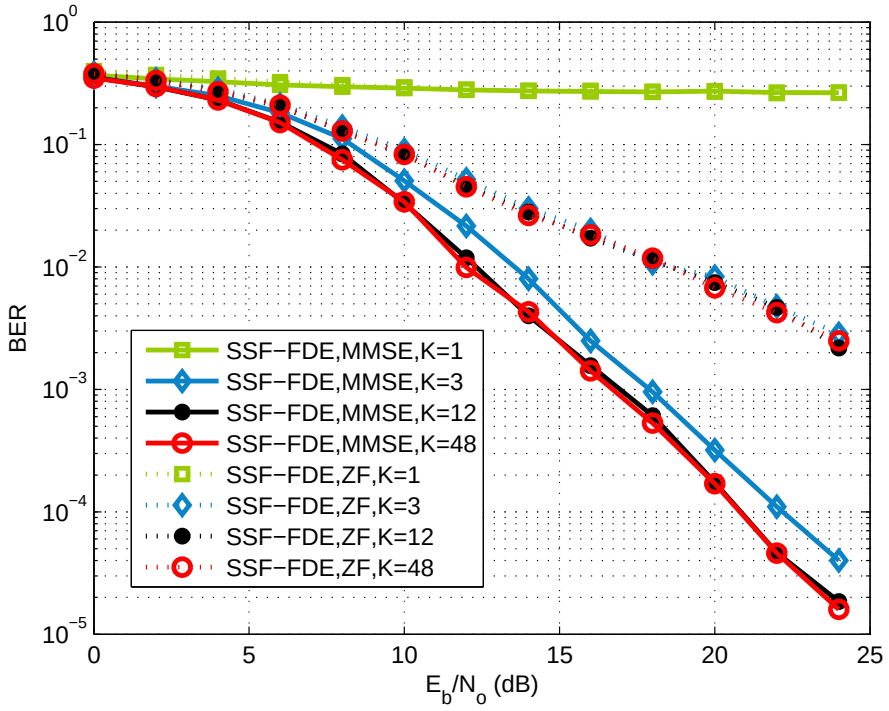

Figure 33: BER performance for the IRIG-106 dual-h CPM waveform with the SSF-based FDE receiver.

To get information about the comparative performance of the FDE receivers, the BER performance curves for ZF criterion are plotted in Fig. 34, for all techniques. The corresponding curves for MMSE criterion are presented in Fig. 35. We can gather following information from these curves:

- BER performance is almost similar for both SF-based FDE and SSF-based scheme. This implies that the approximation suggested in (179) is very good, and does not cause any palpable performance loss. This observation is valid for both ZF (Fig. 34) and MMSE (Fig. 35) criterion.

- In case of ZF criterion (see Fig. 34), the difference between MF-based and SF-based FDE performance is about 4 dB.

- The last case of MMSE criterion (see Fig. 35) is more interesting. Use of $K > 12$ pulses gives a consistent advantage of about 1-2 dB to the MF-based techniques.

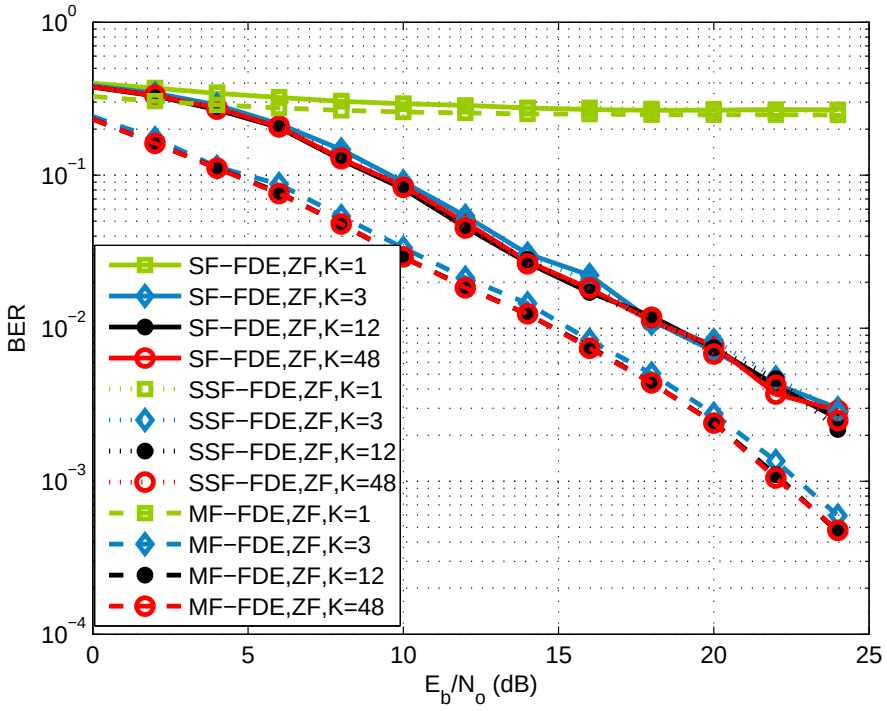

Figure 34: BER for the IRIG-106 dual-h CPM waveform using multiple FDE techniques with the ZF criterion.

However, for the case $K = 3$, where the complexity of the MF-based equalizer is more practical, the performance of MF-based equalizer starts off about 3 dB better than SF-based scheme for low E_b/N_o. However, it drifts slowly to get close to that of SF-based scheme.

From the last observation, we can conclude that the use of MF-based scheme with acceptable complexity ($K \sim 3$) results in almost similar performance for higher values of SNR as that of the case of SSF-based scheme. In a practical system, the ultimate choice between the two cases may be determined by whether the complexity introduced by the MF-bank or the computation of SF-based equalizer is more acceptable.

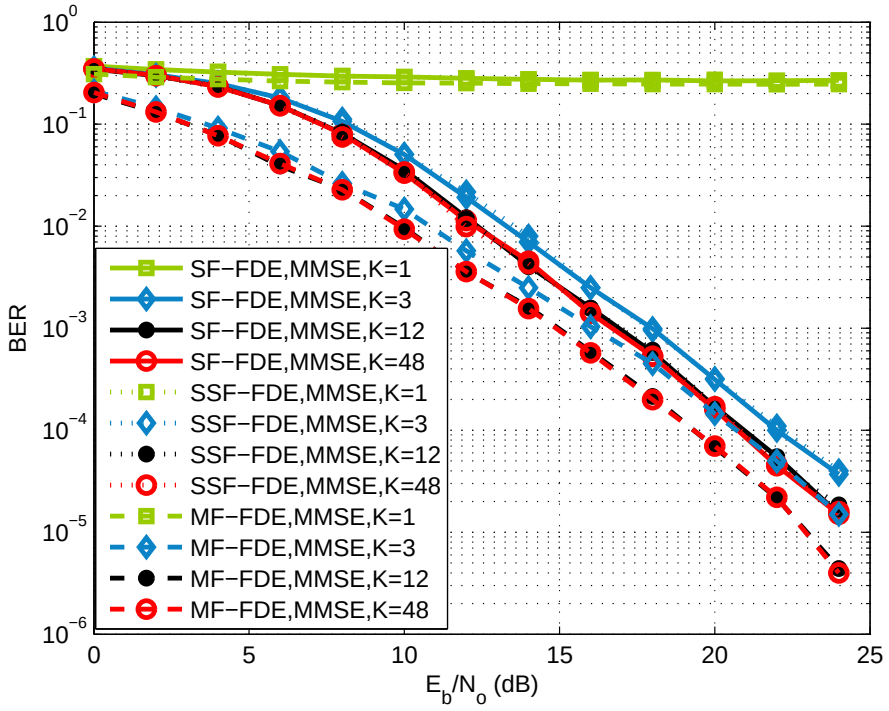

Figure 35: BER for the IRIG-106 dual-h CPM waveform using multiple FDE techniques with the MMSE criterion.

5.6 Summary

In this chapter, we have developed low-complexity techniques to mitigate the effects of intersymbol interference on a multi-h continuous phase modulation (CPM) waveform. Circulant matrix models are derived for both the matched-filter (MF) front end and sampling-filter (SF) front end techniques. Based upon these models, we proposed new architectures for frequency-domain equalization (FDE) and subsequent demodulation. The computational complexity of each of these architectures is then analyzed, and results are reported in terms of the number of front end filters and the number of floating points operatoins (FLOPs) required for various components of the receiver. Several methods have been proposed to achieve further reduction in receiver complexity, e.g., by ignoring low-energy Laurent pulses in the MF-bank, by

using a reduced-state demodulator or by truncating signal correlation while computing the equalizer. It is suggested that by combining these methods in a judicious manner, it is possible to get a substantial reduction in the overall receiver complexity without sacrificing too much performance. This trade-off is studied very carefully by performing detailed numerical simulations on a dual-h CPM waveform affected by an aeronautical-telemetry channel model.

CHAPTER VI

CONCLUSIONS AND FUTURE RESEARCH DIRECTIONS

In this dissertation, we have focused on developing low-complexity techniques for frequency-domain equalization (FDE) of multi-h continuous phase modulation (CPM). We identified that there were two main hurdles to be cleared before reaching this eventual goal. The first problem to be addressed was the specification of the block format to generate a cyclic transmitted multi-h CPM signal. To achieve this purpose, in Chapter 3, we provided a detailed discussion on the structure of the transmitter. Chapter 4 built upon the results of Chapter 3 and contained a detailed description about the construction of the transmitted block. The second issue was that of the design of the receiver, which includes the design of front end to generate statistics, equalizer to mitigate interference, and demodulator to detect symbols. Several solutions to these design problems are proposed, compared, and evaluated in Chapter 5.

6.1 Contributions

The major contributions of this work can be summarized as below:

- In Chapter 3, we showed that the multi-h CPM modulator can be decomposed into a finite-state machine (FSM) and a phase modulator (PM). Further, it was proved that the output of the FSM, called the tilted phase, has a periodic trellis structure. Using this decomposition, we proposed a process of trellis termination for tilted-phase signal. Different segments of the terminating sequence are classified in such a way that each segment terminates one component of the state vector.

- It was also shown in Chapter 3 that the length of the terminating sequence depends upon the parameters of the modulation scheme, e.g., the set of rational modulation indices, the order of the modulation scheme, the number of modulation indices, etc. Upper and lower bounds were proposed on the minimal-length terminating sequence required for a multi-h CPM modulation scheme. Moreover, it was found that the problem of minimizing the number of symbols required to terminate the tilted-phase state is related to a celebrated problem in number theory, called the Diophantine Frobenius Problem (FP). Numerical examples of single-h, dual-h, and triple-h CPM modulation schemes were presented to illustrate the process of finding the minimum-length terminating sequence. These examples also helped to evaluate the sharpness of the proposed upper and lower bounds.

- In Chapter 4, we presented a comprehensive procedure for construction of a transmit block such that the received signal has cyclic property for the duration of the block. The block construction is based upon the results on trellis termination of tilted-phase CPM, discussed in Chapter 3. The cyclic behavior of the received signal enables the use of FFT/IFFT algorithms in the FDE. The selection of the intrafix segment (inserted to ensure the cyclic property) was made to minimize its overhead. The intrafix forces the transmitter state machine to regress to the state it had at the start of the block. The constraints on the symbols of the intrafix, which ensure above condition, were shown to be a set of linear Diophantine equations (LDEs).

- Three different methods were proposed for finding the symbols of the intrafix such that the length of the intrafix is minimized. One of these methods connected the problem of intrafix insertion to the trellis termination of the tilted phase signal. This connection enabled us to state and justify that existing

bounds established on the length of the terminating sequence are effective for the length of the intrafix. It was observed that multi-h CPM schemes typically required a shorter intrafix as compared to single-h CPM schemes having similar modulation parameters. The proposed procedure was applied to the ARTM dual-h CPM scheme.

- In Chapter 5, we focused on the problem of receiver design, to mitigate the effects of ISI introduced by a frequency-selective channel. For this purpose, we presented a new interpretation of the Laurent decomposition for multi-h CPM signals that suppressed the periodicity of the Laurent pulses. This was achieved by merely re-labelling the Laurent pulses and their pseudo-coefficients. However, this seemingly naive step enabled visualizing multi-h CPM as essentially a higher-order single-h CPM, thus paving the way for extension of techniques available for single-h CPM to multi-h CPM.

- We proposed two FDE architectures for multi-h CPM; one that uses a matched-filter front end and the other that uses a single low-pass (anti-aliasing) filter followed by a sampler. For both schemes, we showed that the sampled output of the receiver filter(s) satisfies a circulant matrix model for general multi-h CPM waveforms given that the transmitted signal is cyclic for the duration of the block. The effect of the memory of the modulator and that of the frequency-selective channel is isolated by these models. This isolation enables the equalizer to eliminate exclusively the effect of the channel, while a trellis-based AWGN demodulator can then follow the equalizer to recover the data symbols.

- The reduction in the complexity of the receiver using MF front end was proposed by dropping the MFs and the FDE branches corresponding to low-energy Laurent pulses. It was observed that the loss in performance could be acceptable even when a few significant branches are considered. Similarly, further

complexity reduction can be forced for sampling-based approach by partially truncating the auto-correlation matrix of the multi-h CPM signal.

- Simulation results obtained for the IRIG-106 Tier-2 dual-h CPM waveform were presented in Chapter 5. The wideband aeronautical telemetry channel model was used to perform these simulations. The proposed receiver architectures, i.e., MF-based FDE, SF-based FDE, and SSF-based FDE were compared in terms of terms of their computational complexity and performance. Simulation results indicated that low-complexity designs for FDE can be used without losing much performance.

6.2 Suggestions for Future Research

In the previous section, we listed the major contributions made in this dissertation, in the area of frequency-domain equalization for multi-h CPM. Because of the ever increasing needs for data rates in all communication links, e.g., in aeronautical telemetry, the need to counter channel selectivity, in an efficient manner, is becoming more and more important. We expect that our results will be very useful in solving these and other related issues. We suggest that following possible directions of research can be explored by building upon the foundations laid in this dissertation:

- **Improving the Demodulator Design:** Reducing the complexity of the receiver has been of interest to researchers since the inception of CPM in early 1970s. A lot of work has been done to reduce the complexity of the demodulator, e.g., by using techniques such as decision-feedback sequence estimation [11, 32], differential phase demodulation [29], and by using various decompositions, e.g., Laurent decomposition [55] and principal component analysis [17], etc. In our work, we have focused primarily on complexity reduction for the FDE, and we have employed only the standard ways of reducing the complexity of the demodulator. The intention was to provide a proof of the concept that reduced

complexity FDE can be appropriately combined with simplified multi-h CPM demodulators. On the reduced-complexity demodulation of multi-h CPM, a thorough treatment is provided in [55]. Among several simplification techniques, suggested there, the technique of optimal averaging of the Laurent pulses was reported to be most successful. It is suggested that these advanced complexity reduction methods can be combined with our FDE design to provide a better trade-off between BER performance and complexity.

- **Laurent Decomposition for Separable CPM:** As we observed in Chapter 5, our ability to reduce the complexity of MF-based FDE design was limited by the number of Laurent pulses with significant energy. A special type of CPM, called separable CPM [56], is defined such that the phase shaping function has certain symmetry properties. This separability leads to a considerable reduction in the number of Laurent pulses required for exact representation of such CPM signals [57]. A possible extension of this work may be to define separable multi-h CPM signal, and try to find its concise Laurent decomposition. Our results in Chapter 3, related to Frobenius Number, can be used in this work to compute the number of Laurent pulses for a given multi-h CPM signal.

- **Space-time Codes for Multi-h CPM:** In the last few years, a considerable amount of work has been done on the development of space-time block codes for CPM signals. For example, very interesting theoretical results are developed in the context of space-time block codes for single-h CPM considering rank and determinant criterion [58]. An application to tier-1 ARTM modulation, i.e., SO-QPSK, has been presented in [59]. Very recently, STBCs have also been applied to multi-h CPM [60]. It will be very interesting to develop STBC techniques for ARTM dual-h CPM modulation scheme.

- **Advanced Channel Coding Techniques for Multi-h CPM:** In Chapter 5, we have provided BER simulation results for an uncoded system. To reduce the BER further, to acceptable quantities for a practical telemetry system, it is recommended to employ modern coding techniques. The re-discovery of low-density parity check (LDPC) codes in the last decade has led to a renewed interest in channel coding. Recently, LDPC codes have been applied to Tier-1 SO-QPSK modulation scheme [61]. We recommend that LDPC and other codes should also be explored for application to Tier-2 dual-h CPM modulation scheme.

APPENDIX A

PROOF OF THEOREM 1

Proof: By (28) and (29), $\exists\ l \in \mathbb{N}_H$ such that

$$\gcd(\mathrm{K_l}, \mathrm{P}) = 1. \tag{180}$$

Take $V_i^{(\Gamma)} = 0, \forall\ i \in \mathbb{N}_H \backslash l$. It is sufficient to show that $\exists\ V_l^{(\Gamma)} \geq 0$ and $m \in \mathbb{N}$ such that

$$mP + V_l^{(\Gamma)}(-K_l) = \Gamma. \tag{181}$$

An integer (possibly negative) solution $(m, V_l^{(\Gamma)})$ to this LDE exists iff $\gcd(\mathrm{P}, -\mathrm{K_l})|\Gamma$. This holds true for all Γ, by (180). Let (m_0, v_0) be one of these solutions. Then it can be shown that for any $j \in \mathbb{Z}$, $(m_j, v_j) := (m_0 + jP, V_0 - j(-K_l))$ generates the solution set. Thus, $\exists\ J \in \mathbb{N}$, such that $m_J \geq 1$ and $v_J \geq 0$. Defining $m = m_J$ and $V_l^{(\Gamma)} = v_J$ completes the proof. ■

APPENDIX B

PROOF OF THEOREM 2

B.1 Proof of Lower Bound

Let $B_0^+(\zeta) := \{\mathbf{V^{(\Gamma)}} \in \mathbb{N}^H | \, \|\mathbf{V^{(\Gamma)}}\|_\infty \leq \zeta\}$ be an $\|.\|_\infty$-norm closed ball of radius ζ, centred at origin, where $\mathbb{N}^H$ is the set of all non-negative integer H-tuples, and $\zeta \in \mathbb{N}$. By this definition, each coordinate of $V^{(\Gamma)}$, i.e, $V_k^{(\Gamma)}$, satisfies $V_k^{(\Gamma)} \leq \zeta$. Observe that the total number of lattice points in this ball is equal to the number of permutations generated by H coordinates, each taking values from the set $\{0, 1, ..., \zeta\}$, i.e., $\mathrm{Card}[\mathrm{B}_0^+(\zeta)] = (\zeta + 1)^{\mathrm{H}}$. A TSS with P elements can be contained in this ball iff $P \leq (\zeta + 1)^H$, which is equivalent to the lower bound on ζ above. This is the most efficient arrangement possible for P elements of a TSS according to the minimum number of symbols criterion. Note that equality holds when P is an integer power of H. ■

B.2 Proof of Upper Bound

The upper bound on ζ can be proved by way of contradiction. Let's assume that there exists an optimal TSS, $\mathbf{V}$ such that $\zeta \geq P$. This implies that $\exists$ for some Γ, $\kappa = \{k_1, ..., k_j, ..., k_J\} \subset \mathbb{N}_H$, such that

$$V_k^{(\Gamma)} = \begin{cases} \alpha_k^{(\Gamma)} P + \beta_k^{(\Gamma)} & \text{if } k \in \kappa \\ \beta_k^{(\Gamma)} & \text{otherwise} \end{cases}, \tag{182}$$

where $1 \leq j \leq J < H$, $\alpha_k^{(\Gamma)} \geq 1$ and $0 \leq \beta_k^{(\Gamma)} < P$ are all positive integers. For this solution, (27) thus satisfies

$$\sum_{k \in \kappa} K_k(\alpha_k^{(\Gamma)} P + \beta_k^{(\Gamma)}) + \sum_{k \notin \kappa} K_k \beta_k^{(\Gamma)} = mP - \Gamma, \tag{183}$$

for some integer m. Shifting terms with $\alpha_k^{(\Gamma)}$ to the right, we get

$$\sum_{k=0}^{H-1} K_k \beta_k^{(\Gamma)} = \bar{m}P - \Gamma, \tag{184}$$

where $\bar{m} := m - \sum_{k\in\kappa} \alpha_k^{\Gamma} K_k$ is an integer. Since $\Gamma \in \mathbb{N}_P$, and all the coefficients are non-negative, one can see that $\bar{m} \in \mathbb{N}$. This implies that $W_k^{(\Gamma)} = \beta_k^{(\Gamma)}$ is another valid solution to (27), such that $\|\mathbf{W}^{(\mathbf{\Gamma})}\|_\infty < P \leq \|\mathbf{V}^{(\mathbf{\Gamma})}\|_\infty$. Thus $\mathbf{V}$ is not an optimal TSS, which is contradictory to the assumption. ■

APPENDIX C

PROOF OF THEOREM 3

C.1 Lower Bound

Let's consider a TSS, $\mathbf{V}^{(\mathbf{\Gamma})}$, with P elements such that every $(H-1)$-simplex for $0 \leq C \leq P-1$ has a lattice point corresponding to each value of Γ. This ideal scenario of P consecutive solution curves can only occur when condition of relative primality holds. Otherwise, if $d = \gcd(\mathbb{K}) > 1$, lattice points occur only on every d-th simplex. Now it can be observed that ζ cannot be smaller than the point of minimum $\|.\|_\infty$-norm on the $(H-1)$-simplex with $C = P-1$. This specific point is at the intersection of this simplex and $\|.\|_\infty$-norm closed ball of radius

$$r \leq \zeta, \tag{185}$$

and has all the coordinates $\mathbf{V}_{\mathbf{k}}^{(\mathbf{\Gamma})} = r$, $\forall\ k \in \mathbb{N}_H$. If it is a lattice point, then (27) satisfies the following:

$$r \sum_{k=0}^{H-1} K_k = P - 1, \tag{186}$$

which along with (185) justifies the validity of the lower bound. ■

C.2 Upper Bound

The condition of relative primality implies that every $(H-1)$-simplex has integer lattice points, possibly with negative coordinates. However, $C > g(\mathbb{K})$ guarantees at least one non-negative lattice point on the simplex. So in the worst case, the last lattice point belongs to the simplex with $C = g(\mathbb{K}) + P$, such that it has largest $\|.\|_\infty$-norm of all points on that simplex. If $j \in \mathbb{N}_H$ is such that $K_j = \min_k K_k$, then this point will be equal to the j-th intercept of the simplex $C = g(\mathbb{K}) + P$. This worst-case condition thus proves the upper bound. ■

APPENDIX D

PROOF OF LEMMA 1

Proof: Note that $\eta(2, V_j^{\gamma})) = 0$, $\forall V_j^{\gamma} \in \mathbb{Z}$, which implies that the second term in (70) is zero. First assertion, i.e., (1) follows from the evaluation of first term for $M = 2$. For assertion (2), it is assumed without loss of generality that both a and b are non-negative. Since M is fixed, the first argument of μ can be dropped for notational simplicity. η_a is used as a simplified notation for $\eta(M, a)$. If $\bar{a} = \lfloor \frac{a}{M-1} \rfloor$ and $\bar{b} = \lfloor \frac{b}{M-1} \rfloor$ are as defined, then $a = (M-1)\bar{a} + \eta_a$, and $b = (M-1)\bar{b} + \eta_b$. Now consider,

$$\mu(a) - \mu(b) = (\bar{a} - \bar{b}) + [2 - (\eta_a)_2]\, I(\eta_a) - [2 - (\eta_b)_2]\, I(\eta_b) \ . \tag{187}$$

Since $a > b$, one must have $\bar{a} \geq \bar{b}$. When $\eta_b = 0$, it is trivial that $\mu(a) \geq \mu(b)$. So, one only need to check for $\eta_b \neq 0$. Three different scenarios are considered as follows.

$\bar{a} \geq \bar{b} + 2$: For this condition (using the minimum value of all the terms in (187)), and $\mu(a) - \mu(b) \geq 2 + 0 - 2 = 0$.

$\bar{a} = \bar{b} + 1$: If $\eta_a \neq 0$, then $\mu(a) - \mu(b) \geq 1 + 1 - 2 = 0$. Now, if $\eta_a = 0$, the second term in (187) vanishes, and $\mu(a) - \mu(b) = 1 - [2 - (\eta_b)_2]$. Thus, $\mu(a) < \mu(b)$ only when η_b is even. Now, for this to hold $a = (M-1)(\bar{b}+1)$ and $b = (M-1)\bar{b} + \eta_b$. Since $M-1$ is odd, it is clear that $a - b = (M-1) - \eta_b$ satisfies the two specified exceptions in the statement, i.e., $a - b < M - 1$ and $a - b$ is odd. Otherwise, $\mu(a) \geq \mu(b)$.

$\bar{a} = \bar{b}$: Since $a > b$, this implies that $\eta_a > \eta_b > 0$ (ignoring the trivial $\eta_b = 0$ case). From (187), and the fact that $\eta_a \neq 0$, $\mu(a) - \mu(b) = (\eta_b)_2 - (\eta_a)_2$. Note that $\mu(a) \geq \mu(b)$ holds except when η_b is even and η_a odd. For this case, $\mu(a) = \mu(b) - 1$. Since, $\bar{a} = \bar{b}$, a and b are such that $a = (M-1)\bar{b} + \eta_a$ and $b = (M-1)\bar{b} + \eta_b$. It is easy to see that even in this case, $a - b < M - 1$ and $a - b$ is an odd integer. ■

APPENDIX E

PROOF OF THEOREM 4

Proof: Since the cost function is same in both the optimization problems (66) and (80), it is sufficient to show that the set of constraints are equivalent for both. On comparison of (61) and (68), it is observed that only the first summation term is different. For a fixed value of F, and Γ_F, let the x_i's be the feasible symbols satisfying the constraint (61). If $\mathbf{V}^{(\gamma)}$ is defined as in (69), then $\mathbf{V}^{(\gamma)} \in \mathsf{D}(\mathbf{J}_F)$ and (68) is satisfied. Now assume that $\mathbf{V}^{(\gamma)} \in \mathsf{D}(\mathbf{J}_F)$ satisfies (68) for a fixed value of F and γ_F. The vector constructed by intrafix symbols corresponding to the j-th modulation index is represented by $\mathbf{x}(J_F^{(j)})$, and define it as $\mathbf{x}(J_F^{(j)}) := z_{|J_F^{(j)}|}(V_j^{(\gamma)})$ (see (75)). Using this definition, the summation terms in (61) and (68) can be shown to be equal.

When F is a multiple of H, all modulation indices K_j have equal number of symbols F/H in the intrafix. So, the domain of the problem is as specified in (81). The constraints of the two problems ((80) and (81)) are also equal. It is sufficient to show that the two objectives functions are equivalent. Let $\kappa_1 = \Omega H$ and $\kappa_2 = (\Omega + 2i)H$, for $\Omega, i \in \mathbb{Z}^+$ be two possible lengths of the intrafix. Then, from the definition (67), $\mathbf{J}_{\kappa_1} = \Omega \mathbf{1}_H$ and $\mathbf{J}_{\kappa_2} = (\Omega + 2i)\mathbf{1}_H$. Since $(\kappa_1 - \kappa_2)_2 = 0$, and from the definition (76), $\mathsf{d}(\Omega) \subset \mathsf{d}(\Omega + 2\mathsf{i})$, it follows from (79) that $D(\mathbf{J}_{\kappa_1}) \subset D(\mathbf{J}_{\kappa_2})$.

Let $\mathbf{W}^{(\gamma)} \in D(\mathbf{J}_{\kappa_2}) \backslash D(\mathbf{J}_{\kappa_1})$ be a feasible vector. Such a vector exists if $D(\mathbf{J}_{\kappa_2}) \backslash D(\mathbf{J}_{\kappa_1})$ is non-empty (true for $\kappa_1 \neq \kappa_2$) and $D(\mathbf{J}_{\kappa_2})$ is defined such that every vector is feasible (may not be optimal) for some $\gamma \in \Gamma_{\kappa_2}$. At least one component (in particular, the one largest in absolute value) of $\mathbf{W}^{(\gamma)}$, say $W_j^{(\gamma)}$, for $j \in \mathbb{N}_H$, is such that $W_j^{(\gamma)} \in d(\Omega + 2i) \backslash d(\Omega)$ and thus $\mu(W_j^{(\gamma)}, M) > \Omega$. While for all vectors $\mathbf{V} \in D(\mathbf{J}_{\kappa_1})$,

such that $\mu(||\mathbf{V}||_\infty, M) \leq \Omega$, it holds that

$$\mu(||\mathbf{W}^{(\gamma)}||_\infty, M) = \mu(W_j^{(\gamma)}, M) \tag{188}$$

$$> \mu(||\mathbf{V}||_\infty, M). \tag{189}$$

The equality above is due to the fact that μ is a function of absolute value of the first argument. Since $(||\mathbf{W}^{(\gamma)}||_\infty - ||\mathbf{V}||_\infty)_2 = 0$ (from (76) and (72)), it follows from the second claim of Lemma 1 that $||\mathbf{W}^{(\gamma)}||_\infty > ||\mathbf{V}||_\infty$.

For the third assertion, assume that two vectors, $\mathbf{V}^{(\gamma)} \in \mathsf{D}(\frac{\kappa_v}{H}\mathbf{1}_H)$ and $\mathbf{W}^{(\gamma)} \in \mathsf{D}(\frac{\kappa_w}{H}\mathbf{1}_H)$ are such that $||\mathbf{W}^{(\gamma)}||_\infty > ||\mathbf{V}^{(\gamma)}||_\infty$. Also, assume that $\mathsf{D}(\frac{\kappa_v}{H}\mathbf{1}_H)$ and $\mathsf{D}(\frac{\kappa_w}{H}\mathbf{1}_H)$ are smallest feasible sets containing these vectors, respectively. For binary ($M = 2$) modulation schemes, $\mu(V, 2) = |V|$, for any $V \in \mathbb{Z}$. This implies that $\mu(||\mathbf{W}^{(\gamma)}||_\infty, 2) > \mu(||\mathbf{V}^{(\gamma)}||_\infty, 2)$, and hence, $\kappa_w > \kappa_v$. Thus choosing a vector contained in an infinity-norm ball of smaller radius ensures that it leads to less number of symbols in the intrafix.

Assume that F satisfies (61), i.e., $\exists$, $\mathbf{V}^{(\gamma)} \in \mathsf{D}(\mathbf{J}_F)$, for each $\gamma_F \in \Gamma_F$. By adding and subtracting a term from this modulo equality,

$$\sum_{i=N-(F+1)}^{N-1} K_{(i)_H} x_i + \bar{\gamma} \equiv 0 \bmod(2P), \tag{190}$$

where $\bar{\gamma} := (\gamma - K_{(N-F)_H} x_{N-F})_{2P}$. Choosing $x_{N-F} = 1 \in \mathbb{M}$ as the additional symbol of the intrafix, and realizing that transformation from γ to $\bar{\gamma}$ is a bijective transformation from Γ_F to Γ_{F+1}, implies the result. ■

REFERENCES

[1] J. B. Anderson, T. Aulin, and C.-E. Sundberg, *Digital Phase Modulation*. New York, NY: Plenum Press, 1986.

[2] M. Mouly, *The GSM System for Mobile Communications*. Bay Foreign Language Books, 1992.

[3] *Bluetooth Special Interest Group*, Specifications of the Bluetooth System, Ver. 1.2, Nov. 2003.

[4] I. Sasase and S. Mori, "Multi-h phase-coded modulation," *IEEE Commun. Mag.*, vol. 29, no. 12, pp. 46 – 56, Dec. 1991.

[5] D. Stephens and K. Kreitzer, "High data rate UHF SATCOM," in *Proceedings MILCOM 97*, vol. 3, Nov. 1997, pp. 1443–1447.

[6] M. Geoghegan, "Description and performance results for a multi-h CPM telemetry waveform," *Proc. 21st Cent. Military Commun. Conf. MILCOM 2000*, Los Angeles, CA, pp. 353 – 357, Oct. 2000.

[7] M. Rice, A. Davis, and C. Bettweiser, "Wideband channel model for aeronautical telemetry," *IEEE Trans. Aerosp. Electron. Syst.*, vol. 40, no. 1, pp. 57 – 69, Jan. 2004.

[8] M. Rice and M. Jensen, "Multipath propagation for helicopter-to-ground MIMO links," in *Military Communications Conference, MILCOM 2011*, Nov. 2011, pp. 447–452.

[9] F. Pancaldi, G. Vitetta, R. Kalbasi, N. Al-Dhahir, M. Uysal, and H. Mheidat, "Single-carrier frequency domain equalization," *IEEE Signal Process. Mag.*, vol. 25, no. 5, pp. 37 – 56, Sept. 2008.

[10] G. L. Stüber, *Principles of Mobile Communications, 3rd ed.* New York, NY: Springer, Sept. 2011.

[11] J. Tan and G. L. Stüber, "Frequency-domain equalization for continuous phase modulation," *IEEE Trans. Wireless Commun.*, vol. 4, no. 5, pp. 2479 – 2490, Sept. 2005.

[12] W. V. Thillo, J. Nsenga, R. Lauwereins, V. Ramon, A. Bourdoux, and F. Horlin, "A New Symbol Block Construction for CPM with Frequency Domain Equalization," *Proc. IEEE Int. Conf. Commun. ICC '08*, Beijing, China, pp. 4321 – 4325, May 2008.

[13] W. Zhendao, G. B. Giannakis, "Wireless multicarrier communications," *IEEE Signal Process. Mag.*, vol. 17, no. 3, pp. 29 – 48, May 2000.

[14] B. E. Rimoldi, "A decomposition approach to CPM," *IEEE Trans. Inf. Theory*, vol. 34, no. 2, pp. 260 – 270, Mar. 1988.

[15] J. L. R. Alfonsín, *The Diophantine Frobenius Problem.* New York, NY: Oxford University Press USA, 2005.

[16] W. Tang and E. Shwedyk, "A quasi-optimum receiver for continuous phase modulation," *IEEE Transactions on Communications*, vol. 48, no. 7, pp. 1087–1090, July 2000.

[17] P. Moqvist and T. Aulin , "Orthogonalization by principal components applied to CPM," *IEEE Trans. Commun.*, vol. 51, no. 11, pp. 1838 – 1845, Nov. 2003.

[18] P. Laurent, "Exact and approximate construction of digital phase modulations by superposition of amplitude modulated pulses (AMP)," *IEEE Trans. Commun.*, vol. 34 , no. 2 , pp. 150 – 160, Feb. 1986.

[19] U. Mengali and M. Morelli, "Decomposition of M-ary CPM signals into PAM waveforms," *IEEE Trans. Inf. Theory*, vol. 41, no. 5, pp. 1265 – 1275, Sept. 1995.

[20] G. K. Kaleh, "Simple coherent receivers for partial response continuous phase modulation," *IEEE J. Sel. Areas Commun.*, vol. 7, no. 9, pp. 1427–1436, Dec. 1989.

[21] E. Perrins and M. Rice, "PAM decomposition of M-ary multi-h CPM," *IEEE Trans. Commun.*, vol. 53, no. 12, pp. 2065 – 2075, Dec. 2005.

[22] E. Perrins and M. Rice, "Reduced-complexity detectors for Multi-h CPM in aeronautical telemetry," *IEEE Transactions on Aerospace and Electronic Systems*, vol. 43, no. 1, pp. 286–300, Jan. 2007.

[23] W. Van Thillo, F. Horlin, V. Ramon, A. Bourdoux, and R. Lauwereins, "Novel block constructions using an intrafix for CPM with frequency domain equalization," *IEEE Transactions on Wireless Communications*, vol. 9, no. 3, pp. 951–955, Mar. 2010.

[24] F. Pancaldi and G. Vitetta, "Equalization algorithms in the frequency domain for continuous phase modulations," *IEEE Trans. Commun.*, vol. 54, no. 4, pp. 648 – 658, Apr. 2006.

[25] W. V. Thillo, F. Horlin, J. Nsenga, V. Ramon, A. Bourdoux, and R. Lauwereins, "Low-complexity linear frequency domain equalization for continuous phase modulation," *IEEE Trans. Wireless Commun.*, vol. 8, no. 3, pp. 1435 – 1445, Mar. 2009.

[26] J. G. Proakis, *Digital Communications, 4th ed.* New York, NY: McGraw-Hill, 2001.

[27] E. Perrins and M. Rice, "Optimal and reduced complexity receivers for M-ary multi-h CPM," *IEEE Wireless Commun. Netw. Conf. WCNC '04*, vol. 2, pp. 1165 – 1170, Mar. 2004.

[28] B. W. Peterson, D. R. Stephens, W. H. Tranter, "DFSE equalization of dual-h CPM over UHF MILSATCOM channels," *Proc. IEEE Military Commun. Conf. MILCOM '02*, vol. 2, pp. 1406 – 1411, Oct. 2002.

[29] C. Park and B. Womack, "Frequency domain processing for cyclic prefix-assisted multi-h CPM block transmission," *Proc. IEEE Military Commun. Conf. MILCOM '11*, pp. 329 – 333 , Nov. 2011.

[30] C.-E Sundberg, "Continuous phase modulation," *IEEE Commun. Mag.*, vol. 24, no. 4, pp. 25 – 38, Apr. 1986.

[31] J. B. Anderson and C. -E. W. Sundberg, "Advances in constant envelope coded modulation," *IEEE Commun. Mag.*, vol. 29 , no. 12, pp. 36 – 45, Dec. 1991.

[32] A. Duel-Hallen and C. Heegard, "Delayed decision-feedback sequence estimation," *IEEE Trans. Commun.*, vol. 37, no. 5, pp. 428 – 436, May 1989.

[33] G. D. Jr. Forney , "The Viterbi algorithm," *Proc. IEEE*, vol. 61, no. 3, pp. 268 – 278, Mar. 1973.

[34] H. C. Guren, N. Holte, "Decision feedback sequence estimation for continuous phase modulation on a linear multipath channel," *IEEE Trans. Commun.*, vol. 41, no. 2, pp. 280 – 284, Feb. 1993.

[35] A. Svensson, "Reduced state sequence detection of partial response continuous phase modulation," *IEEE Proc. on Commun., Speech, Vision*, vol. 138, no. 4, pp. 256 – 268, Aug. 1991.

[36] N. Benvenuto and S. Tomasin, "On the comparison between OFDM and single carrier modulation with a DFE using a frequency-domain feedforward filter," *IEEE Trans. Commun.*, vol. 50, no. 6, pp. 947 – 955, June 2002.

[37] D. Falconer, S. L. Ariyavisitakul, A. Benyamin-Seeyar, and B. Edison, "Frequency domain equalization for single-carrier broadband wireless systems," *IEEE Commun. Mag.*, vol. 40, no. 4, pp. 58 – 66, Apr. 2002.

[38] N. Benvenuto, R. Dinis, D. Falconer, and S. Tomasin, "Single Carrier Modulation With Nonlinear Frequency Domain Equalization: An Idea Whose Time Has Come – Again," *Proc. IEEE*, vol. 98, no. 1, pp. 69 – 96, Jan. 2010.

[39] B. Ozgul, M. Koca, and H. Delic, "Double turbo equalization of continuous phase modulation with frequency domain processing," *IEEE Trans. Commun.*, vol. 57, no. 2, pp. 423 – 429, Feb. 2009.

[40] R. H. H. Yang, "A generalized decomposition approach to multi-h continuous phase modulation," *IEEE Int. Symp. Inf. Theory ISIT '03*, pp. 148 – 148, June 2003.

[41] S. Lin and J. Jr. Costello, *Error Control Coding, 2nd ed.* New Jersey, USA: Pearson Prentice Hall, 2004.

[42] O. Joerssen and H. Meyr, "Terminating the trellis of turbo-codes," *Electron. Lett.*, vol. 30, no. 16, pp. 1285 – 1286, Aug. 1994.

[43] J. Hokfelt, O. Edfors, and T. Maseng, "On the theory and performance of trellis termination methods for turbo codes," *IEEE J. Sel. Areas Commun.*, vol. 19, no. 5, pp. 838 – 847, May 2001.

[44] P. Moqvist and T. Aulin , "Trellis termination in CPM," *Electron. Lett.*, vol. 36, no. 23, pp. 1940 – 1941, Nov. 2000.

[45] T. Koshy, *Elementary Number Theory with Applications, 2nd ed.* San Diego, CA, USA: Academic Press, 2007.

[46] J. Huber, W. Liu, "An alternative approach to reduced-complexity CPM-receivers," *IEEE J. Sel. Areas Commun.*, vol. 7, no. 9, pp. 1437 – 1449, Dec. 1989.

[47] Q. Zhao, and G. L. Stüber, "Robust time and phase synchronization for continuous phase modulation," *IEEE Trans. Commun.*, vol. 54, no. 10, pp. 1857 – 1869, Oct. 2006.

[48] G. A. Jones and J. M. Jones, *Elementary Number Theory,* London, UK: Springer-Verlag, 2005.

[49] S. Bocker and Z. Lipták, "The Money Changing Problem Revisited: Computing the Frobenius Number in Time $O(ka_1)$," *Coll. Math. Soc. János Bolyai, Finite and Infinite Sets*, vol. 3595, pp. 965–974, 2005.

[50] B. Vizvári, "On the connection of the Frobenius Problem and the Knapsack Problem," *Coll. Math. Soc. János Bolyai, Finite and Infinite Sets*, vol. 37, pp. 799–819, 1993.

[51] A. Brauer, "On a Problem of Partitions," *Am. J. Math.*, vol. 64, no. 1, pp. 299 – 312, 1942.

[52] S. Saleem and G. L. Stüber, "Trellis termination of multi-h CPM and the Diophantine Frobenius Problem," *IEEE Trans. Commun.*, vol. 59, no. 8, pp. 2196 – 2205, Aug. 2011.

[53] S. Saleem and G. L. Stüber, "Linear Diophantine Constrained Intrafix for Frequency Domain Equalization of Multi-h CPM," *IEEE Transactions on Communications*, vol. 60, no. 8, pp. 2265–2274, Aug. 2012.

[54] P. P. Vaidyanathan , S. Phoong, and Y. Lin, *Signal Processing and Optimization for Transceiver Systems.* Cambridge University Press, 2010.

[55] E. Perrins and M. Rice, "A new performance bound for PAM-based CPM detectors," *IEEE Trans. Commun.*, vol. 53, no. 10, pp. 1688 – 1696, Oct. 2005.

[56] G. Cariolaro and A. M. Cipriano, ""An equivalence principle for separable CPM signals," *Personal, Indoor and Mobile Radio Communications. PIMRC '04*, Sept. 2004, pp. 1347–1350.

[57] G. Cariolaro and A. M. Cipriano, "Minimal PAM decompositions of CPM signals with separable phase," *IEEE Transactions on Communications*, vol. 53, no. 12, pp. 2011–2014, Dec. 2005.

[58] A. G. Zajic, G. L. Stüber, "A SpaceTime Code Design for CPM: Diversity Order and Coding Gain," *IEEE Transactions on Information Theory*, vol. 55, no. 8, pp. 3781–3798, Aug. 2009.

[59] M. Rice and M. Jensen, "Space Time Coding for Aeronautical Telemetry," *presented at the Instrumentation Test Technical Symposium*, New Orleans, LA, 2004.

[60] M. A. Hisojo, J. Lebrun and L. Deneire, "Wireless Robotics: Generalization of an Efficient Approach with Multi-h CPM Signaling and L2-Orthogonal Space-Time Coding," *Wireless Personal Communications, Springer*, vol. 70, no. 3, pp. 1183–1198, 2013.

[61] E. Perrins, "FEC Systems for Aeronautical Telemetry," *IEEE Transactions on Aerospace and Electronic Systems*, vol. 49, no. 4, pp. 2340–2352, Oct. 2014.

[62] M. Rice and E. Satorius, "Equalization techniques for multipath mitigation in aeronautical telemetry," *IEEE Military Commun. Conf. MILCOM '04*, vol. 1, pp. 65 – 70, Oct. 2004.

[63] G. Mayer, "Trends in Aeronautical Wideband Telemetry Applicable to Science Missions with Aircraft and Balloon," *Proc. 19th ESA Symp. on European Rocket and Balloon Programmes and Related Research*, Bad Reichenhall, Germany, pp. 1 – 5, June 2009.

[64] F. Pancaldi and G. M. Vitetta , "Block channel equalization in the frequency domain," *IEEE Trans. Commun.*, vol. 53, no. 3, pp. 463 – 471, Mar. 2005.

[65] M. P. Wylie-Green, "A new finite Series expansion of continuous phase modulated waveforms," *IEEE Trans. Commun.*, vol. 55, no. 8, pp. 1547 – 1556, Aug. 2007.

[66] T. Aulin and C.-E. Sundberg, "Continuous Phase Modulation–Part I: Full Response Signaling," *IEEE Trans. Commun.*, vol. 29, no. 3, pp. 196 – 209, Mar. 1981.

[67] T. Aulin, N. Rydbeck and C.-E. Sundberg, "Continuous Phase Modulation–Part II: Partial Response Signaling," *IEEE Trans. Commun.*, vol. 29, no. 3, pp. 210 – 225, Mar. 1981.

[68] J. Anderson and D. Taylor, "A bandwidth-efficient class of signal-space codes," *IEEE Trans. Inf. Theory*, vol. 24, no. 6, pp. 703 – 712, Nov. 1978.

[69] C. Park, R. W. Heath, and T. S. Rappaport, "Frequency-Domain Channel Estimation and Equalization for Continuous-Phase Modulations With Superimposed Pilot Sequences," *IEEE Trans. Veh. Tech.*, vol. 58, no. 9, pp. 4903 – 4908, Nov. 2009.

[70] C. Park and B. Womack, "Continuous phase modulation receivers based on frequency domain processing," *Proc. IEEE Military Commun. Conf. MILCOM '09*, pp. 1 – 7 , Oct. 2009.

[71] H. Sari, G. Karam, and I. Jeanclaude, "Transmission techniques for digital terrestrial TV broadcasting," *IEEE Commun. Mag.*, vol. 33, no. 2, pp. 100 – 109, Feb. 1995.

[72] G. Cariolaro, "A system-theory approach to decompose CPM signals into PAM waveforms," *IEEE Trans. Commun.*, vol. 58, no. 1, pp. 200 – 210, Jan. 2010.

[73] O. Popescu, M. Saquib, D. C. Popescu, and M. D. Rice, "Interference Mitigation in Aeronautical Telemetry Systems using Kalman Filter," *IEEE Trans. Aerosp. and Electron. Syst.*, vol. 43, no. 4, pp. 1624 – 1630, Oct. 2007.

[74] M. Wylie-Green, E. Perrins, and T. Svensson, "Introduction to CPM-SC-FDMA: A Novel Multiple-Access Power-Efficient Transmission Scheme," *IEEE Trans. Commun.*, vol. 59, no. 7, pp. 1904 – 1915, July 2011.

[75] X. Huang and Y. Li, "The PAM decomposition of CPM signals with integer modulation index," *IEEE Trans. Commun.*, vol. 51, no. 4, pp. 543 – 546, Apr. 2003.

[76] N. Svensson, "On Optimum and Suboptimum Coherent Detection of Continuous Phase Modulation on a Two-Ray Multipath Fading Channel," *IEEE Trans. Commun.*, vol. 35, no. 10, pp. 1041 – 1049, Oct. 1987.

[77] M. Rice and X. Dang, "Aeronautical telemetry using offset QPSK in frequency selective multipath," *IEEE Trans. Aerosp. Electron. Syst.*, vol. 41, no. 2, pp. 758 – 767, Apr. 2005.

[78] M. Rice, A. Davis, and C. Bettweiser, "Wideband channel model for aeronautical telemetry," *IEEE Trans. Aerosp. Electron. Syst.*, vol. 40, no. 1, pp. 57 – 69, Jan. 2004.

[79] W. V. Thillo, J. Nsenga, F. Horlin, A. Bourdoux, and R. Lauwereins, "The Generalized Linear Decomposition of Multilevel CPM Signals," *IEEE Int. Conf. Acoustics, Speech Signal Process. ICASSP '07*, vol. 3, pp. 645 – 648, Apr. 2007.

[80] M. P. Wylie-Green, "A New Finite Series Representation for Continuous Phase Modulation," *IEEE Military Commun. Conf. MILCOM '06*, pp. 1 – 7, Oct. 2006.

[81] C. Brown and P. J. Vigneron, "Equalisation and iterative reception for spectrally efficient CPM in multipath environments," *Proc. IEEE Military Commun. Conf. MILCOM '10*, pp. 1719 – 1724, Oct. 2010.

[82] G. Cariolaro, A. Vigato, "Representation of a CPM Modulator through a Finite-State Sequential Machine," *IEEE Int. Conf. Commun. ICC '07.*, pp. 2625 – 2629, June 2007.

[83] E. Haas, "Aeronautical channel modeling," *IEEE Trans. Veh. Tech.*, vol. 51, no. 2, pp. 254 – 264, Mar. 2002.

VITA

Sajid Saleem completed his B.Sc and M.S. degrees in Electrical Engineering from National university of Science and Technology (NUST), Pakistan, in 2006 and 2008, respectively. He was awarded President Gold Medal for academic distinction in his bachelors degree. Before starting his doctoral degree, he worked as a design engineer at Centre of Research and Engineering (CARE), Islamabad. Sajid Saleem worked towards his doctoral degree, as a Fulbright fellow at Wireless Systems Laboratory, Georgia Institute of Technology, from 2009 to 2013. During this time, he also completed an M.S. degree in Mathematics at Georgia Tech. The topic of his doctoral research was frequency-domain equalization for multi-h continuous phase modulation. Sajid spent summer of 2011 at Corporate R&D Qualcomm, San Deigo, where he focused on improving robustness of multi-user beamforming problem. His research interests broadly lie in the applications of the theory of detection, estimation, and digital signal processing to develop physical layer techniques for wireless communications.